Mechanistic and Pharmacological Studies of 11β-hydroxylase (P450 11B1) and Aldosterone Synthase (P450 11B2)

by

Juan J. Valentín-Goyco

A dissertation submitted in partial fulfillment
of the requirements for the degree of
Doctor of Philosophy
(Pharmacology)
in the University of Michigan
2024

Doctoral Committee:

Professor Richard J. Auchus, Chair
Professor Rita Bernhardt, Universität des Saarlandes
Associate Professor Jorge A. Iñiguez-Lluhí
Professor Neil Marsh
Professor Janet Smith

Juan J. Valentín-Goyco

juvalent@umich.edu

ORCID iD: 0000-0001-9120-6511

Dedication

Mi trayectoria académica ha sido posible gracias al trabajo, esfuerzo y sacrificio de mi madre, Maribel Goyco Rivera, y padre, Juan Valentín Cordero. A pesar de todas las visicitudes que han sobrellevado, siempre han puesto mi bienestar y futuro por delante. Ambos me han motivado a alcanzar mi potencial, y por ello les estoy eternamente agradecido.

My academic career has been possible thanks to the work, effort, and sacrifice of my mother, Maribel Goyco Rivera, and father, Juan Valentín Cordero. Despite all the hardships they have endured, they have always put my well-being and future first. They have both motivated me to reach my potential, and for that, I am eternally grateful.

Acknowledgments

I am immensely grateful to my mentor, Dr. Richard Auchus, who provided me with the opportunity to pursue fascinating scientific research and helped me flourish as an independent scientist. Thank you for motivating and inspiring me to strive for excellence. I highly appreciate your constructive criticism, patience, and enthusiasm for research. Pursuing my graduate degree has been a challenging experience, and having a supportive mentor has been indispensable throughout this journey.

I would like to express my gratitude to my committee members, namely Drs. Rita Bernhardt, Jorge A. Iñiguez-Lluhí, Neil Marsh, and Janet Smith, for their support and invaluable discussions throughout the past several years. I want to extend a special appreciation to Dr. Jorge A. Iñiguez-Lluhí, who has been a constant source of encouragement since my first year as a Ph.D. student in the Department of Pharmacology.

Thanks to my lab members, Neikelyn Burgos Tirado and Nirupama Sumangala Korada, with whom I am happy to have shared this experience. I am also thankful to have been mentored by Dr. Sangchoul Im, an excellent biochemist who has taught me many of the techniques necessary for my research project.

Graduate school has been a rollercoaster of emotions, but I am appreciative of my friends' support. Special thanks go to Cristina Acosta Guijarro and Susan Seijo Méndez, whom I have known and cherished since high school, for their constant help and encouragement. To Sofia

González Martínez, thanks for being a kind and supportive friend. I feel incredibly fortunate to have had the opportunity to meet all of you in this lifetime.

I am appreciative of the wonderful friends I have made during this experience, including Candilliane Serrano Zayas, Austin B. Shannon, Loyda Morales Rodríguez, Gissell Sánchez, Liz Jaeckel, Caroline Hernández-Casner Josh Lott, Anthony García, Tasmine Clement, Nathalie Momplaisir, and Tenzin Ngodup. Each one of you has been a source of inspiration and motivation for me throughout this journey. I feel fortunate to have crossed paths with all of you.

As a graduate student, I am very appreciative of all the senior students who mentored and guided me through the most challenging part of my life. Specifically, I would like to thank Andrea Pesch and Naincy Chandan for their genuine support.

I want to also express my sincere gratitude to my biggest supporter in Michigan, Mark Hartwig, for his constant encouragement and unwavering support. Additionally, I am grateful to Susan, my feline companion, for being with me since my first year as a Ph.D. student.

Table of Contents

List of Tables

List of Figures

Abstract

The cytochrome P450 enzymes, 11β-hydroxylase (P450 11B1), and aldosterone synthase (P450 11B2) carry out the final stages of cortisol and aldosterone synthesis in the adrenal glands. Cortisol, the primary glucocorticoid, plays a crucial role in regulating glucose homeostasis, stress, and immune responses. Excessive production of cortisol, however, leads to Cushing syndrome, which is characterized by a range of debilitating symptoms. These symptoms include hypertension, suppressed immunity, depression, and infertility, among others. Conversely, aldosterone regulates water, sodium, and potassium homeostasis. When aldosterone is produced in excess, it results in primary aldosteronism, the most prevalent form of secondary hypertension. The development of selective inhibitors for P450 11B1 and P450 11B2 has received significant attention due to their roles in endocrine disorders. Unfortunately, the high sequence identity of 93% between both homologous enzymes has hindered the development of such inhibitors, particularly for P450 11B2.

P450 11B2 catalyzes the production of aldosterone in three successive hydroxylation reactions: the 11β-hydroxylation of 11-deoxycorticosterone (DOC) to corticosterone, then the 18-hydroxylation to 18-hydroxycorticosterone, and last 18-oxidation to aldosterone. In contrast, P450 11B1 catalyzes the formation of cortisol from 11-deoxycortisol via a one-step 11β-hydroxylation reaction. Both enzymes can perform 11β-hydroxylation reactions on both 11-deoxycortisol and DOC; however, only P450 11B2 can produce aldosterone from the latter. While it has been shown that P450 11B2 carries out aldosterone synthesis through a processive mechanism, the factors that limit aldosterone production from 11B1 are still not well understood.

To address the disparities in the catalytic activities of P450 11B1 and P450 11B2, we performed two assessments. Firstly, we evaluated their inhibition by osilodrostat (LCI699), a newly approved medication for Cushing syndrome. Secondly, our goal was to identify the distinct biochemical properties of P450 11B2 that limit the 18-oxygenation activities and processivity of P450 11B1. To evaluate LCI699-mediated inhibition, we conducted an analysis of steroid synthesis in the NCI-H295R human adrenocortical cancer cell line. Subsequently, we investigated LCI699 inhibition in cells stably expressing individual human steroidogenic P450 enzymes, utilizing either HEK-293 or V79 cells. Lastly, we assessed the direct binding of LCI699 to purified enzymes incorporated into phospholipid nanodiscs. Our research has demonstrated that osilodrostat is a potent inhibitor of both P450 11B1 and P450 11B2. We also demonstrate partial inhibition of P450 11A1 and no inhibition of P450 17A1 and P450 21A2.

To understand the mechanism that enables and hinders aldosterone synthesis in P450 11B2 and P450 11B1, respectively, we introduced point mutations at residue 320, which partially exchanges the activities of both enzymes. We then investigated NADPH coupling efficiencies, binding kinetics and affinities, and product formation of purified P450 11B1 and P450 11B2, wild-type, and residue 320 mutations (V320A and A320V, respectively) in phospholipid vesicles and nanodiscs. Altogether, our findings suggest that coupling efficiencies do not directly correlate with an increase in 18-hydroxylase activity. In contrast, slow intermediate dissociation inversely correlates with 18-oxygenation activities in wild-type and mutant enzymes. Therefore, we conclude that slow intermediate dissociation kinetics, rather than high NADPH coupling efficiency, is the major property that enables P450 11B2 – but not P450 11B1 – to synthesize aldosterone via a processive mechanism.

Chapter 1
Introduction

1.1 Overview of Adrenal Steroid Biosynthesis

Steroid hormones regulate a wide range of physiological and developmental processes in the body. These hormones are synthesized from cholesterol, a 27-carbon molecule consisting of four rings and a side chain, and have a very similar structural composition. Although humans can produce cholesterol from acetate, most of the cellular supply of cholesterol comes from plasma low-density lipoproteins (LDLs) that are derived from the cholesterol in our diet [1].

The initial stage of steroidogenesis occurs in the mitochondria, where the steroidogenic acute regulatory protein (StAR) aids the movement of cholesterol from the outer mitochondrial membrane (OMM) to the inner mitochondrial membrane (IMM) [2]. Once transported to the IMM, the pathway begins with the cleavage of the cholesterol side chain by cytochrome P450 11A1 to yield pregnenolone, the primary intermediate in the production of most of the steroid hormones (Figure 1.1) [1].

Mineralocorticoids, which regulate sodium and potassium homeostasis, are synthesized in the *zona glomerulosa* through three separate enzymes. Firstly, 3β-hydroxysteroid dehydrogenase type 2 (HSD3β2) converts pregnenolone to progesterone. Progesterone is converted to 11-deoxycorticosterone by 21-hydroxylase (P450 21A2). Finally, aldosterone synthase (P450 11B2) metabolizes 11-deoxycorticosterone in three successive reactions to produce aldosterone.

Unlike mineralocorticoids, glucocorticoids, such as cortisol, are synthesized in the *zona fasciculata* and regulate the metabolism of glucose, proteins, and fats. The enzyme P450 17A1 catalyzes the 17α-hydroxylation of pregnenolone and progesterone, resulting in the formation of 17OH-progesterone and 17OH-pregnenolone. The HSD3β2 enzyme then converts 17OH-pregnenolone to 17OH-progesterone, which is necessary to produce 11-deoxycortisol through the action of P450 21A2. Finally, the synthesis of cortisol is completed by 11β-hydroxylase (P450 11B1), an enzyme closely related to P450 11B2.

Steroidogenesis also involves the production of various sex hormones, such as androgens and estrogens. The *zona reticularis* is responsible for synthesizing adrenal androgen and 19-carbon precursors. Two of the most abundant adrenal androgens are dehydroepiandrosterone (DHEA) and its sulfate (DHEAS). The enzyme P450 17A1 facilitates the two-step synthesis of DHEA from pregnenolone and the production of androstenedione (A4) from progesterone. Sulfotransferase 2A1 (SULT2A1) conjugates DHEA to DHEAS. The adrenal gland also produces small amounts of testosterone through the action of 17β-hydroxysteroid dehydrogenase type 5 (17βHSD5) on A4. A4 is also converted to testosterone in peripheral tissues. However, most of the testosterone, as well as the estrogens, are produced in the gonads. Both DHEA and DHEAS have minor steroidogenic activity and are secreted in greater quantities than A4. Their main function is to serve as an androgen precursor, and these 19-carbon steroids are further metabolized into more potent androgens and estrogens in the gonads [3].

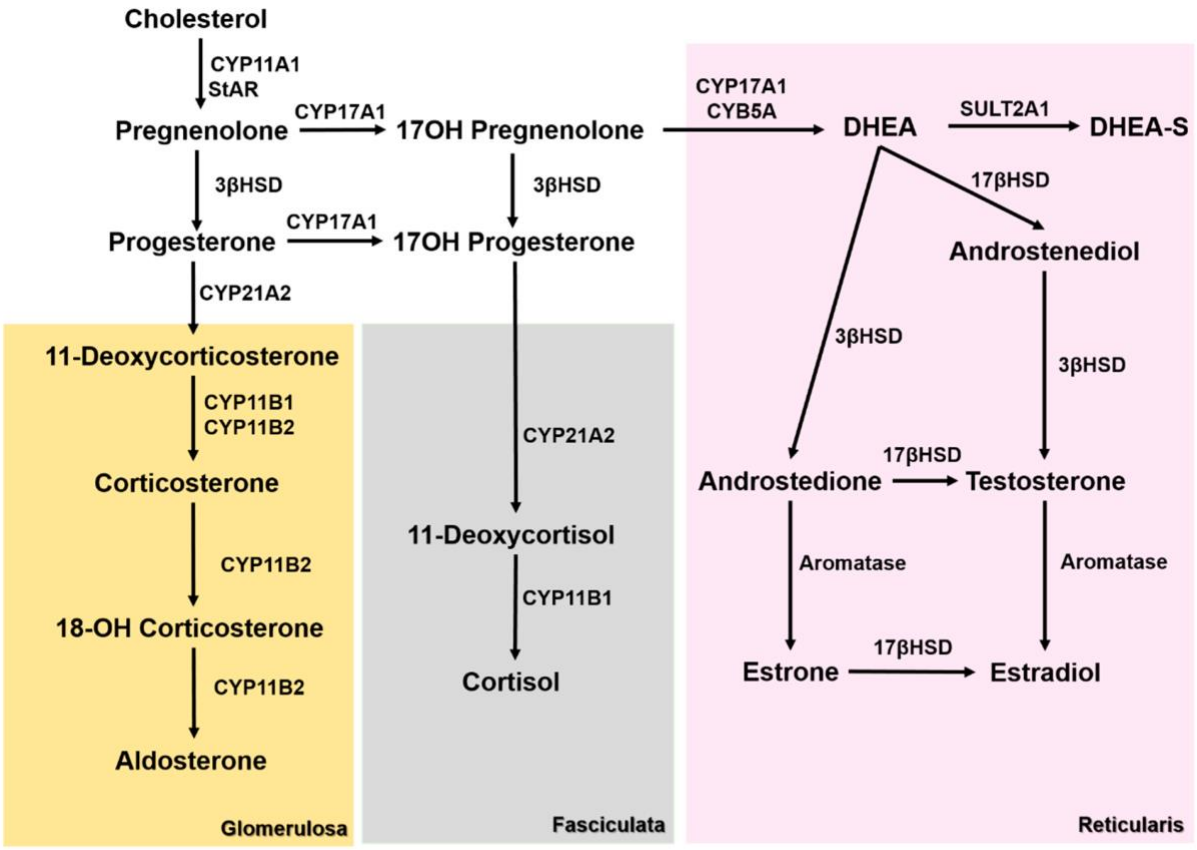

Figure 1.1 **Overview of adrenal steroidogenic pathways in different adrenal cortex zones**. Abbreviation: 3β-hydroxysteroid dehydrogenase (3βHSD), 17β-hydroxysteroid dehydrogenase (17βHSD), Cytochrome B5A (CYB5A), cholesterol side chain cleavage enzyme (CYP11A1), 11β-hydroxylase (CYP11B1), aldosterone synthase (CYP11B2), 17α-Hydroxylase (CYP17A1),21α-hydroxylase (CYP21A2), dehydroepiandrosterone (DHEA), dehydroepiandrosterone sulfate (DHEA-S), steroidogenic acute regulatory protein (StAR), and Sulfotransferase 2A1 (SULT2A1). The figure was adapted from Pereira S. *et al.* [4].

1.1.1 The 11β-hydroxylase and Aldosterone Synthase Enzymes

The enzymes 11β-hydroxylase (P450 11B1) and aldosterone synthase (P450 11B2) are responsible for the final steps in the biosynthesis of cortisol and aldosterone, respectively. Cortisol, the primary human glucocorticoid, is synthesized in the *zona fasciculata* of the adrenal cortex by P450 11B1. Expression of the human *CYP11B1* gene is limited to the *zona fasciculata* and adjacent *zona reticularis*. In contrast, aldosterone secretion and *CYP11B2* gene expression occur only in the *zona glomerulosa*.

In humans, the genes for *CYP11B1* and *CYP11B2* are located close to each other on chromosome 8, about 40 kb apart, and show a sequence identity of ~ 93% [5]. The major function of P450 11B1 is the 11β-hydroxylation of 11-deoxycorticortisol to yield cortisol (Figure 1.2). In contrast, P450 11B2 can carry out various other reactions. The biosynthesis of aldosterone begins with the 11β-hydroxylation of 11-deoxycorticosterone to make corticosterone. This is followed by an 18-hydroxylation to yield 18-hydroxycorticosterone and 18-oxidation to produce aldosterone. While both enzymes possess 11β-hydroxylation activity, they diverge in their 18 hydroxylase and 18-oxidase activities. Despite having 93% sequence identity, P450 11B1 has only a fraction of the 18-hydroxylase activity of P450 11B2 and lacks 18-oxidase activity.

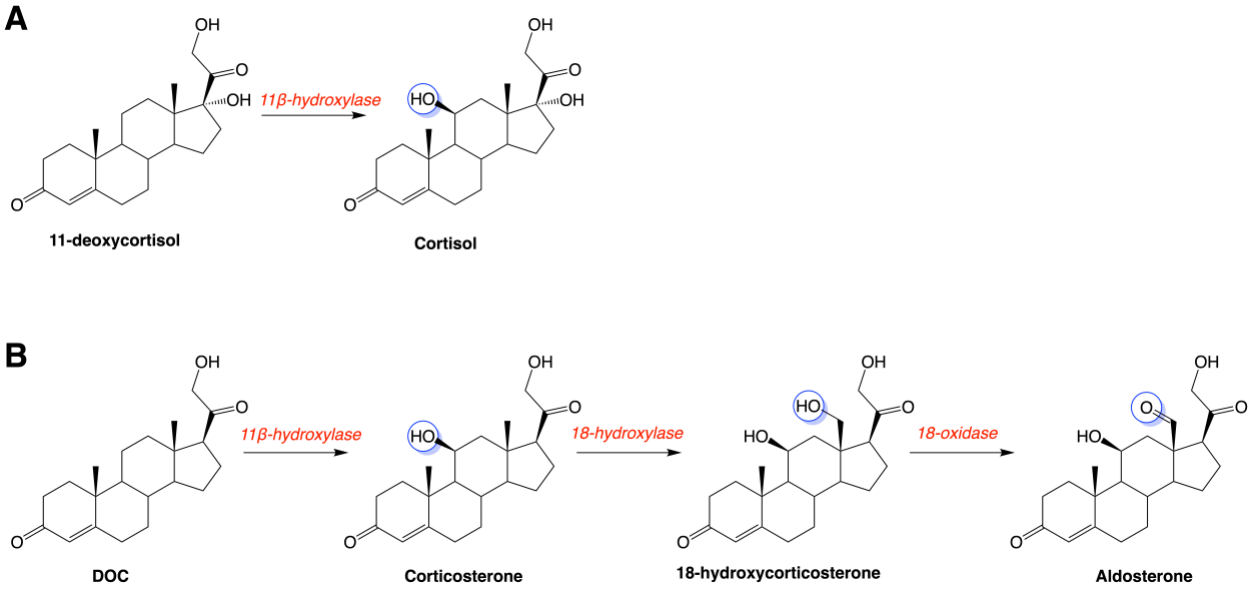

Figure 1.2 **Reactions catalyzed by cytochrome P450 11B1 and 11B2 in the adrenal glands.** Panel A shows the synthesis of cortisol from 11-doxycortisol. Panel B shows the synthesis of aldosterone from DOC.

1.1.2 Cellular Modulation of 11β-hydroxylase and Aldosterone Synthase

The regulation of cytochrome P450 11B enzymes is complex and involves two distinct physiological systems: the hypothalamic–pituitary–adrenal axis (HPA) and the renin–angiotensin system (RAS) [6]. The latter system modulates cytochrome P450 11B2 expression in the *zona*

glomerulosa of the adrenal cortex. In normal physiology, during volume depletion, the juxtaglomerular cells in the kidneys secrete the enzyme renin [7]. Renin cleaves angiotensinogen to angiotensin I, which is converted to angiotensin II by the angiotensin-converting enzyme in endothelial cells. Ultimately, angiotensin II binds to and activates angiotensin II receptors located on cells of the adrenal *zona glomerulosa*, resulting in the expression of cytochrome P450 11B2 and subsequent production of aldosterone from DOC (Figure 1.2). The synthesized aldosterone binds to mineralocorticoid receptors in the kidney, which results in the dissociation of heat shock proteins from the receptors and subsequent dimerization. These aldosterone-bound homodimers translocate to the nucleus and enhance the transcription of genes encoding serum glucocorticoid kinase 1 (SGK-1) and, ultimately, the three subunits of the epithelial sodium channel (ENaC) [8]. Within the cytosol, ENaC interacts with the ubiquitin protein ligase Nedd4, which hinders its trafficking to the cell surface. SGK-1 prevents this interaction by phosphorylation of serine residues in Nedd4. Altogether, these processes increase blood pressure primarily by enhancing sodium retention and potassium excretion in the kidneys.

Unlike P450 11B2, the expression of P450 11B1 in the *zona fasciculata* is regulated by the HPA axis [9]. Physical and environmental stressors cause the production of the corticotropin-releasing factor in the hypothalamus and initiate the release of the adrenocorticotropic hormone (ACTH) from the anterior pituitary [10]. ACTH binds to receptors on adrenocortical cells, activating adenylyl cyclase and, subsequently, increasing intracellular cyclic AMP (cAMP) [9]. This cAMP rise results in the activation of protein kinase (PKA), which leads to the phosphorylation of cholesterol ester hydrolase and the subsequent conversion of cholesterol esters to free cholesterol. These kinases also phosphorylate transcription factors, including members of the cAMP response element binding (CREB) protein family, which leads to the expression of P450

11B1, as well as other enzymes required for cortisol synthesis [5]. Much like aldosterone-mediated cellular signaling, circulating cortisol binds to glucocorticoid receptors and regulates physiological processes such as glucose metabolism and immune response through gene transcription [11].

1.1.3 Role of 11β-hydroxylase and Aldosterone Synthase in Disease

Due to the pivotal functions of both P45011B homologous enzymes in steroid production, their dysregulation can cause life-threatening illnesses. For example, defects in the *CYP11B1* gene cause 11β-hydroxylase deficiency (11OHD), the second most frequent cause of congenital adrenal hyperplasia (CAH) [12]. 11OHD is characterized by elevated 11-deoxycortisol and low cortisol levels, and symptoms include but are not limited to, virilization of the external genitalia, hyperpigmentation, accelerated skeletal maturation, and hypertension [13]. In contrast, excessive cortisol production can lead to Cushing syndrome (CS). CS can be classified into two major categories based on the underlying etiology: ACTH-dependent and ACTH-independent [14]. In the ACTH-dependent subtypes, there is an excess of ACTH due to either a pituitary tumor or an ectopic source, such as a neuroendocrine tumor. The most prevalent form of CS is due to pituitary adenomas, which autonomously secrete ACTH. ACTH-independent CS is due to autonomous cortisol synthesis from carcinoma or hyperplasia. Regardless of the underlying cause, chronic hypercortisolism can lead to various health problems, such as insulin resistance, osteoporosis, and neuropsychiatric disorders like depression. In normal physiology, cortisol is rapidly inactivated by 11β-hydroxysteroid dehydrogenase type 2 (11β-HSD2) in the kidney, which converts cortisol to cortisone, thereby preventing its binding to mineralocorticoid receptors [15]. In CS, excess cortisol secretion overwhelms the regulatory capacity of 11β-HSD2, leading to the activation of mineralocorticoid receptors and the subsequent development of hypertension and hypokalemia.

Much like cortisol, overproduction or underproduction of aldosterone can be harmful to human health. Underproduction, however, is a much more serious threat in early childhood development. Mutations in the *CYP11B2* gene that inactivate P450 11B2 lead to aldosterone synthase deficiency (ASD), which is often manifested in early infancy. ASD results in salt-wasting and failure to thrive if left untreated. There exist two types of ASD, namely ASD type I and ASD type II. The former is caused by mutations in P450 11B2 that impair 18-hydroxylase deficiency, while the latter is attributed to mutations that impair 18-oxidase deficiency [16]. In contrast to ASD, some individuals suffer from a condition called primary aldosteronism, which is characterized by high aldosterone production in the presence of low plasma renin. PA is the major cause of secondary hypertension, and it is estimated that between 5%-10% of all people with hypertension suffer from this disease [17]. In addition, compared to primary hypertension, patients with PA are at higher risk for cardiovascular events (heart failure, stroke, atrial fibrillation, etc.) and target organ damage. PA can be caused by either aldosterone-producing adenomas or bilateral hyperaldosteronism, which is the most common form [17].

1.2 Cytochrome P450 Enzymes

The cytochrome P450 superfamily is a group of proteins that contains a heme prosthetic group in their active site. They were initially discovered as a pigment in rat liver microsomes in 1958 and were identified due to their unique spectroscopic attributes, which include a 450 nm optical absorption peak after exposure to carbon monoxide (CO) [18]. However, Omura and Sato categorized the pigment as a hemeprotein and coined the term "cytochrome P450” in 1962 [19]. These enzymes eventually were found to be involved in various reactions related to the metabolism of drugs and steroid hormones, highlighting their diverse functionalities and generating interest in the fields of biotechnology, agriculture, and drug development and metabolism [20, 21].

To date, scientists have identified 57 distinct types of cytochromes P450 in humans (Table 1.1), which can be classified as either microsomal (Type II) or mitochondrial (Type I) P450 enzymes [22]. In human physiology, these P450s serve diverse functions, including the production of hormones, fatty acids, bile acid synthesis, and the metabolism of xenobiotics, including environmental pollutants and drugs. Their primary function is the monooxygenation of substrates by using molecular oxygen and electrons transferred from NADPH via redox partner proteins. This electron transfer process was first described by Omura through the isolation and reconstitution of activity of 11β-hydroxylase from the adrenal cortex [23]. In the case of mitochondrial enzymes, electron transfer involves adrenodoxin, a soluble ferredoxin-type iron-sulfur (Fe_2S) protein, and the membrane-bound adrenodoxin reductase, a flavoprotein that contains a flavin adenine dinucleotide (FAD) coenzyme [24]. Microsomal P450 enzymes require the membrane-bound cytochrome P450 reductase (CPR), which carries two coenzymes, FAD and a flavin mononucleotide (FMN), and some employ the membrane-bound form of cytochrome b_5 [25].

Enzymes belonging to the cytochrome P450 family are highly diverse and are categorized based on their gene sequences. They are given a family number, for instance, P450 11, and a subfamily letter, such as P450 11B. Each enzyme is then identified by a number for the isoform or individual enzyme, such as P450 11B1 and P450 11B2. Generally, families have 40% sequence identity, while subfamilies have over 55% [26]. Among the 57 identified P450 enzymes in humans, there are 18 families and 41 subfamilies [22]. Between these enzymes, microsomal P450s, such as P450 3A4 and 3A5, have been a major focus for many years as they metabolize most FDA-approved drugs. However, attention has shifted towards mitochondrial enzymes, such as P450 11B1 and 11B2, due to their crucial role in synthesizing steroid hormones and endocrine disorders.

Table 1.1 **Classification of Human Cytochrome P450 Enzymes.***

Steroids	Xenobiotics	Fatty Acids	Eicosanoids	Vitamins	Orphan
1B1	1A1	2J2	2U1	2R1	2A7
7A1	1A2	4A11	4F2	24A1	2S1
7B1	2A6	4A22	4F3	26A1	4X1
8B1	2A13	4B1	4F8	26B1	20A1
11A1	2B6	AF11	5A1	26C1	
11B1	2C8	4F12	8A1	27B1	
11B2	2C9	4F22		27C1	
17A1	2C18	4V2			
19A1	2C19	4Z1			
21A2	2D6				
27A1	2E1				
39A1	2F1				
46A1	2W1				
51A1	3A4				
	3A5				
	3A7				
	3A43				

*Table adapted from Guengerich P.F. [27].

1.2.1 Molecular Structure of Cytochrome P450 Enzymes

Cytochrome P450 enzymes contain a heme prosthetic group and, in the case of eukaryotic organisms, are bound to membranes of the endoplasmic reticulum or mitochondria. The first P450 enzyme purified and crystallized was the water-soluble bacterial P450 enzyme from *Pseudomonas putida*, P450 101A1, otherwise known as P450cam [28, 29]. The structure of P450cam can be described as a singular globular domain comprising 12 alpha helices and five anti-parallel beta sheets (Figure 1.3). The heme prosthetic group is positioned between two long alpha helices, namely Helix I and Helix L, and is buried within a large internal pocket surrounded by hydrophobic amino acid residues.

In general, the structure of all cytochrome P450 enzymes is highly conserved, meaning that the membrane-bound P450s have the same overall conformation as their soluble bacterial counterparts [30]. A critical difference between bacterial and eukaryotic enzymes is the presence

of a membrane anchor [31]. In the case of microsomal P450s, these contain a hydrophobic anchor sequence of 20-25 residues at the amino terminus. This sequence helps to target and anchor the enzymes to the cytosolic face of the membrane of the endoplasmic reticulum. Mitochondrial P450s, however, possess a 20-40 amino acid-long targeting sequence that is proteolytically removed after the enzyme is imported into the mitochondria [32]. Additionally, the membrane-bound mammalian P450 enzymes are partially embedded into the membrane via the F/G loop [33].

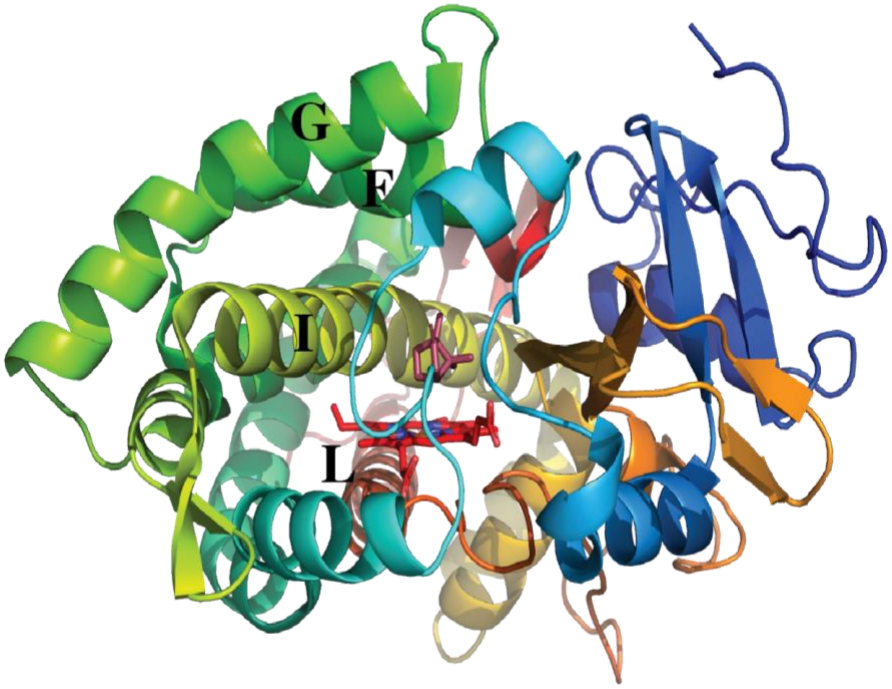

Figure 1.3 **Crystal structure of cytochrome P450cam.** (PDB: 2CCP).

1.2.1.1 Structure of 11β-hydroxylase and Aldosterone Synthase

In 2013, the crystal structures of P450 11B2 were obtained in a complex with either DOC or fadrozole, an inhibitor [34]. The structure of P450 11B1, however, was not published until 2019, albeit only in a complex with fadrozole [35]. Both structures reveal the characteristic cytochrome P450 fold, and an active site lined with hydrophobic residues. Upon comparing P450 11B

structures with bound fadrozole, it was found that despite most active site residues being identical, each enzyme binds to a different drug enantiomer. The P450 11B1 crystal bound to the *S*-enantiomer, while the P450 11B2 crystal bound to the *R*-enantiomer of fadrozole (Figure 1.4). In both enzymes, the nitrogen atom of fadrozole is directly coordinated with the heme iron, as it is typically observed with azole-bound inhibitors. A significant difference in the binding of these enantiomers is the orientation of the benzonitrile group, which projects towards the β1 sheet in P450 11B1, but towards the I Helix in P450 11B2. The authors attribute the preferential binding phenomenon to the "unique active-site architecture" of these homologous enzymes [35]. Specifically, they highlight differences in the placement and orientation of residues in the active site roof.

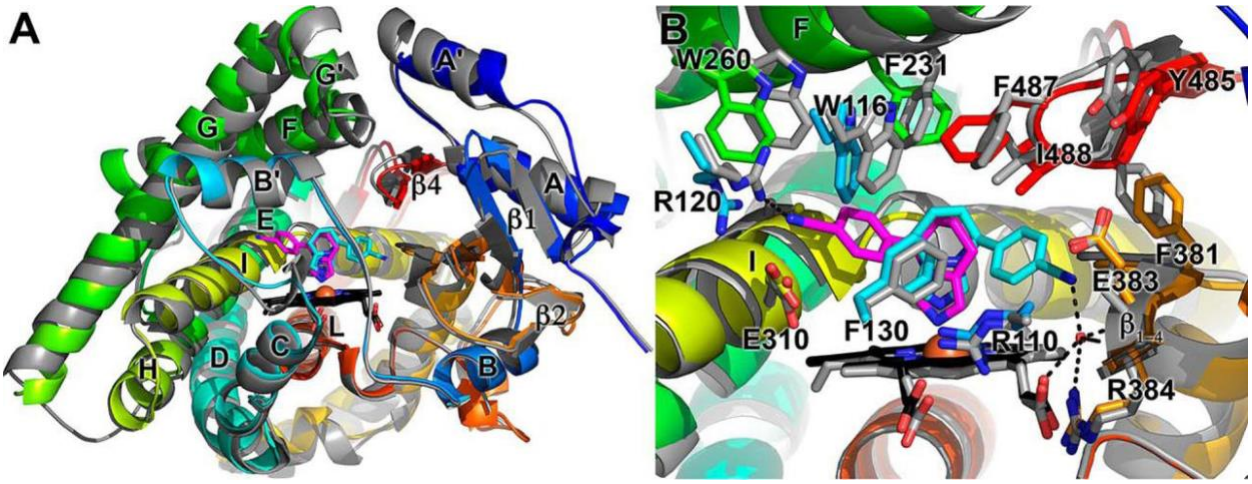

Figure 1.4 **Structural alignments of P450 11B1 and P450 11B2 structures in complex with fadrozole.** Panel A shows P450 11B1 (in colors) and P450 11B2 (gray ribbons with magenta fadrozole, PDB:4FDH). Panel B shows active site rearrangement for selective (S)- and (R)-fadrozole binding. The figure was adapted from Brixius-Anderko S. *et al.* [35].

Another prominent difference that exists between the enzymes P450 11B1 and 11B2 is in regard to the structure of the I helix, which participates in substrate binding. In both enzymes, the

I helix exhibits a slight break as it transits over the heme, leading to the formation of a non-helical region. However, the break in P450 11B1 is longer, consisting of five amino acid residues, while in P450 11B2, it is shorter, consisting of only two amino acid residues [35], with residue 320 situated after this break. Residue 320, which is a valine in P450 11B2, but an alanine in P450 11B1, has been demonstrated to be significant in the synthesis of aldosterone. Replacing alanine with valine at this position has been shown to enhance and confer 18-hydroxylase and 18-oxidase activity in P450 11B1 [36]. Several other key residues that are important for these activities, including residue 320, have been identified through sequence alignment and mutagenesis studies of P450 11B1 and 11B2 [36]. However, the mechanism by which these residues promote aldosterone synthesis has not been explored in the scientific literature.

1.2.2 Mechanism of P450 Catalyzed Reactions

When unliganded, P450 enzymes exist in a ferric resting state, where a water molecule is directly coordinated with the heme group [37]. Substrate binds to the active site and displaces this water molecule but does not bind covalently to the iron. Substrate binding triggers a high spin shift, resulting in the transfer of one electron and the reduction of the ferric iron (Fe^{3+}) to the ferrous iron (Fe^{2+}) state. Upon entering the ferrous state, molecular oxygen binds to heme, resulting in the formation of the [$Fe^{2+}O_2$] complex. Following oxygen binding, a second reduction and proton transfer occurs, which generates a ferric hydroperoxo species, [Fe^{3+}-OOH], commonly referred to as compound 0. Compound 1 is then formed when a second proton added to the distal oxygen promotes the cleavage of the O-O bond of compound 0, resulting in the release of a water molecule. Compound 1 abstracts a hydrogen atom from the substrate, leading to the formation of compound 2 and the substrate radical. Finally, the formation of the hydroxylated product occurs when the

substrate radical recombines with the hydroxyl group of compound 2. As a result of this reaction, the product is released, and the enzyme is returned to its initial state.

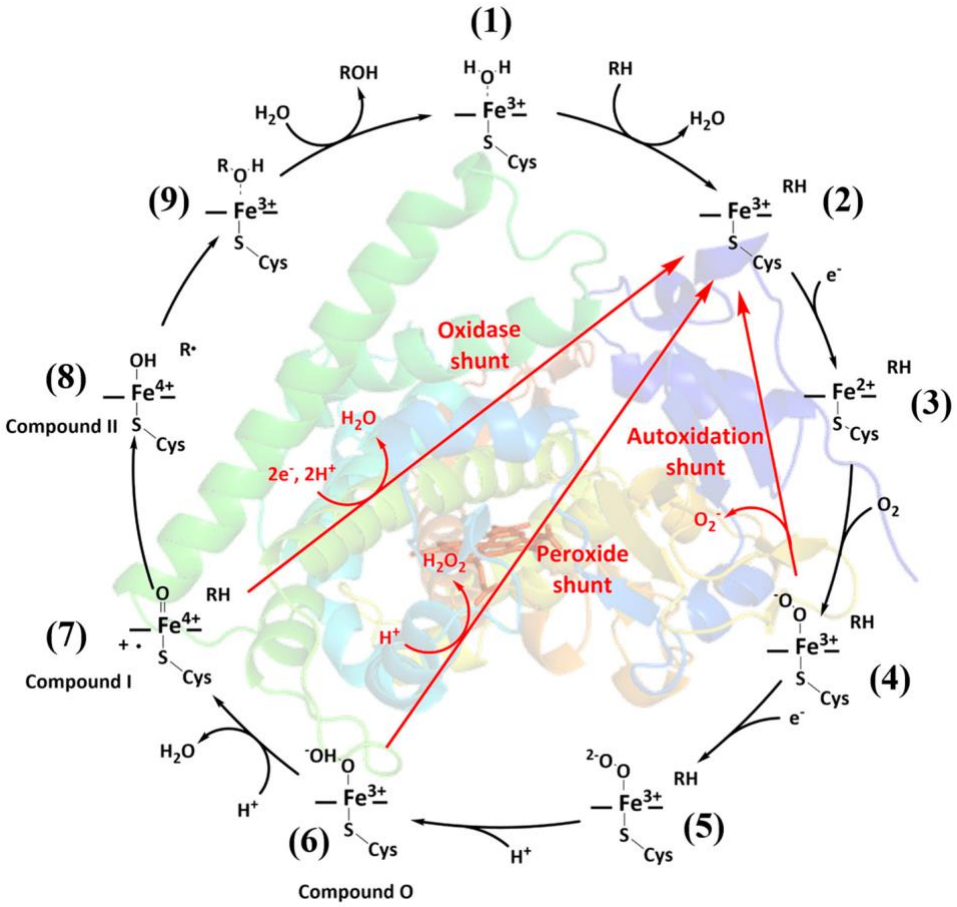

Figure 1.5 **The catalytic cycle of cytochrome P450 enzymes.** The red arrows indicate the pathways for uncoupling. Figure obtained from Meng S. *et al.*[38].

In some instances, the catalytic cycle of P450 enzymes may be inefficient and lead to the release of unmetabolized substrate and reactive oxygen species [38]. This cycle can produce superoxide, hydroperoxide, or extra water, depending on which step is affected (Figure 1.5). The efficiency with which a P450 enzyme consumes NADPH is often referred to as coupling efficiency, and it is defined as the ratio of formed products to consumed NADPH. P450 enzymes often exhibit high coupling efficiency towards their natural substrates. For instance, the bacterial P450 BM3 from *Bacillus megaterium* has up to 88% coupling efficiency towards myristic acid and up to 93% towards palmitic acid [39]. In contrast, xenobiotic metabolizing enzymes, such as

P450 3A4, show a wide range of coupling efficiencies with many compounds that are substrates. P450 17A1 has been shown to have a coupling efficiency of 46% for its 17-hydroxylase activity; however, the coupling efficiency is much lower for its 17,20-lyase activity, which can be partially or completely rescued with the addition of cytochrome b_5 [40].

1.2.3 Spectroscopic Features of Cytochrome P450 Enzymes

The presence of a heme prosthetic group imparts a unique and scientifically useful characteristic in P450 enzymes: their distinct UV-visible spectra. The heme exhibits an absorption spectrum between the 400 and 500 nm range, featuring a Soret band with a peak at ~ 418 nm when the enzyme is in its resting state, low-spin state [18, 41]. Upon substrate binding, the iron atom undergoes a transition from a low- to a high-spin state, resulting in a shift of the Soret band from a wavelength of ~ 418 to ~ 390 nm. This type of binding is commonly known as Type I binding, which is characterized by the ligand replacing the distal water molecule, leading to the iron transitioning to a high-spin and pentacoordinate state. To qualitatively assess the type of binding, difference spectra are commonly obtained by subtracting the signal of the unliganded P450 from the complexed enzyme. Type I difference spectra show a peak at ~ 390 nm and a trough at ~ 418 nm (Figure 1.6).

In contrast to substrate binding, when the P450 enzymes bind to azole-containing inhibitors, the maximum of the Soret band shifts from ~ 418 to ~ 425 nm [42]. This shift is attributed to the strong coordination of the nitrogen atom with the heme, resulting in a hexacoordinate and low-spin state, as is observed with the binding of fadrozole to cytochrome P450 11B1 and 11B2. As such, typical Type II difference spectra show a peak and a trough at ~ 425 nm and ~ 390 nm, respectively. Some ligands may induce a third form of binding known as Reverse Type I, which is characterized by a maximum at ~ 420 nm. This type of binding is believed

to occur through the ligation of a non-nitrogen heteroatom to the heme, typically involving hydroxyl groups [43].

These spectral changes serve as a useful tool to assess ligand binding through various approaches. For instance, by titrating increasing amounts of ligand to a quartz cuvette containing a P450 enzyme of interest, the equilibrium dissociation constant (K_d) can be calculated [43]. The K_d is quantified by subtracting the absorbance minimum from the maximum of the difference spectra and plotting this value as a function of ligand concentration. To determine specific binding and dissociation rates, and to evaluate the overall binding mechanism, a stopped-flow apparatus is often employed [43]. This instrument is designed to measure reaction kinetics precisely by monitoring time-dependent changes in absorbance in a millisecond time scale.

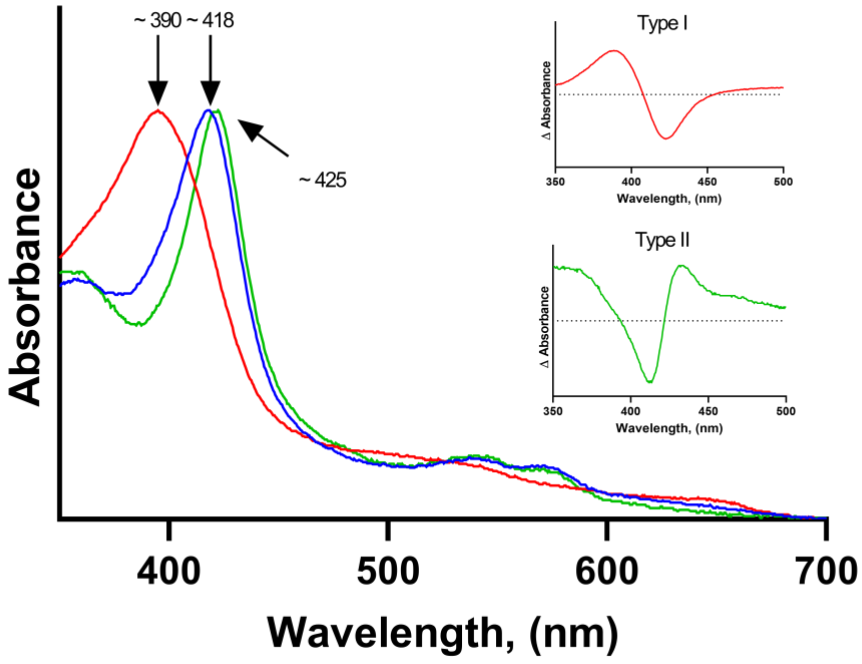

Figure 1.6 **Representative cytochrome P450 UV-visible spectra.**

Another helpful application of P450 spectra is the quantification of functional protein, which is essential for accurate biochemical analysis. As initially observed in 1958 with rat liver microsomes, P450 enzymes in the Fe^{2+} state can bind carbon monoxide (CO) with a high affinity [18]. This P450-CO complex produces a spectrum with a pronounced peak at ~ 450 nm (Figure 1.7). To quantify functional protein, purified P450 enzymes are diluted with buffer in a quartz cuvette, which is saturated with CO gas prior to reducing with sodium dithionite ($Na_2S_2O_4$) [44]. The spectra are then measured in a UV-visible spectrophotometer in the 400 to 500 nm range. A reference cuvette that contains P450 enzyme and $Na_2S_2O_4$ but is not bubbled with CO is also used to correct for background signal and protein loss. Ultimately, the concentration of the enzyme is calculated with the use of Beer's law and the corresponding extinction coefficient for 450 nm (91 $mM^{-1}cm^{-1}$). An inactive or damaged form of 450 enzymes is associated with a peak at 420 nm in this assay [45].

The 450 nm absorbance maximum observed with cytochrome P450 enzymes is due to the coordination of a cysteine residue with the heme iron. The distinction between P420 and P450 forms has been attributed to the protonation of the cysteine thiolate ligand and the substitution of the cysteine ligand by a neighboring histidine [46, 47]; however, the latter has been shown not to be a requirement for the conversion of P450 to P420, as established in a study in which three different histidine residues that are in close proximity to the heme in P450cam were mutated to glycine [48]. Regardless of the underlying cause for the conversion, the appearance of the 420 nm peak occurs during harsh chemical treatments or due to protein instability. While the back conversion of P420 to P450 is widely considered improbable, it continues to be a topic of active research within the sphere of cytochrome P450.

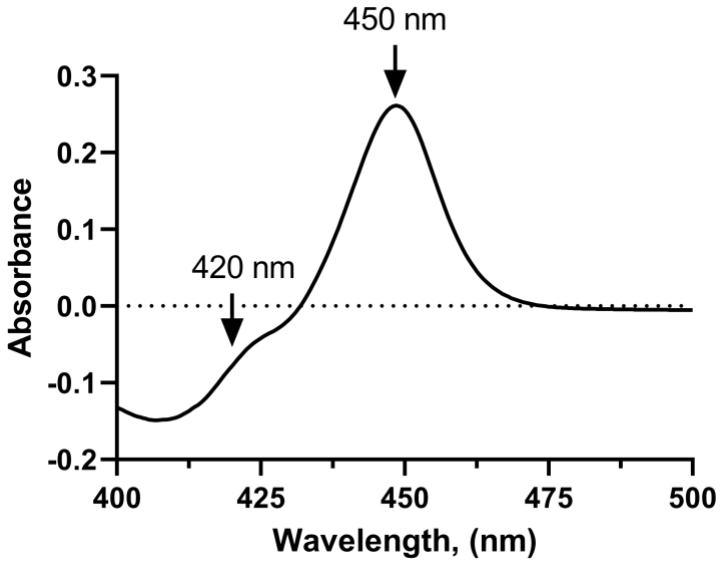

Figure 1.7 **CO-binding spectrum from purified cytochrome P450 11B1.**

1.2.4 Modulation of P450 Activity by Redox Partners

The catalytic activity of all cytochrome P450 enzymes requires interaction with their respective redox partners to efficiently transfer electrons. For microsomal enzymes, the transfer of electrons occurs via cytochrome P450 reductase (CPR), which contains FAD and FMN domains. The FAD domain accepts two electrons from NADPH. These electrons are then transferred one at a time to the FMN domain, which then passes them on to the P450 enzyme. Based on the x-ray crystal structure of CPR, CPR must undergo conformational changes to transfer electrons to the P450 [49, 50]. A "closed" conformation of CPR allows the interaction between the FAD and FMN domains, thereby supporting intramolecular electron transfer. Meanwhile, the "open" conformation allows for the FMN-containing domain to transiently interact and transfer the received electron to the P450 enzyme.

While CPR is the primary redox partner for all microsomal P450 enzymes, its interaction differs for each P450. For example, in the case of P450 17A1 and P450 21A2, their fusion to the FMN-containing domain of CPR differentially impacted their binding to ligands. Both wild-type P450 17A1 and P450 21A2 can bind to 17α-hydroxyprogesterone with similar affinity. The FMN-fused P450 17A1 exhibited a significant 43% reduction in the dissociation constant (K_d) in comparison to the FMN-fused P450 21A2, which demonstrated a 27% reduction in the K_d [51]. The fusion of the FMN domain did not affect the binding of the steroidogenic inhibitor, ketoconazole, to P450 17A1; however, the FMN-fusion significantly altered the binding of ketoconazole to P450 21A2 by raising the K_d value by 31% [51].

In the case of mitochondrial P450 enzymes, such as P450 11B1 and P450 11B2, steroid metabolism is carried out with the help of the soluble Fe_2S_2 protein adrenodoxin and the membrane-bound flavoprotein adrenodoxin reductase. Much like what is observed with the microsomal P450s and CPR, there is evidence that suggests that adrenodoxin can allosterically modulate the activity and ligand binding affinity of mitochondrial P450s [52-54]. Although adrenodoxin dimers have been reported in the literature, it is believed that the monomeric protein is the form responsible for the transfer of electrons to the P450 enzyme [55]. In this process, two electrons from NADPH are transferred to adrenodoxin reductase. The reduced adrenodoxin reductase then transfers one electron at a time to adrenodoxin, which then shuttles the electron to the mitochondrial P450 (Figure 1.8).

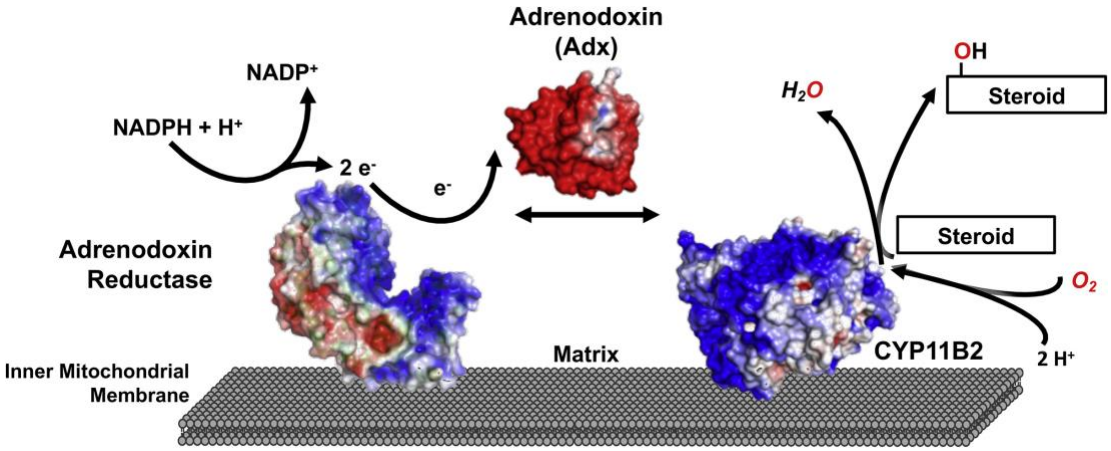

Figure 1.8 **Catalytic system of cytochrome P450 11B2.** The figure was adapted from Brixius-Anderko S. *et al.* [52].

Adrenodoxin's α-helix-3 facilitates interactions between adrenodoxin and adrenodoxin reductase, as well as between adrenodoxin and P450 enzymes. This interaction was characterized by the engineering and subsequent crystallization of an adrenodoxin-P450 11B2 fusion protein. The crystal structure of this fusion protein confirmed that negatively charged residues (Asp72, Glu73, and Asp76) in α-helix-3 interact with positively charged residues in helix K (Arg366 and Lys370) of P450 11B2 [52]. Previous functional studies have also confirmed the interaction of these two helices. For example, exchanging the arginine at the 366 position for lysine in P450 11B1 and 11B2 results in a significant reduction of their 11β-hydroxylase activity [54].

In addition, incubating P450 11B2 with increasing concentrations of adrenodoxin significantly enhances substrate turnover (k_{cat}). This trend is also observable in the binding of substrates. Specifically, equimolar concentrations of adrenodoxin and P450 11B2 yield a K_d of 17 µM, whereas a 40-fold excess of adrenodoxin results in a K_d of 11 µM [52]. Adrenodoxin has also been shown to affect the inhibition of P450 11B2. Studies have demonstrated that increasing concentrations of adrenodoxin can enhance the effectiveness of osilodrostat, a drug approved in

2020 by the FDA for treating Cushing syndrome [52]. Similarly, the same results have been observed for P450 11B1 when it is incubated with increasing concentrations of adrenodoxin [53].

1.3 Conclusions and Research Goals

Despite progress in understanding cytochrome P450 11B1 and 11B2 biochemistry, questions remain about their divergent enzymatic activities. P450 11B1 shares good 11β-hydroxylase activity with P450 11B2; however, the 18-hydroxylase activity of P450 11B1 is poor. Furthermore, P450 11B2, but not P450 11B1, produces aldosterone from DOC through a processive mechanism, a reaction sequence in which intermediates undergo a subsequent reaction faster than dissociation from the active site [56].

Given the lack of therapeutics for the treatment of primary aldosteronism (PA), being able to differentiate these two homologous enzymes biochemically is important. Novartis developed osilodrostat (LCI-699) as a P450 11B2 inhibitor to treat PA. LCI-699 is based on the *R*-enantiomer (FAD286) of the P450 inhibitor fadrozole [57]. Even though FAD286 reduced plasma and urine aldosterone levels in transgenic mice overexpressing renin, there was still a lack of selectivity for P450 11B2 [58]. Selectivity was improved by adding a fluorine atom to the benzonitrile in FAD286, thereby creating LCI-699. Although promising, clinical trials of osilodrostat showed that participants suffered from side effects associated with the inhibition of P450 11B1. Osilodrostat was then repurposed as a P450 11B1 inhibitor to treat Cushing syndrome and is now commercially available as Isturisa [59]. Nonetheless, advancements have been made in recent times towards the development of selective P450 11B2 inhibitors as a randomized, double-blind, placebo-controlled clinical study has demonstrated the efficacy of dexfadrostat in suppressing aldosterone production [60].

The aim of this dissertation is first to characterize osilodrostat inhibition of P450 11B1 and 11B2 and, secondly, to establish the factors that regulate aldosterone synthase activity. While it was shown that P450 11B2 produces aldosterone in a processive mechanism, the question remains: how is P450 11B2 able to produce aldosterone while its counterpart, P450 11B1, cannot? An in-depth understanding of the complex reactions catalyzed by both isoenzymes, particularly the kinetic parameters that allow processivity for P450 11B2, might enable the development of selective inhibitors and progress our knowledge of cytochrome P450 enzymes and steroid metabolism.

1.4 Bibliography

1. Miller, W.L. and R.J. Auchus, *The molecular biology, biochemistry, and physiology of human steroidogenesis and its disorders.* Endocr Rev, 2011. **32**(1): p. 81-151.
2. Bose, H.S., V.R. Lingappa, and W.L. Miller, *Rapid regulation of steroidogenesis by mitochondrial protein import.* Nature, 2002. **417**(6884): p. 87-91.
3. Papadopoulou-Marketou, N., E. Kassi, and G.P. Chrousos, *Adrenal Androgens and Aging*, in *Endotext*, K.R. Feingold, et al., Editors. 2000: South Dartmouth (MA).
4. Pereira, S.S., et al., *Incomplete Pattern of Steroidogenic Protein Expression in Functioning Adrenocortical Carcinomas.* Biomedicines, 2020. **8**(8).
5. Schiffer, L., et al., *The CYP11B subfamily.* J Steroid Biochem Mol Biol, 2015. **151**: p. 38-51.
6. Rainey, W.E., *Adrenal zonation: clues from 11beta-hydroxylase and aldosterone synthase.* Mol Cell Endocrinol, 1999. **151**(1-2): p. 151-60.
7. Sparks, M.A., et al., *Classical Renin-Angiotensin system in kidney physiology.* Compr Physiol, 2014. **4**(3): p. 1201-28.
8. Flores, S.Y., et al., *Aldosterone-induced serum and glucocorticoid-induced kinase 1 expression is accompanied by Nedd4-2 phosphorylation and increased Na+ transport in cortical collecting duct cells.* J Am Soc Nephrol, 2005. **16**(8): p. 2279-87.
9. Waterman, M.R. and L.J. Bischof, *Cytochromes P450 12: diversity of ACTH (cAMP)-dependent transcription of bovine steroid hydroxylase genes.* FASEB J, 1997. **11**(6): p. 419-27.
10. Ramamoorthy, S. and J.A. Cidlowski, *Corticosteroids: Mechanisms of Action in Health and Disease.* Rheum Dis Clin North Am, 2016. **42**(1): p. 15-31, vii.
11. Hupfeld, C.J. and J.A. Iñiguez-Lluhí, *Adrenocorticotropic Hormone, Adrenal Steroids, and the Adrenal Cortex*, in *Goodman & Gilman's: The Pharmacological Basis of Therapeutics*, L.L. Brunton and B.C. Knollmann, Editors. 2023, McGraw-Hill Education.

12. Yau, M., J. Gujral, and M.I. New, *Congenital Adrenal Hyperplasia: Diagnosis and Emergency Treatment*, in *Endotext*, K.R. Feingold, et al., Editors. 2000: South Dartmouth (MA).
13. Turcu, A.F. and R.J. Auchus, *Adrenal steroidogenesis and congenital adrenal hyperplasia.* Endocrinol Metab Clin North Am, 2015. **44**(2): p. 275-96.
14. Raff, H. and T. Carroll, *Cushing's syndrome: from physiological principles to diagnosis and clinical care.* J Physiol, 2015. **593**(3): p. 493-506.
15. Luft, F.C., *11beta-Hydroxysteroid Dehydrogenase-2 and Salt-Sensitive Hypertension.* Circulation, 2016. **133**(14): p. 1335-7.
16. Merakou, C., et al., *Molecular Analysis of the CYP11B2 Gene in 62 Patients with Hypoaldosteronism Due to Aldosterone Synthase Deficiency.* J Clin Endocrinol Metab, 2021. **106**(1): p. e182-e191.
17. Byrd, J.B., A.F. Turcu, and R.J. Auchus, *Primary Aldosteronism: Practical Approach to Diagnosis and Management.* Circulation, 2018. **138**(8): p. 823-835.
18. Klingenberg, M., *Pigments of rat liver microsomes.* Arch Biochem Biophys, 2003. **409**(1): p. 2-6.
19. Omura, T. and R. Sato, *A new cytochrome in liver microsomes.* J Biol Chem, 1962. **237**: p. 1375-6.
20. Cooper, D.Y., et al., *Photochemical Action Spectrum of the Terminal Oxidase of Mixed Function Oxidase Systems.* Science, 1965. **147**(3656): p. 400-2.
21. Estabrook, R.W., D.Y. Cooper, and O. Rosenthal, *The Light Reversible Carbon Monoxide Inhibition of the Steroid C21-Hydroxylase System of the Adrenal Cortex.* Biochem Z, 1963. **338**: p. 741-55.
22. Nelson, D.R., *Cytochrome P450 diversity in the tree of life.* Biochim Biophys Acta Proteins Proteom, 2018. **1866**(1): p. 141-154.
23. Omura, T.S., E.;Estabrook, R. W.; Cooper, D. Y.; Rosenthal, O. , *Isolation from adrenal cortex of a nonheme iron protein and a flavoprotein functional as a reduced triphosphopyridine nucleotide-cytochrome P-450 reductase.* Arch Biochem Biophys, 1966. **117**(3): p. 660-673.
24. Omura, T., *Mitochondrial P450s.* Chem Biol Interact, 2006. **163**(1-2): p. 86-93.
25. Srejber, M., et al., *Membrane-attached mammalian cytochromes P450: An overview of the membrane's effects on structure, drug binding, and interactions with redox partners.* J Inorg Biochem, 2018. **183**: p. 117-136.
26. Esteves, F., J. Rueff, and M. Kranendonk, *The Central Role of Cytochrome P450 in Xenobiotic Metabolism-A Brief Review on a Fascinating Enzyme Family.* J Xenobiot, 2021. **11**(3): p. 94-114.
27. Guengerich, F.P., *Ninety-eight semesters of cytochrome P450 enzymes and related topics-What have I taught and learned?* J Biol Chem, 2024. **300**(2): p. 105625.
28. Poulos, T.L., B.C. Finzel, and A.J. Howard, *High-resolution crystal structure of cytochrome P450cam.* J Mol Biol, 1987. **195**(3): p. 687-700.
29. Poulos, T.L., et al., *The 2.6-A crystal structure of Pseudomonas putida cytochrome P-450.* J Biol Chem, 1985. **260**(30): p. 16122-30.
30. Guengerich, F.P., M.R. Waterman, and M. Egli, *Recent Structural Insights into Cytochrome P450 Function.* Trends Pharmacol Sci, 2016. **37**(8): p. 625-640.
31. Black, S.D., *Membrane topology of the mammalian P450 cytochromes.* FASEB J, 1992. **6**(2): p. 680-5.

32. Ou, W.J., et al., *Processing-independent in vitro translocation of cytochrome P-450(SCC) precursor across mitochondrial membranes.* J Biochem, 1986. **100**(5): p. 1287-96.
33. Headlam, M.J., M.C. Wilce, and R.C. Tuckey, *The F-G loop region of cytochrome P450scc (CYP11A1) interacts with the phospholipid membrane.* Biochim Biophys Acta, 2003. **1617**(1-2): p. 96-108.
34. Strushkevich, N., et al., *Structural insights into aldosterone synthase substrate specificity and targeted inhibition.* Mol Endocrinol, 2013. **27**(2): p. 315-24.
35. Brixius-Anderko, S. and E.E. Scott, *Structure of human cortisol-producing cytochrome P450 11B1 bound to the breast cancer drug fadrozole provides insights for drug design.* J Biol Chem, 2019. **294**(2): p. 453-460.
36. Bottner, B., K. Denner, and R. Bernhardt, *Conferring aldosterone synthesis to human CYP11B1 by replacing key amino acid residues with CYP11B2-specific ones.* Eur J Biochem, 1998. **252**(3): p. 458-66.
37. Guengerich, F.P., *Mechanisms of Cytochrome P450-Catalyzed Oxidations.* ACS Catal, 2018. **8**(12): p. 10964-10976.
38. Meng, S., et al., *The molecular basis and enzyme engineering strategies for improvement of coupling efficiency in cytochrome P450s.* Biotechnol Adv, 2022. **61**: p. 108051.
39. Cryle, M.J. and J.J. De Voss, *Is the ferric hydroperoxy species responsible for sulfur oxidation in cytochrome p450s?* Angew Chem Int Ed Engl, 2006. **45**(48): p. 8221-3.
40. Peng, H.M., et al., *Cytochrome b5 Activates the 17,20-Lyase Activity of Human Cytochrome P450 17A1 by Increasing the Coupling of NADPH Consumption to Androgen Production.* Biochemistry, 2016. **55**(31): p. 4356-65.
41. Wagner, G.C., M.M. Palcic, and H.B. Dunford, *Absorption spectra of cytochrome P450CAM in the reaction with peroxy acids.* FEBS Lett, 1983. **156**(2): p. 244-8.
42. Locuson, C.W., J.M. Hutzler, and T.S. Tracy, *Visible spectra of type II cytochrome P450-drug complexes: evidence that "incomplete" heme coordination is common.* Drug Metab Dispos, 2007. **35**(4): p. 614-22.
43. Yoshimoto, F.K. and R.J. Auchus, *Rapid kinetic methods to dissect steroidogenic cytochrome P450 reaction mechanisms.* J Steroid Biochem Mol Biol, 2016. **161**: p. 13-23.
44. Guengerich, F.P., et al., *Measurement of cytochrome P450 and NADPH-cytochrome P450 reductase.* Nat Protoc, 2009. **4**(9): p. 1245-51.
45. Martinis, S.A., et al., *Probing the heme iron coordination structure of pressure-induced cytochrome P420cam.* Biochemistry, 1996. **35**(46): p. 14530-6.
46. Wells, A.V., et al., *Resonance Raman investigations of Escherichia coli-expressed Pseudomonas putida cytochrome P450 and P420.* Biochemistry, 1992. **31**(18): p. 4384-93.
47. Perera, R., et al., *Neutral thiol as a proximal ligand to ferrous heme iron: implications for heme proteins that lose cysteine thiolate ligation on reduction.* Proc Natl Acad Sci U S A, 2003. **100**(7): p. 3641-6.
48. Gable, J.A., S. Tripathi, and T.L. Poulos, *Structural Insights on the Conversion of Cytochrome P450 to P420.* ACS Omega, 2022. **7**(22): p. 18481-18485.
49. *Two conformations are better than one: domain motion in cytochrome P450 reductase. conformational equilibria revealed by nmr and small-angle X-ray scattering.* J Biol Chem, 2009. **284**(52): p. e99972.

50. Wang, M., et al., *Three-dimensional structure of NADPH-cytochrome P450 reductase: prototype for FMN- and FAD-containing enzymes.* Proc Natl Acad Sci U S A, 1997. **94**(16): p. 8411-6.
51. Burris-Hiday, S.D. and E.E. Scott, *Allosteric modulation of cytochrome P450 enzymes by the NADPH cytochrome P450 reductase FMN-containing domain.* J Biol Chem, 2023. **299**(9): p. 105112.
52. Brixius-Anderko, S. and E.E. Scott, *Structural and functional insights into aldosterone synthase interaction with its redox partner protein adrenodoxin.* J Biol Chem, 2021. **296**: p. 100794.
53. Loomis, C.L., S. Brixius-Anderko, and E.E. Scott, *Redox partner adrenodoxin alters cytochrome P450 11B1 ligand binding and inhibition.* J Inorg Biochem, 2022. **235**: p. 111934.
54. Peng, H.M. and R.J. Auchus, *Molecular Recognition in Mitochondrial Cytochromes P450 That Catalyze the Terminal Steps of Corticosteroid Biosynthesis.* Biochemistry, 2017. **56**(17): p. 2282-2293.
55. Jay, N., J.E. McGlohon, and D.F. Estrada, *Interactions of human mitochondrial Ferredoxin 1 (Adrenodoxin) by NMR; modulation by cytochrome P450 substrate and by truncation of the C-terminal tail.* J Inorg Biochem, 2023. **249**: p. 112370.
56. Reddish, M.J. and F.P. Guengerich, *Human cytochrome P450 11B2 produces aldosterone by a processive mechanism due to the lactol form of the intermediate 18-hydroxycorticosterone.* J Biol Chem, 2019. **294**(35): p. 12975-12991.
57. Hargovan, M. and A. Ferro, *Aldosterone synthase inhibitors in hypertension: current status and future possibilities.* JRSM Cardiovasc Dis, 2014. **3**: p. 2048004014522440.
58. Fiebeler, A., et al., *Aldosterone synthase inhibitor ameliorates angiotensin II-induced organ damage.* Circulation, 2005. **111**(23): p. 3087-94.
59. Duggan, S., *Osilodrostat: First Approval.* Drugs, 2020. **80**(5): p. 495-500.
60. Mulatero, P., et al., *CYP11B2 inhibitor dexfadrostat phosphate suppresses the aldosterone-to-renin ratio, an indicator of sodium retention, in healthy volunteers.* Br J Clin Pharmacol, 2023. **89**(8): p. 2483-2496.

Chapter 2

Selectivity of Osilodrostat as an Inhibitor of Human Steroidogenic Cytochromes P450[1]

2.1 Introduction

Osilodrostat (LCI699) is the first FDA-approved cortisol synthesis inhibitor for treating Cushing disease (CD). Most commonly occurring in women and with an incidence of 0.2-5.0 per million people per year, overt Cushing syndrome (CS) is a life-threatening illness characterized by chronic overproduction of cortisol [1]. The most prevalent cause of CS is pituitary adenomas (CD), which autonomously secrete excessive adrenocorticotropic hormone (ACTH) [1]. In such cases, the first line of treatment involves the surgical removal of the tumors. While effective in skilled centers, patients may require pharmacologic treatment post-surgery, as the risk of recurrence is high (15-66%) [2]. Hypercortisolemia can cause hypertension, skin atrophy, glucose intolerance, depression, and other co-morbid conditions [3]; consequently, adequate control of cortisol production is essential to prevent morbidity and mortality in patients with CS. LCI699 inhibits steroid 11β-hydroxylase (P450 11B1), thereby preventing the conversion of 11-deoxycortisol to cortisol. In two phase III trials, LCI699 normalized 24-hour urine-free cortisol in significantly more CD patients than placebo and maintained disease control over many months, with improvement in disease-related co-morbidities [4-6].

[1] The content of this chapter has been published: Valentín-Goyco, J., Liu, J., Peng, H. M., Oommen, J., & Auchus, R. J. (2023). Selectivity of osilodrostat as an inhibitor of human steroidogenic cytochromes P450. The Journal of steroid biochemistry and molecular biology, 231, 106316. https://doi.org/10.1016/j.jsbmb.2023.106316

Initially, however, LCI699 was developed by Novartis as an aldosterone synthase (P450 11B2) inhibitor for the treatment of hypertension, including primary aldosteronism, the most common form of secondary hypertension. P450 11B2 catalyzes the final three steps of aldosterone synthesis from 11-deoxycorticosterone (DOC). While *in-vitro* studies established some selectivity of LCI699 for P450 11B2 over P450 11B1, phase II clinical studies revealed that LCI699 led to the accumulation of 11-deoxycortisol [7] and a slight reduction in ACTH-stimulated serum cortisol [8]. Given these findings, LCI699 was then successfully repurposed as a P450 11B1 inhibitor.

While *in-vitro* studies have shown that LC699 is a potent P45011B1 and P450 11B2 inhibitor, with reported IC_{50} values of 2.5 nM and 0.7 nM, respectively, few studies have established the global effects of LCI699 on adrenal steroidogenesis [9, 10]. A recent study compared the steroid profiles of patients with ACTH-dependent CS treated with either LCI699 or metyrapone, a drug used off-label in the United States (and approved by the European Medicines Agency) for treating CS [11]. Despite the markedly greater potency of LCI699 over metyrapone *in-vitro* as a P450 11B1 inhibitor, this study found that LCI699 caused less accumulation of 11-deoxycortisol and androgens than metyrapone, despite similar normalization of urine-free cortisol. Because P450 11B1 inhibition allows accumulation of cortisol intermediates, particularly 17-hydroxyprogesterone, which can be converted to androgens, the authors suggested that LCI699 also inhibits P450 17A1 (17-hydroxylase/17,20-lyase) and P450 21A2 (21-hydroxylase), but the data could not exclude simultaneous inhibition of P450 11A1 (cholesterol side-chain cleavage enzyme). Given these findings, we comprehensively characterized the effects of LCI699 on human adrenal steroidogenesis and on the adrenal cytochromes P450, P450 11A1, P450 11B1, P450 11B2, P450 17A1, and P450 21A2 (Figure 2.1). We examined the effects of LCI699 on steroid synthesis in the NCI-H295R human adrenocortical cancer cell line, in V79 or HEK-293 cells stably

expressing individual steroidogenic P450 enzymes, and with purified recombinant steroidogenic P450 enzymes.

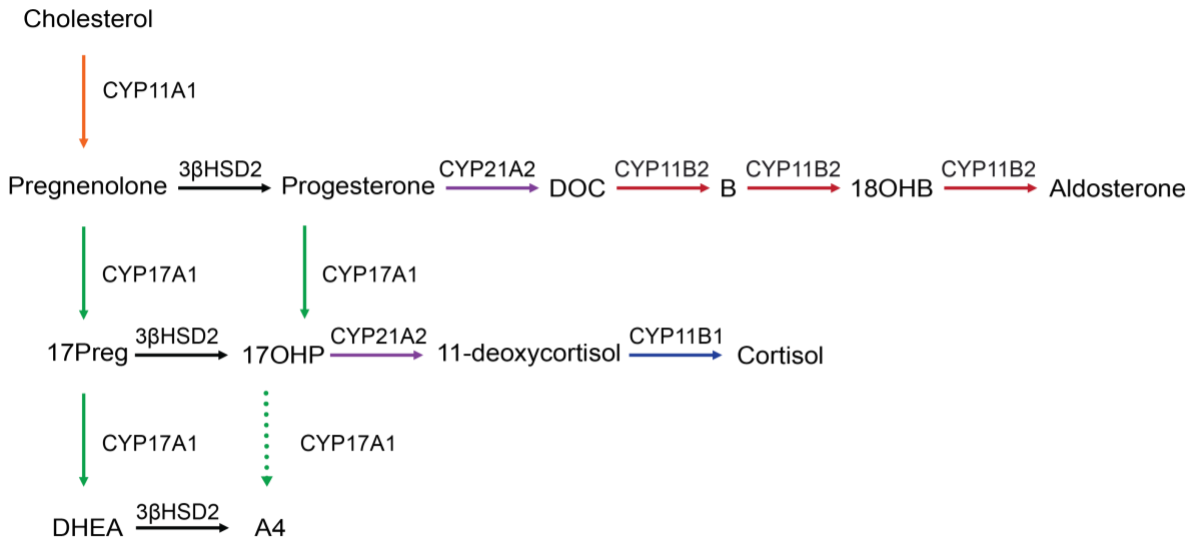

Figure 2.1 **Overview of the steroidogenic pathways.** Different colors are used to highlight the involvement of individual enzymes in multiple reactions. Abbreviations: B, corticosterone; 18OHB, 18-hydroxycorticosterone; DHEA, dehydroepiandrosterone; 17Preg, 17-hydroxypregnenolone; 17OHP, 17-hydroxyprogesterone; A4, androstenedione; 3βHSD2, 3β-hydroxysteroid dehydrogenase type 2; other enzyme abbreviations as in the text.

2.2 Materials and Methods

2.2.1 Reagents and Chemicals

LCI699 was obtained as gifts from Novartis Pharmaceuticals and from Prof. Emily Scott, University of Michigan (obtained from Selleckchem). The sources of biochemicals [12-14] and reagents for mass spectrometry, including steroid calibrators and internal standards, [15, 16] are as described previously or as specified in subsections 2.2-2.6.

2.2.2 Cellular Inhibition Assay

After treatment with 10 μM forskolin in medium with 1% serum for 72 h, NCI-H295R cells were seeded in 12 well plates at 80% confluency and experimentally treated in serum-free medium with 0-1000 nM LCI699, 1000 nM ketoconazole, or 1000 nM metyrapone (final ethanol

content <1% v/v). The medium was removed at 24 h, and steroids were assayed by liquid chromatography-tandem mass spectrometry (LC-MS/MS) as described [16]. The Δ^5-steroids pregnenolone, 17-hydroxypregnenolone, and dehydroepiandrosterone we measured in parallel [14]. These steroids combined amounted to only <5% the amount of 11-deoxycortisol + cortisol; consequently, no further analysis was performed with these data.

HEK-293 cell lines stably expressing P450 17A1 or P450 21A2 and V79 cells stably expressing P450 11A1, P450 11B1, or P450 11B2 were generated as described for AKR1C9 [17]. Briefly, cells were transfected in 10 cm dishes with 1.5 μg of pcDNA3 plasmid driving expression of each enzyme using FuGENE6. Cells were split 1:25 or thinner 48 h after transfection and then treated with medium containing G418 at 1.6 mg/mL to select for clones with stable plasmid integration. Individual clones were picked with a sterile pipette, expanded in medium with 0.5 mg/mL G418, and tested for enzyme activity. Clones with high activity were subsequently used for inhibition experiments.

V79 or HEK-293 cell lines were seeded in 12 well plates at 80% confluency and incubated in a medium containing 1 μM substrate and 0-1000 nM LCI699 (final ethanol content <1% v/v). Aliquots of medium were removed after 5 hrs, and steroids were extracted and analyzed by LC-MS/MS. The substrates used were 22*R*-hydroxycholesterol for P450 11A1, progesterone for P450 17A1, 17-hydroxyprogesterone for P450 21A2, 11-deoxycortisol for P450 11B1, and corticosterone rather than DOC for P450 11B2, to limit the number of intermediate steroids and facilitate data analysis.

The half-maximal inhibitory concentrations (IC_{50}) were calculated using GraphPad Prism software version 9.0.0 for Mac OS X. For the NCI-H295R cells, the measured products were plotted as a function of inhibitor concentration. In the case of the stable cell lines, the percent

inhibition was plotted as a function of inhibitor concentration. Data were fit to the dose-response inhibitor (three-parameter) equation.

2.2.3 Protein Expression in Escherichia coli and Purification

P450 11B2 and P450 11B1 were expressed as previously reported [18]. After expression, the pelleted cells were resuspended in cold lysis buffer (50 mM potassium phosphate buffer (pH 8.0), 20% (v/v) glycerol, 0.5 M sodium chloride, protease inhibitor cocktail (Bimake), 0.1 mM DTT) and passed once through a French press system at 16,000 PSI. Proteins were solubilized through the slow addition of 1.5% (w/v) sodium cholate and 1.5% (v/v) Tween 20, and the supernatant was collected after 20 minutes of centrifugation at 35,000 RPM at 4 °C. The lysate was incubated overnight with Ni-NTA resin (Qiagen) previously equilibrated with 3 column volumes (CV) of equilibration buffer (50 mM potassium phosphate buffer (pH 8.0), 20% (v/v) glycerol, 0.5 M sodium chloride, 1% (w/v) sodium cholate, 1% (v/v) Tween 20, 0.1 mM DTT). The resin was loaded into a column and washed with 5 CV of washing buffer 1 (50 mM potassium phosphate buffer (pH 8.0), 20% (v/v) glycerol, 0.5 M sodium chloride, 1% (w/v) sodium cholate, 1% (v/v) Tween 20, 10 mM imidazole, 0.1 mM DTT) and then with 5 CV of washing buffer 2 (50 mM potassium phosphate buffer (pH 8.0), 20% (v/v) glycerol, 1% (w/v) sodium cholate, 1% (v/v) Tween 20, 20 mM imidazole, 0.1 mM DTT, 0.1 mM ATP). P450 11B proteins were eluted with 5 CV of elution buffer (50 mM potassium phosphate buffer (pH 7.4), 20% (v/v) glycerol, 0.5% (w/v) sodium cholate, 0.05% (v/v) Tween 20, 250 mM imidazole, 0.1 mM TCEP). Imidazole was removed by buffer exchange using PD-10 columns (GE Healthcare, 8.3 mL bed volume). The proteins were further purified with His-Select resin (Millipore) by using the same buffers. P450 11A1, adrenodoxin, adrenodoxin reductase, and membrane-scaffold protein 1D1 (MSP1D1) were expressed and purified as previously reported [19-22].

2.2.4 P450-nanodiscs Preparation

The procedure was adapted from a previously described method [21]. P450-nanodiscs were prepared by mixing the MSP1D1, cholate-solubilized lipids, and P450 enzymes in a 1:64:0.05 ratio in disc buffer (100 mM potassium phosphate (pH 7.4), 50 mM NaCl, 20 mM sodium cholate buffer), using 16:0-18:1 PC (POPC) and 16:0-18:1 PS (POPS) lipids at a 4:1 (POPC:POPS) ratio. The resulting reaction mixture was incubated on a shaker at 4°C. After 1 h of incubation, 0.25 g/mL of Bio-Beads™ (Bio-Rad) was added to slowly remove sodium cholate and to initiate nanodisc assembly. After another 1 h, an additional 0.50 g/mL of Bio-Beads™ was added, for a total of 0.75 g/mL. The sample was incubated in a tube rotator overnight at 10 RPM. The sample was aspirated from the Bio-Beads and centrifuged at 13,000 x *g* for 5 minutes before purification through size-exclusion chromatography on a Superdex 200 10/300 GL column using an Akta model UPC-900 FPLC and 50 mM potassium phosphate buffer (pH 7.4). P450 and MSP1D1 incorporation into the nanodiscs was assessed through SDS gel electrophoresis and SEC analysis. Purified nanodiscs were stored at 4°C and used within 2-3 days.

2.2.5 Reconstituted Enzyme Assay

Assays contained 0.16 μM P450 11B2, 9.6 μM adrenodoxin, and 0.16 μM adrenodoxin reductase in 0.2 mL 50 mM potassium phosphate buffer (pH 7.4). The reaction mixture was pre-incubated at 37°C for 5 min, followed by the addition of either 10 μM LCI699 or 0.5 μM DOC dissolved in ethanol (final ethanol content <1% v/v) and pre-incubated at 37°C for 8 min. In some experiments, either inhibitor or substrate was next added to have both compounds present but added in a different order. NADPH (1 mM) was added, and the final incubation was continued at 37°C for 10 min to allow the synthesis of quantifiable 18-hydroxylase and 18-oxidase products.

The reaction was stopped by the addition of 20 µL of 0.1 M HCl, followed by vortexing. Steroids were extracted and analyzed using LC-MS/MS [16].

2.2.6 Ligand Binding Assays

Substrate and inhibitor binding affinities to P450 11A1, P450 11B1, and P450 11B2 enzymes were determined by monitoring UV-visible (350–700 nm) spectral changes. P450-nanodiscs were diluted to 0.16 µM with 50 mM potassium phosphate (pH 7.4) in a 1-cm quartz cuvette. After a 5 min incubation at 25°C, increasing amounts of ligand stocks in ethanol were added (final ethanol content ≤1% v/v). Difference spectra were obtained by subtracting the absorbance signal of individual titration concentrations from the spectra of P450-nanodiscs in the absence of titrant. The absorbance differences (at the wavelength maximum and minimum) were then plotted as a function of the added ligand concentrations. Dissociation constants (K_d) were calculated using GraphPad Prism software version 9.0.0 for Mac OS X. For substrate binding analysis, data were fitted to the one-site-binding equation. For LCI699 binding to P450 11B1 and P450 11B2, the data obtained required fitting to the tight-binding Morrison equation (1) [23].

$$\Delta A = \Delta A_{max} \frac{([E] + [L] + K_d) - \sqrt{([E] + [L] + K_d)^2 - 4[E][L]}}{2[E]} \quad (1)$$

The binding affinities of LCI699 for P450 11B1 and P450 11B2 were also calculated using a competition binding assay with DOC. P450-nanodiscs were pre-incubated with DOC for 8 minutes, after which increasing amounts of LCI699 were added (final ethanol content < 4% v/v). The absorbance differences (at the wavelength maximum and minimum) were then plotted against the log of the added LCI699 concentrations. The resulting curves were analyzed using a dose-response inhibitor (four-parameter) equation in GraphPad Prism. The dissociation constant for LCI699 (K_d) was calculated from the IC_{50} obtained using the Cheng-Prusoff equation (2), where

K_D is the binding constant for DOC and "IC_{50}" refers to the concentration of LCI699 that achieves 50% DOC displacement. In this case, the equation is used with binding parameters rather than enzymatic activity/inhibition constants, using the same theoretical basis of active-site competition.

$$K_d = \frac{\mathrm{IC}_{50}}{1 + \frac{[\mathrm{DOC}]}{K_D}} \quad (\mathbf{2})$$

2.3 Results

2.3.1 Effect of LCI699 on Steroidogenesis in NCI-H295R Cells

To assess the global effects of LCI699 on adrenal steroidogenesis, NCI-H295R cells were utilized [24]. To stimulate steroid production, the cells were pre-treated with 10 μM forskolin prior to incubation with fresh serum-free medium containing various concentrations of LCI699, 1000 nM ketoconazole, or 1000 nM metyrapone. Conditioned medium aliquots were collected 24 h post-treatment and analyzed via LC-MS/MS.

LCI699 inhibited cortisol and aldosterone production in a dose-dependent manner to 13 ± 4% and 2 ± 3% of baseline with IC_{50} values of 8.4 ± 1.5 nM and 3.2 ± 0.9 nM, respectively (Figure 2.2). Furthermore, corticosterone fell to 1 ± 2% of the baseline while androstenedione remained unchanged (Figure 2.2). These data are consistent with potent inhibition of P450 11B1 and P450 11B2 with little "overflow" of 21-carbon precursors into the adrenal 19-carbon steroidogenesis pathway via P450 17A1. In contrast, 11-deoxycortisol but not DOC appeared to increase at higher concentrations of LCI699, but these changes did not reach statistical significance (Figure 2.2). Unlike the human adrenal zona fasciculata, however, NCI-H295R cells are relatively deficient in P450 11B1 expression similar to most adrenocortical carcinomas [25], such that the cortisol content of the conditioned medium is roughly half that of 11-deoxycortisol at baseline. The sum

of 11-deoxycortisol + cortisol remained relatively constant across all LCI699 concentrations, yet the abundance of 11-deoxycortisol relative to cortisol limited our ability to detect rises in 11-deoxycortisol. Similarly, aldosterone concentrations were an order of magnitude lower than DOC, which minimized DOC accumulation from P450 11B2 inhibition; furthermore, forskolin treatment does not induce maximal aldosterone production [26].

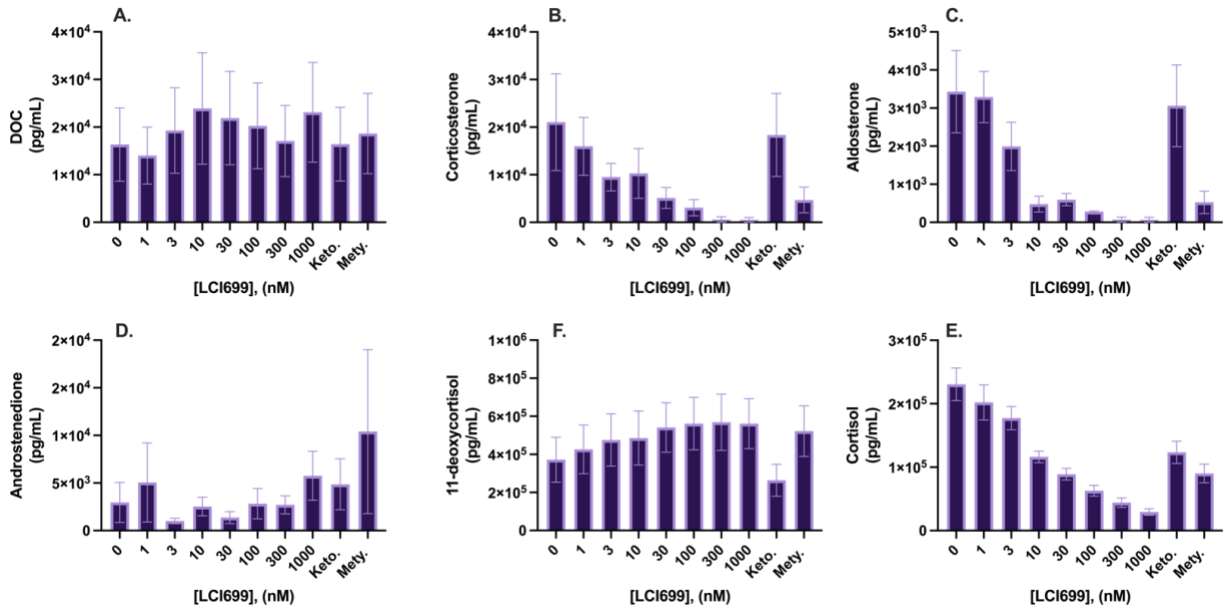

Figure 2.2 **Inhibition of steroid production in NCI-H295R cells**. After forskolin stimulation, H295R cells were treated with 0-1000 nM LCI699, 1000 nM ketoconazole (Keto.), 1000 nM metyrapone (Mety.), or vehicle in a fresh serum-free medium. Steroid levels measured by LC-MS/MS are given as the mean ± standard error of the mean (SEM) of three individual experiments.

2.3.2 V79 and HEK-293 Cell Lines Stably Expressing Individual Enzymes

To corroborate the results obtained from NCI-H295R cells, HEK-293 and V79 Chinese hamster cells stably expressing individual steroidogenic P450 enzymes were generated. V79 cells have been employed to study mitochondrial P450 enzymes, as they lack endogenous P450 activity and do not require co-transfection with redox partners (Adx and its reductase) [15,16]. HEK-293 cells, on the other hand, have been widely employed to study microsomal cytochrome P450-

mediated drug and steroid metabolism [27]. In V79 cells expressing P450 11B1, LCI699 inhibited the conversion of 11-deoxycortisol to cortisol with an IC_{50} of 9.5 ± 0.5 nM (Figure 2.3). In comparison, LCI699 inhibited the conversion of corticosterone to aldosterone with an IC_{50} of 0.28 ± 0.06 nM in V79 cells expressing P450 11B2. In V79 cells expressing P450 11A1, LCI699 showed partial (<25%) inhibition of pregnenolone formation at 1000 nM. In HEK-293 cells stably expressing P450 17A1 or P450 21A2, LCI699 showed negligible activity inhibition (<1%) at concentrations up to 1000 nM. These data confirm that LCI699 potently inhibits P450 11B1 and P450 11B2 with negligible inhibition of P450 17A1 and P450 21A2 yet partial inhibition of P450 11A1 at high concentrations.

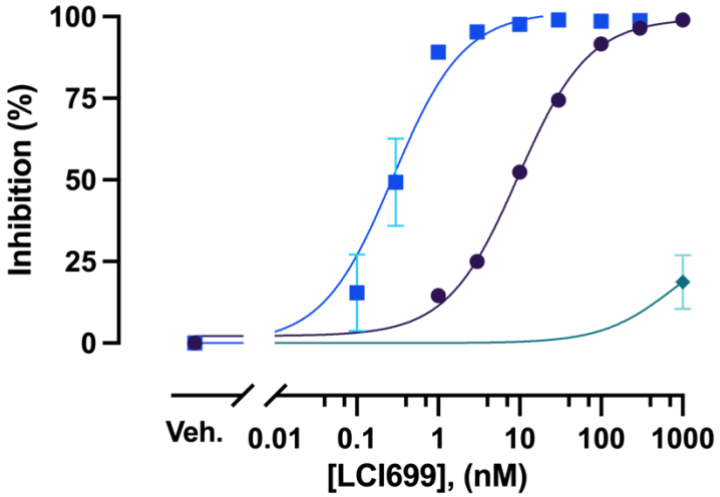

Figure 2.3 **Inhibition of P450 11A1, P450 11B1, and P450 11B2 activity in V79 cells**. Cells were plated and incubated in a medium containing 1 μM 22-*R*-hydroxycholesterol, 11-deoxycortisol, and corticosterone for P450 11A1(♦), P450 11B1(●), and P450 11B2(■) expressing cells, respectively, and 0-1000 nM LCI699. Data were fit to the dose-response inhibitor (three-parameter) equation to determine the half-maximal inhibitory concentration (IC_{50}) of 9.5 ± 0.5 nM and 0.28 ± 0.06 nM for P450 11B1 and P450 11B2, respectively. Data represent the mean ± standard error of the mean (SEM) of three individual experiments.

2.3.3 Ligand Binding Titrations in Nanodiscs

To directly determine the equilibrium binding constants (K_d) of LCI699 with adrenal mitochondrial P450 enzymes, we performed spectroscopic studies with P450s incorporated into

lipid nanodiscs. LCI699 binds tightly to purified P450 11B2 and P450 11B1 in nanodiscs and affords type II spectral changes (Figure 2.4). Data from the optical titration were fit to the tight-binding model in equation (1) and yielded K_d values of 0.6 ± 2.0 nM and 0.3 ± 0.9 nM for P450 11B1 and P450 11B2, respectively. The large relative errors in these measurements are due to the sharpness of the inflection point under conditions where K_d << [enzyme], and difference spectra using lower enzyme concentrations would be too weak to measure. While these values should be interpreted with some caution, the data are consistent with our cell-culture results. In contrast, P450 11A1 showed much weaker binding to LCI699 with a K_d of 18.8 ± 4.5 μM derived from a robust titration curve (Figure 2.4).

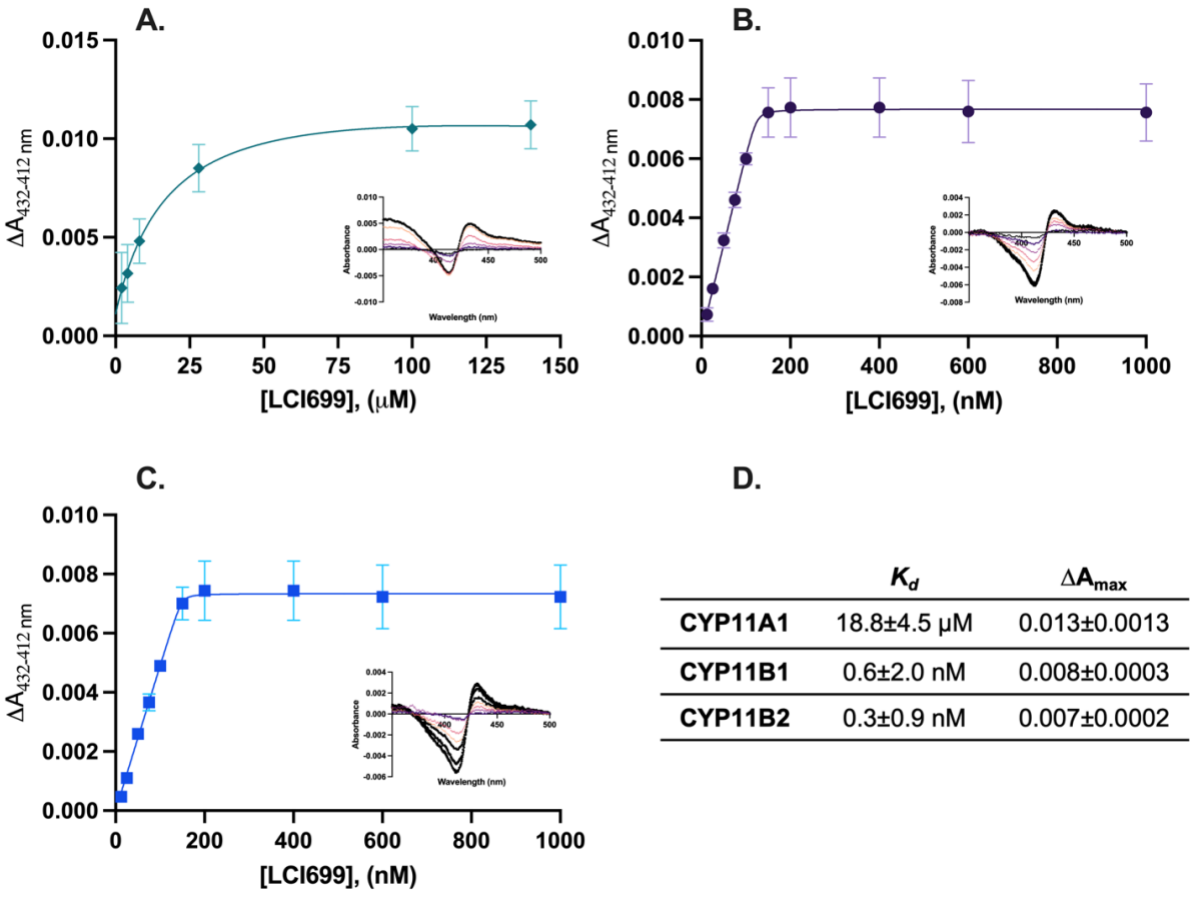

	K_d	ΔA_{max}
CYP11A1	18.8±4.5 μM	0.013±0.0013
CYP11B1	0.6±2.0 nM	0.008±0.0003
CYP11B2	0.3±0.9 nM	0.007±0.0002

Figure 2.4 **Equilibrium binding titration of LCI699 to P450-incorporated nanodiscs**. (A) P450 11A1(♦), (B) P450 11B1(•), and (C) P450 11B2(■) nanodiscs at 0.16 μM were equilibrated with increasing concentrations of LCI699 in 50 mM potassium phosphate buffer (pH 7.4). (D) Calculated equilibrium dissociation constants (K_d). The

inserted image in each panel shows the difference spectra between samples with and without LCI699. Data represent the mean ± standard deviation of three individual experiments.

2.3.4 Competitive Binding Experiments

Given the limitations of the direct binding experiments, we also determined the K_d of LCI699 for P450 11B1 and P450 11B2 using competition experiments with our P450-nanodisc system. In this strategy, we relied on the distinct spectral shifts induced upon binding of substrate (DOC) and LCI699 inhibitor to the P450s, which allowed us to monitor displacement of substrate at various LCI699 concentrations. To this end, both P450 11B1 and P450 11B2 were incubated with the common substrate DOC (K_D determined as 420 and 270 nM with P450 11B1 and P450 11B2, respectively) prior to the addition of LCI699. During titration with inhibitor, the spectrum gradually shifted from Type I to Type II (Figure 2.5 A). LCI699 completely outcompeted DOC (25 μM) bound to P450 11B1 in nanodiscs and yielded an IC_{50} of 90 ± 3 nM (Figure 2.5 B). Using the Cheng-Prussoff equation (2), these data afforded a K_d of 1.5 ± 0.1 nM, with a similar value yet much lower relative error than the direct binding experiments. Thus, the two binding studies consistently yield K_d values for LCI699 binding to P450 11B1 of close to 1 nM. In contrast, concentrations up to 10 μM of LCI669 could not fully shift the spectrum of P450 11B2 in nanodiscs from Type I to Type II (Figure 2.6 A, B), suggesting that LCI699 cannot fully outcompete the previously bound DOC (0.5 μM). The addition of Adx further limited DOC displacement from P450 11B2 by LCI699 (Fig. 2.6 B).

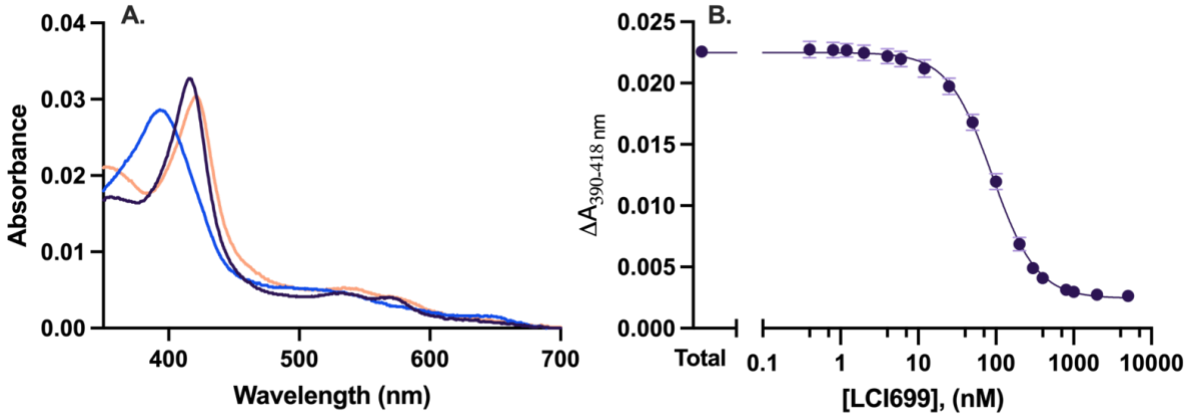

Figure 2.5 **P450 11B1-nanodiscs competitive binding assay**. (A) UV-visible spectral changes of 0.16μM P450 11B1-nanodiscs in 50 mM potassium phosphate buffer (pH 7.4). The addition of 25 μM DOC causes the absorption maximum of the Soret band to shift from 417 nm (dark purple) to 390 nm (blue). Subsequently, with increasing concentrations of LCI699, the maximum of the Soret band shifts to 419 nm (orange). (B) Dose-response curve of P450 11B1-nanodisc. Increasing concentrations of LCI699 can outcompete the bound DOC. Data were fit to the dose-response inhibitor (four-parameter) equation to determine the half-maximal inhibitory concentration (IC_{50}) of 90 ± 3 nM. Data represent the mean ± standard deviation of three individual experiments.

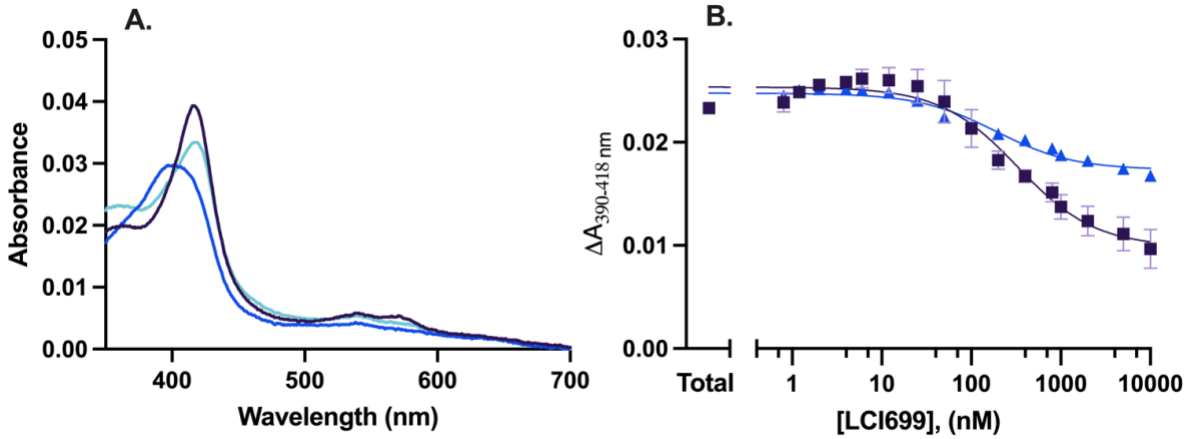

Figure 2.6 **P450 11B2 competition binding assay.** (A) UV-visible spectral changes of 0.16 μM P450 11B2-nanodiscs in 50 mM potassium phosphate buffer (pH 7.4). The addition of 0.5 μM DOC causes the absorption maximum of the Soret band to shift from 417 nm (dark purple) to 390 nm (blue). Subsequently, increasing the concentration of LCI699 up to 10 μM shifts the maximum of the Soret band to 414 nm (cyan). (B) Dose-response curve of P450 11B1-nanodisc with (▲) and without 1.6 μM adrenodoxin (■). LCI699 cannot outcompete the bound DOC in either condition. Data represent the mean ± standard deviation of three individual experiments.

2.3.5 P450 11B2 Inhibition Studies

To address the unexpected results obtained for LCI699 displacement of DOC bound to P450 11B2, we assess LCI699 inhibition of P450 11B2-catalyzed DOC turnover. Pre-incubation

of P450 11B2 nanodiscs with LCI699 (10 µM) completely abrogated aldosterone production, with only traces of the initial product corticosterone formed from 0.5 µM DOC. Conversely, pre-incubation with the same concentrations of DOC followed by sequential addition of LCI699 and then NADPH yielded similar amounts of aldosterone as in the absence of LCI699, yet much fewer total products, when including corticosterone and 18-hydroxycorticosterone intermediates (Figure 2.7). When P450 11B2 was pre-incubated with 0.5 µM corticosterone, addition of 10 µM LCI699 did not completely inhibit 18-hydroxycorticosterone and aldosterone formation (1% the yield without LCI699, not shown). These data are consistent with a population of P450 11B2•DOC complexes that does not dissociate during the timeframe of the experiment and affords aldosterone despite subsequent exposure to LCI699.

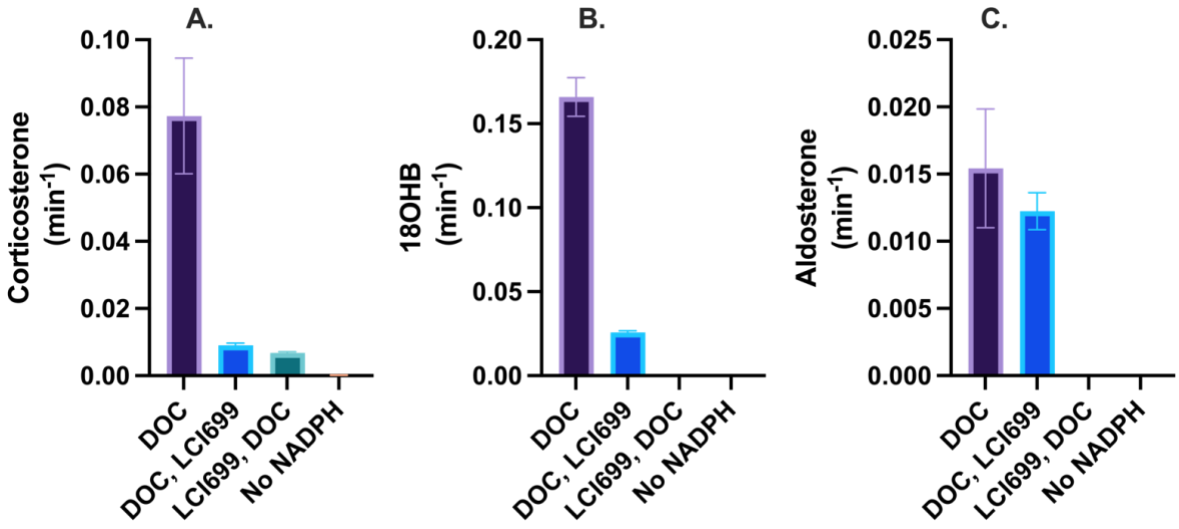

Figure 2.7 **LCI699-mediated inhibition of P450 11B2-nanodiscs.** Corticosterone (A), 18-hydroxycorticosterone (B), and aldosterone (C) were quantified with LC-MS/MS. P450 11B2-nanodiscs (0.16 µM) were pre-incubated with either DOC (0.5 µM) or LCI699 (10 µM) in 50 mM potassium phosphate buffer (pH 7.4) before the addition of either NADPH (first bar), LCI699 or DOC in the order specified, then NADPH (second and third bars), or no NADPH control (fourth bar). Data represent the mean ± standard deviation of three individual experiments.

2.4 Discussion

Using three different model systems, we confirmed that LCI699 is a potent inhibitor of P450 11B1 and P450 11B2, with IC_{50} of 0.1-10 nM using V79 or NCI-H295R cells. Using purified

recombinant enzymes, spectral binding studies required quadratic fitting and substrate competition experiments to calculate K_d values (~1 nM) due to such tight binding. In contrast, we found no inhibition of P450 17A1 or P450 21A2 at LCI699 concentrations up to 1000 nM. We also detected partial inhibition of P450 11A1 at 1000 nM LCI699 and spectroscopic evidence of binding to the heme iron of P450 11A1 with a K_d of 18.8 μM. In all systems, LCI699 was about a more potent inhibitor of P450 11B2 than of P450 11B1. The internally consistent data from several different systems affirm the selectivity of LCI699 for the adrenal mitochondrial P450s in the order P450 11B2>P450 11B1>>P450 11A1.

While ligand binding and activity of microsomal (type 2) P450s have been extensively studied using nanodiscs [28, 29], we report the first data obtained with mitochondrial (type 1) P450 enzymes in nanodiscs. With microsomal P450 systems, the redox partner POR must be also incorporated in the nanodisc on the same side as the P450, which might account for the low specific activity often seen relative to liposomal reconstituted systems. In contrast, mitochondrial P450s use adrenodoxin, a soluble iron-sulfur protein, as the direct electron transfer protein. Hence, every mitochondrial P450 in a population of nanodiscs will have full access to its redox partner adrenodoxin from the solution, which allows maximal reconstitution of activity. We have found that both substrate binding and turnover are as efficient or better using P450 11B1 and P450 11B2 in nanodiscs as in liposomal reconstituted assays (data not shown).

An unexpected result was that the addition of LCI699 could neither completely displace P450 11B2-bound DOC nor block its metabolism to aldosterone (Figure 2.6, 2.7), despite extremely tight LCI699 binding when added alone (Figure 2.4). A possible explanation for this behaviour, which is consistent with the data in Figure 2.7, is two populations of P450 11B2 molecules, one of which has a very slow dissociation rate of DOC. This finding is consistent with

the high processivity of P450 11B2 with DOC as the substrate, which maximizes aldosterone production [30]. These data might explain the incomplete reduction of aldosterone observed in clinical trials of LCI699 [5, 31], despite its high potency as a P450 11B2 inhibitor. Our data suggest that LCI699 exposure would have to remain constantly high relative to intra-adrenal DOC to fully inhibit aldosterone production during clinical use. In contrast, LCI699 completely displaced DOC from P450 11B1, which is consistent with the efficacy observed in the treatment of CD, in which it rapidly reduced mean 24-hour urine-free cortisol. On the other hand, aldosterone is often low in CS due to the mineralocorticoid activity of excess cortisol, so the clinical significance of these findings remains ambiguous.

Furthermore, we observed consistent inhibition of and binding of LCI699 to P450 11A1, albeit incomplete and weak relative to its effects on P450 11B1 and P450 11B2. Nevertheless, this finding might explain the results of a retrospective study, which found less cortisol precursor accumulation in patients with ACTH-dependent CS during LCI699 treatment than for those treated with metyrapone [11]. This study also found higher substrate/product ratios in patients treated with LCI699 than for metyrapone, suggesting partial P450 21A2 (17OHP/11-deoxycortisol) and P450 17A1 inhibition (17OHP/androstenedione); however, the authors recognized that reduced substrate influx could also explain their data, and 21-deoxycortisol was not measured. Our data are consistent with the latter explanation that LCI699 partially inhibits P450 11A1 but not P450 21A2 or P450 17A1, and our data are consistent with the reduction of total steroid production in HAC15 cells treated with LCI699 [10]. The limited precursor accumulation in experiments with LCI699 treatment of NCI-H295R cell cultures should be interpreted cautiously (Figure 2.2), because these cells are relatively deficient in P450 11B1 activity compared to the normal adrenal cortex and produce much less aldosterone than cortisol.

The limitations of our studies are similar to those for any pharmacologic experiments using model systems. The calculated inhibition and binding constants observed, while consistent in rank order for the three mitochondrial P450 enzymes, varied among the systems used. Differences in accessible substrate concentrations, enzyme expression, and cellular penetration/efflux of the drug might explain some of this variance. In addition, we did not study the influence of adrenodoxin in detail with purified enzymes, and we neither determined nor varied the abundance of adrenodoxin in the V79 or NCI-H295R cells. The data in Figure 2.7 suggest that adrenodoxin enhances substrate binding for P450 11B2, as previously shown [30], and another study demonstrated that adrenodoxin enhances, in a concentration-dependent manner, the catalytic efficiency, substrate affinity, and potency of LCI699 as an inhibitor of purified P450 11B1 [32]. More detailed biochemical studies of LCI699 *in-vitro* and analyses of steroid changes in treated patients will enhance our understanding of the drug's pharmacology and guide its use in patients with CS.

2.5 Bibliography

1. Lacroix, A., et al., *Cushing's syndrome.* Lancet, 2015. **386**(9996): p. 913-27.
2. Pivonello, R., et al., *The Treatment of Cushing's Disease.* Endocr Rev, 2015. **36**(4): p. 385-486.
3. Melmed, S., *Pituitary-Tumor Endocrinopathies.* N Engl J Med, 2020. **382**(10): p. 937-950.
4. Pivonello, R., et al., *Efficacy and safety of osilodrostat in patients with Cushing's disease (LINC 3): a multicentre phase III study with a double-blind, randomised withdrawal phase.* Lancet Diabetes Endocrinol, 2020. **8**(9): p. 748-761.
5. Fleseriu, M., et al., *Long-term outcomes of osilodrostat in Cushing's disease: LINC 3 study extension.* Eur J Endocrinol, 2022. **187**(4): p. 531-541.
6. Gadelha, M., et al., *Randomized Trial of Osilodrostat for the Treatment of Cushing Disease.* J Clin Endocrinol Metab, 2022. **107**(7): p. e2882-e2895.
7. Schumacher, C.D., R.E. Steele, and H.R. Brunner, *Aldosterone synthase inhibition for the treatment of hypertension and the derived mechanistic requirements for a new therapeutic strategy.* J Hypertens, 2013. **31**(10): p. 2085-93.
8. Calhoun, D.A., et al., *Effects of a novel aldosterone synthase inhibitor for treatment of primary hypertension: results of a randomized, double-blind, placebo- and active-controlled phase 2 trial.* Circulation, 2011. **124**(18): p. 1945-55.

9. Menard, J., et al., *Aldosterone synthase inhibition: cardiorenal protection in animal disease models and translation of hormonal effects to human subjects.* J Transl Med, 2014. **12**: p. 340.
10. Creemers, S.G., et al., *Osilodrostat Is a Potential Novel Steroidogenesis Inhibitor for the Treatment of Cushing Syndrome: An In Vitro Study.* J Clin Endocrinol Metab, 2019. **104**(8): p. 3437-3449.
11. Bonnet-Serrano, F., et al., *Differences in the spectrum of steroidogenic enzyme inhibition between Osilodrostat and Metyrapone in ACTH-dependent Cushing syndrome patients.* Eur J Endocrinol, 2022. **187**(2): p. 315-322.
12. Peng, H.M. and R.J. Auchus, *Molecular Recognition in Mitochondrial Cytochromes P450 That Catalyze the Terminal Steps of Corticosteroid Biosynthesis.* Biochemistry, 2017. **56**(17): p. 2282-2293.
13. Peng, H.M., C. Barlow, and R.J. Auchus, *Catalytic modulation of human cytochromes P450 17A1 and P450 11B2 by phospholipid.* J Steroid Biochem Mol Biol, 2018. **181**: p. 63-72.
14. Peng, H.M., et al., *Cytochrome b5 Activates the 17,20-Lyase Activity of Human Cytochrome P450 17A1 by Increasing the Coupling of NADPH Consumption to Androgen Production.* Biochemistry, 2016. **55**(31): p. 4356-65.
15. Turcu, A.F., et al., *Comprehensive Analysis of Steroid Biomarkers for Guiding Primary Aldosteronism Subtyping.* Hypertension, 2020. **75**(1): p. 183-192.
16. Wright, C., et al., *Abiraterone acetate treatment lowers 11-oxygenated androgens.* Eur J Endocrinol, 2020. **182**(4): p. 413-421.
17. Papari-Zareei, M., A. Brandmaier, and R.J. Auchus, *Arginine 276 controls the directional preference of AKR1C9 (rat liver 3α-hydroxysteroid dehydrogenase) in human embryonic kidney 293 cells.* Endocrinology, 2006. **147**: p. 1591-1597.
18. Brixius-Anderko, S. and E.E. Scott, *Structure of human cortisol-producing cytochrome P450 11B1 bound to the breast cancer drug fadrozole provides insights for drug design.* J Biol Chem, 2019. **294**(2): p. 453-460.
19. Woods, S.T., et al., *Expression of catalytically active human cytochrome p450scc in Escherichia coli and mutagenesis of isoleucine-462.* Arch Biochem Biophys, 1998. **353**(1): p. 109-15.
20. Maharaj, A., et al., *Predicted Benign and Synonymous Variants in CYP11A1 Cause Primary Adrenal Insufficiency Through Missplicing.* J Endocr Soc, 2019. **3**(1): p. 201-221.
21. Luthra, A., et al., *Nanodiscs in the studies of membrane-bound cytochrome P450 enzymes.* Methods Mol Biol, 2013. **987**: p. 115-27.
22. Tuckey, R.C., et al., *Production of 22-hydroxy metabolites of vitamin d3 by cytochrome p450scc (CYP11A1) and analysis of their biological activities on skin cells.* Drug Metab Dispos, 2011. **39**(9): p. 1577-88.
23. Morrison, J.F., *Kinetics of the reversible inhibition of enzyme-catalysed reactions by tight-binding inhibitors.* Biochim Biophys Acta, 1969. **185**(2): p. 269-86.
24. Gazdar, A.F., et al., *Establishment and characterization of a human adrenocortical carcinoma cell line that expresses multiple pathways of steroid biosynthesis.* Cancer Res, 1990. **50**(17): p. 5488-96.
25. Arlt, W., et al., *Urine steroid metabolomics as a biomarker tool for detecting malignancy in adrenal tumors.* J Clin Endocrinol Metab, 2011. **96**(12): p. 3775-84.

26. Holland, O.B., et al., *Angiotensin increases aldosterone synthase mRNA levels in human NCI-H295 cells.* Mol Cell Endocrinol, 1993. **94**(2): p. R9-13.
27. Capper, C.P., et al., *Functional characterization of the G162R and D216H genetic variants of human CYP17A1*. J Steroid Biochem Mol Biol, 2018. **178**: p. 159-166.
28. Zarate-Perez, F. and J.C. Hackett, *Conformational selection is present in ligand binding to cytochrome P450 19A1 lipoprotein nanodiscs.* J Inorg Biochem, 2020. **209**: p. 111120.
29. Nath, A., et al., *Allosteric effects on substrate dissociation from cytochrome P450 3A4 in nanodiscs observed by ensemble and single-molecule fluorescence spectroscopy.* J Am Chem Soc, 2008. **130**(47): p. 15746-7.
30. Reddish, M.J. and F.P. Guengerich, *Human cytochrome P450 11B2 produces aldosterone by a processive mechanism due to the lactol form of the intermediate 18-hydroxycorticosterone.* J Biol Chem, 2019. **294**(35): p. 12975-12991.
31. Bertagna, X., et al., *LCI699, a potent 11beta-hydroxylase inhibitor, normalizes urinary cortisol in patients with Cushing's disease: results from a multicenter, proof-of-concept study.* J Clin Endocrinol Metab, 2014. **99**(4): p. 1375-83.
32. Loomis, C.L., S. Brixius-Anderko, and E.E. Scott, *Redox partner adrenodoxin alters cytochrome P450 11B1 ligand binding and inhibition.* J Inorg Biochem, 2022. **235**: p. 111934.

Chapter 3

Kinetics of Intermediate Release Enhances P450 11B2-catalyzed Aldosterone Synthesis[2]

3.1 Introduction

The mineralocorticoid aldosterone regulates the final 2% of sodium reabsorption in the kidneys, which maintains sodium homeostasis and optimal plasma volume. The production of aldosterone from the zona glomerulosa of the adrenal cortex is tightly regulated, primarily through the renin-angiotensin II system [1]. The enzyme cytochrome P450 11B2 (aldosterone synthase) catalyzes the last three consecutive reactions of aldosterone synthesis using substrate 11-deoxycorticosterone (DOC): 11β-hydroxylation to corticosterone, then 18-hydroxylation to 18-hydroxycorticosterone (18OHB), and finally 18-oxidation to aldosterone (Figure 3.1 A).[2] The renin-independent expression of the *CYP11B2* gene, which encodes P450 11B2, leads to primary aldosteronism (PA), the most common form of secondary hypertension [3]. Given its critical position in blood pressure regulation and the pathogenesis of PA, P450 11B2 has become a promising pharmacological target [4]. This approach is challenging, given that P450 11B2 shares 93% sequence identity with the cortisol-producing cytochrome P450 11B1 (11β-hydroxylase) [2].P450 11B1 catalyzes 11β-hydroxylation of DOC and 11-deoxycortisol efficiently; however, its 18-hydroxylase activity is very poor compared to P450 11B2, and P450 11B1 completely lacks 18-oxidase activity (Figure 3.1 A). Although site-directed mutagenesis and human genetic studies

[2] The content of this chapter has been published: Valentín-Goyco, J. Im, S.C., & Auchus, R.J. (2024). Kinetics of intermediate release enhances P450 11B2-catalyzed aldosterone synthesis. Biochemistry. https://doi.org/10.1021/acs.biochem.3c00725

have explored the specific amino acids responsible for the divergence in activity repertoires for P450 11B1 and P450 11B2, the biochemical and biophysical parameters that govern the 18-oxygenation reactions remain unknown.

Other multi-step steroidogenic cytochrome P450 enzymes (P450 17A1, P450 19A1) catalyze their reaction sequences in a distributive manner, with intermediates released from the active site and re-binding to the enzyme for the next catalytic reaction(s) [5, 6]. In contrast, aldosterone production follows a processive mechanism, where the three reactions occur without intermediates dissociating from the active site of P450 11B2 [7]. The authors of this study attribute this mechanism to an equilibrium in aqueous solution that strongly favors the 18OHB tautomer in the lactol (cyclic 20-acetal) form, because solution-borne 18OHB is a poor substrate for the 18-oxidase reaction (Figure 3.1 B). Consequently, this model implies that nascent 18OHB produced from DOC via corticosterone exists transiently in the acyclic 20-keto form, and only those molecules retained in the active site of P450 11B2 in this tautomer are subsequently metabolized to aldosterone.

While processivity might be essential for aldosterone production via P450 11B2, the differences with P450 11B1, which lacks processivity and corresponding 18-oxygenase activities, are not known. Structural and functional studies provide little insight into how the active site of these enzymes discriminates capacity for aldosterone synthesis. The crystal structures of both P450 11B enzymes reveal that active site residues are mostly identical, with slight differences in placement and orientation [8, 9]. The effects of certain residues, which are conserved among species yet differ for the two enzymes, on their respective activity repertoires were assessed almost 20 years prior to the resolution of their structures [10]. These studies substituted conserved residues from P450 11B2 into the I-helix of P450 11B1 and enhanced or enabled 18-hydroxylase and 18-

oxidase activities, respectively, for P450 11B1. While informative, the biochemical mechanism by which these residues modulate the 18-oxygenation activities of P450 11B enzymes was not elucidated. Poor coupling of subsequent reactions, faster dissociation rates, and lower affinities toward intermediate steroids might prohibit for P450 11B1 the processivity observed for P450 11B2.

Of all the residues studied, exchanges at position 320 yielded the greatest activity changes. P450 11B1 mutation V320A exhibited approximately 20% of the aldosterone synthase activity of P450 11B2 in transfected COS-1 cells. Conversely, P450 11B2 mutation A320V reduced aldosterone production, especially in combination with a second mutation [11]. Given these data, we interrogated the binding kinetics and affinities, coupling, and product formation of purified P450 11B1 and P450 11B2, wild-type and residue 320 mutations in phospholipid nanodiscs [12] and phospholipid vesicle preparations [13]. Our data identify critical mechanistic distinctions between the two highly similar enzymes, which enable P450 11B2 to synthesize aldosterone.

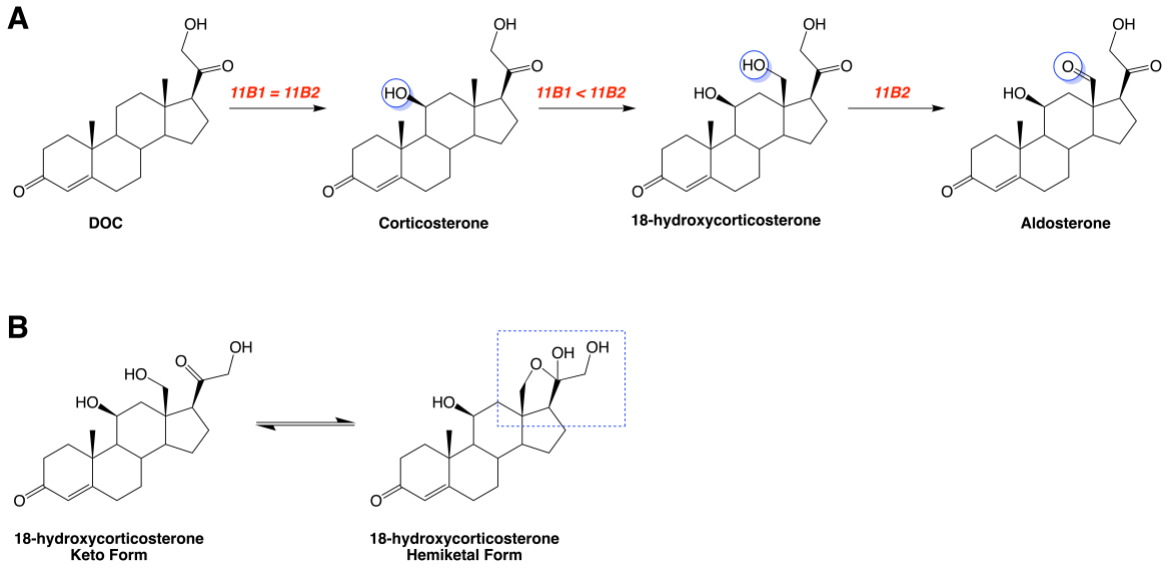

Figure 3.1 **Reactions catalyzed by cytochrome P450 11B1 and P450 11B2 (A) and interconversion between the open and lactol form of 18-hydroxycorticosterone (B).**

3.2 Materials and Methods

3.2.1 Materials

Ampicillin, 5-aminolevulinic acid, Tween 20, and the His-Select resin were obtained from Sigma (St. Louis, MO). Tris (2-carboxyethyl)phosphine hydrochloride (TCEP-HCl) and isopropyl β-D-thiogalactopyranoside (IPTG) were purchased from Gold Biotechnology (St. Louis, MO). Sodium cholate was acquired from Chem-Impex International (Wood Dale, IL). The Coomassie Plus Reagent from Pierce (Rockford, IL) was utilized to determine protein purity. We obtained potassium phosphate monobasic and dibasic, glycerol, as well as Terrific and Luria broths from Research Product International (Mount Prospect, IL). Chloramphenicol was obtained from Fisher Scientific, and adenosine-5'-triphosphate (ATP) was purchased from Roche. All steroid substrates were obtained from Steraloids (Newport, RI). The sources of biochemicals and reagents for mass spectrometry, such as steroid calibrators and internal standards, have been previously described [14].

3.2.2 Plasmid Construction

pCWori+ plasmids containing the human *CYP11B1* and *CYP11B2* cDNAs were a gift from Dr. Emily Scott, University of Michigan. The plasmids encode for N-terminal truncated proteins missing the mitochondrial leader sequences with the septapeptide MAKKTSS prior to the amino acid 31 of the WT sequences and a four-histidine tag located at the C terminus [8, 15]. QuikChange XL II (Agilent) site-directed mutagenesis kit was utilized to generate the V320A and A320V mutations in P450 11B1 and P450 11B2, respectively. The following primers were used: 11B1VA-sense, 5'–CCGTCGATACTACCGCTTTTCCTCTCCTGATG–3'; 11B1VA-antisense, 5'–CATC AGGAGAGGAAAAGCGGTAGTATCGACG–3'; 11B2AV-sense, 5' GTAGCGT GGACACCA

CCGTATTCCCGCTGCTGATGAC–3'; and 11B2AV-antisense, 5'–GTCATC AGCAGCGGGA ATACGGTGGTGTCCACGCTA–3'. The sequences of the protein-coding regions and the presence of the desired mutations in each plasmid were confirmed by DNA sequencing.

3.2.3 Protein Expression in Escherichia coli and Purification

Adrenodoxin, adrenodoxin reductase, membrane-scaffold protein 1D1 (MSP1D1), and the P450 11B enzymes were expressed and purified as previously reported [8, 16, 17].

3.2.4 P450 11B-Nanodisc Preparation

P450 11B-nanodiscs were prepared as previously reported [12]. Briefly, a solution of 16:0-18:1 phosphatidylcholine (POPC) and 16:0-18:1 phosphatidyl serine (POPS), at a ratio of 4:1 (POPC:POPS), was prepared to a concentration of 50 mM in 100 mM potassium phosphate (pH 7.4), 50 mM sodium chloride, and 100 mM sodium cholate. P450 11B enzymes were then mixed with MSP1D1 and the cholate-solubilized lipids in a buffer containing 100 mM potassium phosphate (pH 7.4), 50 mM sodium chloride, and 20 mM sodium cholate at a ratio of 1:64:0.05. After incubation at 4 °C for 1 h, nanodisc formation was initiated with the addition of Biobeads (Bio-Rad) in portions to a total of 0.75 g/mL at 4 °C. The following day, the reaction mixtures were centrifuged to remove beads and protein aggregates, and the P450-containing nanodiscs were purified using a Superdex 200 10/300GL column (GE Healthcare), which had been equilibrated with 50 mM potassium phosphate buffer (pH 7.4) using an ÄKTA model UPC-900 FPLC. Fractions containing nanodiscs were collected and concentrated with an Amicon centrifugation filter (30 kDa).

3.2.5 Activity Assay and NADPH Coupling

At room temperature, 0.1 μM of P450 11B enzymes, wild-type or mutants, were reconstituted at a molar ratio of 1:1:60:200 (P450:AdR:Adx:phospholipids). For P450 11B2 and P450 11B1 dioleoylphosphatidylcholine (DOPC, 18:1) and dilauroylphosphatidylcholine (DLPC, 12:0) vesicles were used, respectively [13]. After 5 minutes, 50 mM potassium phosphate buffer (pH 7.4), prewarmed to 37 °C, and 100 μM of either DOC or corticosterone were added to a final volume of 1 mL in a 1-cm quartz cuvette. The cuvette was further incubated at 37 °C for 5 minutes before the addition of 0.3 mM NADPH in a Shimadzu UV-2600 spectrophotometer with a temperature-controlled cell holder (model TCC-240A). After measuring NADPH consumption at 340 nm for 5 minutes, the reaction was stopped with 0.1 mL of 3 N hydrochloric acid. The sample was then transferred to a 1.5 mL plastic tube, briefly vortexed, and stored at -20 °C. Steroids were then quantified by liquid chromatography-tandem mass spectrometry (LC-MS/ MS) as previously described [18].

3.2.6 Ligand Binding Assay

The binding affinities of DOC and corticosterone to P450 11B enzymes were determined from titrations of UV–visible spectral changes for the Soret bands at 350–700 nm. P450 11B-nanodiscs diluted to 0.16 μM in 50 mM potassium phosphate (pH 7.4) were incubated at 25 °C for 5 min in a quartz cuvette with a 1-cm path length. Small volumes of ligand stock solutions in 95% ethanol were then titrated into the cuvette (final ethanol concentrations <1% (v/v). Difference spectra were generated by subtracting the absorbance spectra at each concentration from the spectra of P450-nanodiscs in the absence of titrant. The differences between the maximum (390 nm) and minimum (425nm) peaks of the difference spectra were then plotted as a function of the added ligand concentrations. To calculate the dissociation constants (K_d), the resulting data were

fit using the one-site-binding equation in GraphPad Prism software version 9.0.0 for Mac OS X. All experiments were performed in technical triplicates.

3.2.7 Rates of Ligand Binding

The rates of DOC and corticosterone binding to P450 11B-nanodiscs were determined using an SF61DX2 stopped-flow spectrophotometer (Hi-Tech Scientific) under pseudo-1st-order conditions ([ligand]>>[P450]). P450 11B-nanodiscs were diluted to a concentration of 0.5 µM in 50 mM potassium phosphate buffer (pH 7.4) and 15% glycerol and loaded in syringe #1 of the stopped-flow spectrophotometer with a set temperature of 25 ^{o}C. Equal volumes from syringe #1 were rapidly mixed with buffer containing various concentrations of either DOC or corticosterone from syringe #2. The P450 spectra (330 to 700 nm) were recorded for each condition in the photodiode array mode (200 scans, logarithmic interval). Changes from low-spin to high-spin state were derived from the absorbance changes from 417 to 390 nm. The observed rate constants and amplitudes were calculated by fitting kinetic traces with multiple exponential functions using GraphPad Prism software version 9.0.0 for Mac OS X.

3.2.8 Rates of Ligand Dissociation by Direct Method

The P450 11B protein-ligand complexes were formed by incubating P450 11B-nanodiscs with either DOC or corticosterone at a concentration of two or four times their respective K_d values at room temperature in 50 mM potassium phosphate buffer pH (7.4) with 15% glycerol and loading the complexes into syringe #1. Aliquots from syringe #1 were rapidly mixed with equal volumes of buffer containing (2-hydroxypropyl)-β-cyclodextrin from syringe #2 at 25 times the concentration of the ligand used, to limit ligand re-binding. Kinetic traces were recorded in the photodiode array mode and resulted in the dissociation of ~ 10% of the P450 11B-ligand complex.

Return from high-spin to low-spin state was obtained from the absorbance change from 390 to 416 nm. The obtained kinetic traces were fit to either uniphasic or biphasic exponential functions in the GraphPad Prism software version 9.0.0 for Mac OS X.

3.2.9 Substrate Binding Kinetic Modeling

Kinetic parameters were calculated by using the KinTek Explorer software (version 11.0.1.) for Mac OS X [19]. Triplicate traces from each experiment were averaged and globally fit to the ordinary differential equation for the lock and key (LK), conformational selection (CS), induced fit (IF), and mixed IF-and-CS models. Upper limits of 1000 s^{-1} and 10 μM^{-1} s^{-1} plus lower limits of 0.001 s^{-1} and 0.01 μM^{-1} s^{1} were assigned for the first- and second-order rate constants, respectively.

Lock and Key

$$E \underset{k_{off}}{\overset{[L]k_{on}}{\rightleftharpoons}} EL. \quad (1)$$

Conformational Selection

$$E_1 \underset{k_{-1}}{\overset{k_1}{\rightleftharpoons}} E_2 \underset{k_{off}}{\overset{[L]k_{on}}{\rightleftharpoons}} EL \quad (2)$$

Induced Fit

$$E \underset{k_{off}}{\overset{[L]k_{on}}{\rightleftharpoons}} EL \underset{k_{-1}}{\overset{k_1}{\rightleftharpoons}} EL' \quad (3)$$

Induced Fit + Conformational Selection

$$E_1 \underset{k_{-1}}{\overset{k_1}{\rightleftharpoons}} E_2 \underset{k_{off}}{\overset{[L]k_{on}}{\rightleftharpoons}} EL \underset{k_{-2}}{\overset{k_2}{\rightleftharpoons}} EL' \quad (4)$$

3.2.10 Statistical Analysis

For direct comparisons, *P* values were calculated using one- or two-tailed student's *t*-tests. Statistical significance was determined to be at $P < 0.05$.

3.2.11 Structural Analysis

Images were generated using PyMol version 2.5.7 (Schrödinger, LLC). Proximity measurements were set to 5 Å and were confirmed with direct measurements.

3.3 Results

3.3.1 Steady-State Activities of P450 11B1, P450 11B2, and 320 Mutations in Phospholipid Vesicles

It was previously demonstrated that swapping residues in the I-helix between P450 11B1 and 11B2 can convert P450 11B1 into an aldosterone-producing enzyme in intact cells. This study revealed that some of these mutations can cause P450 11B1 to gain ~40% and ~20% of the 18-hydroxylase and 18-oxidase activities of P450 11B2, respectively. To corroborate these results, we exchanged the residue at the 320 positions between P450 11B1 and 11B2 via site-directed mutagenesis and subsequently expressed and purified the wild-type and mutant enzymes. High purity was achieved for both wild-type and mutant enzymes (Appendix Figure 1), and their reduced carbon monoxide difference spectra showed maximum absorbances at 450 nm (Appendix Figure 2). The activity observed from our optimized phospholipid vesicle system resembles the previously published results; however, P450 11B1-V320A exhibits higher activity in intact cells than in our reconstituted system [10]. Nevertheless, P450 11B2-A320V produced 36% and 15% of the 18OHB and aldosterone, respectively, compared to P450 11B2. Furthermore, the production

of corticosterone remained relatively the same across all conditions, which indicates that these mutations primarily affect the 18-hydroxylase and 18-oxidase activities.

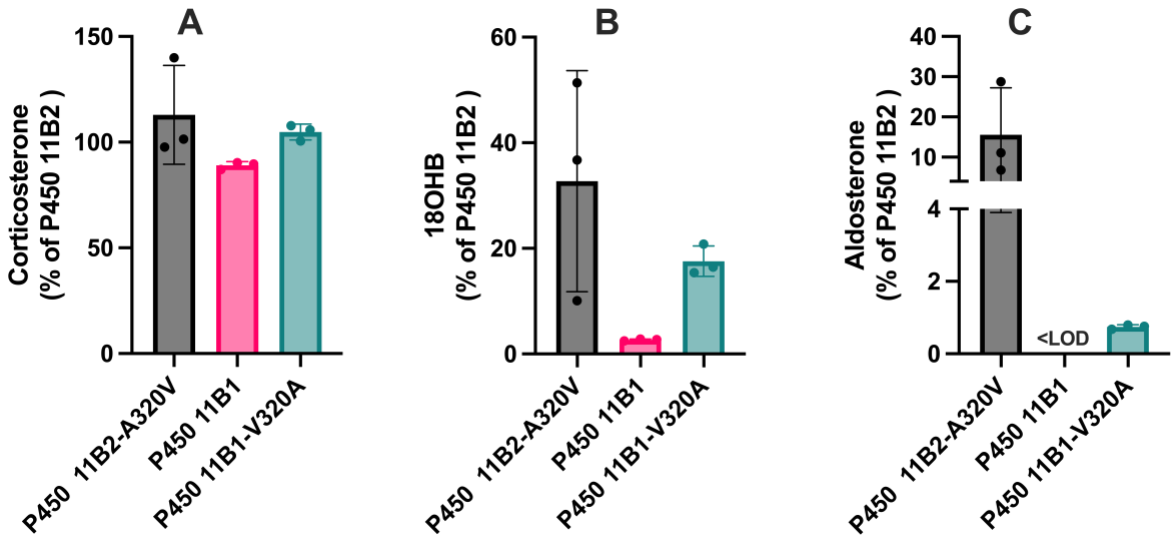

Figure 3.2 **Steady-state activities of wild-type and mutant P450 11B enzymes in phospholipid vesicles.** Data represent the mean ± standard deviation of three experiments (data points) with <25% DOC consumption (100 μM); <LOD = below the limit of detection. Activities of wild-type P450 11B2 were 34.3, 7.8, and 6.3 pmol/min/pmol P450 for corticosterone, 18OHB, and aldosterone, respectively.

3.3.2 Coupling Efficiencies for 11β- and 18-Hydroxylase Reactions

The two most probable explanations for the poor 18-hydroxylase activity of P450 11B1 and for P450 11B2 mutation A320V are a short active-site residence time of nascent corticosterone or poor coupling efficiency of NADPH consumption to product formation. Using our optimized phospholipid vesicle system [13], we found high coupling efficiency with DOC as the substrate for the 11β-hydroxylase reactions of both P450 11B1 and P450 11B2 (65.0 ± 2.4 and 62.8 ± 10.5%, respectively) with robust NADPH consumption (Table 3.1). Although the rates of corticosterone production remained similar for the wild-type and mutant enzymes, NADPH consumption significantly (P = 0.0019) increased for P450 11B1-V320A, which decreased coupling efficiency to 35.2 ± 6.2%. Conversely, NADPH consumption for P450 11B2-A320V was lower than the wild-type enzyme with essentially complete coupling efficiency despite the relatively greater error

in these measurements compared to the other enzymes (Table 3.1). These experiments were conducted under conditions of limited DOC consumption to minimize 18-oxygenation products from subsequent turnovers, and corticosterone was the most abundant product (71 – 99%) for all enzymes, highest for wild-type P450 11B1 and lowest for wild-type P450 11B2. Even with these considerations, we did not find major differences in coupling efficiencies for the 11β-hydroxylase reactions, and our values might underestimate the actual efficiencies.

Starting with corticosterone as the direct substrate, we measured coupling efficiencies for the 18-hydroxylase reaction. Similar to experiments with DOC as the substrate, subsequent conversion to aldosterone was also measured; however, 18OHB was the major product (74 – 97%) under these conditions. Wild-type P450 11B2 exhibited the fastest rates of product formation and NADPH consumption (12.2 ± 1.0 and 35.5 ± 5.3 min^{-1}, respectively) of the four enzymes, with a coupling efficiency of 35.0 ± 4.8%. In contrast, wild-type P450 11B1 showed much lower rates of product formation and NADPH consumption (1.2 ± 0.1 and 5.6 ± 1.1 min^{-1}, respectively), which yields a coupling efficiency of 22.6 ± 5.6%. P450 11B1-V320A, which enhances 18OHB production with DOC as the substrate, only slightly raised 18OHB formation with corticosterone as the substrate but greatly increased NADPH consumption (1.4 ± 0.1 and 65.9 ± 6.7 min^{-1}, respectively), which yields a very poor coupling efficiency of 1.7 ± 0.3%. Conversely, P450 11B2-A320V, which has poor 18-oxygenation activities, mimicked wild-type P450 11B1 in this experiment, with low rates of product formation and NADPH consumption (0.8 ± 0.2 and 2.3 ± 0.1 min^{-1}, respectively) and a coupling efficiency of 42.9 ± 4.5%. These data are inconsistent with higher coupling efficiency for the 18-hydroxylase reaction being a major mechanism that enables aldosterone synthesis via P450 11B2 and P450 11B1-V320A. Overall, the proportionally lower NADPH consumption and 18-hydroxylase activities of wild-type and mutant enzymes reinforce

that DOC is the optimal substrate for aldosterone synthesis, given the processivity of P450 11B2 [7].

Table 3.1 **Rates of NADPH Consumption and Product Formation with Wild-Type P450 11B Enzymes in Phospholipid Vesicles.**

	11β-hydroxylase			18-hydroxylase		
	Product (min^{-1})	**NADPH (min^{-1})**	**Coupling (%)**	**Product (min^{-1})**	**NADPH (min^{-1})**	**Coupling (%)**
P450 11B1	30.5 ± 1.1	46.9 ± 2.4	65.0 ± 2.4	1.2 ± 0.1	5.6 ± 1.1	22.6 ± 5.6
P450 11B1-V320A	35.9 ± 1.6	104.4 ± 13.4	35.2 ± 6.2	1.4 ± 0.1	65.9 ± 6.7	1.7 ± 0.3
P450 11B2	34.2 ± 1.1	55.7 ± 7.3	62.8 ± 10.5	12.2 ± 1.0	35.5 ± 5.3	35.0 ± 4.8
P450 11B2-A320V	38.6 ± 5.6	34.8 ± 16.1	126.8 ± 38.0	0.8 ± 0.2	2.3 ± 0.1	42.9 ± 4.5

3.3.3 Equilibrium Substrate Binding to P450 11B-Nanodiscs

Given that coupling efficiencies did not explain the poor 18-oxygenase activities of P450 11B1, we studied ligand binding and dissociation for DOC and corticosterone. We used phospholipid nanodiscs for P450 11B binding experiments, as recently described for osilodrostat studies [12], given their high stability during prolonged titrations and the tendency for protein precipitation during rapid mixing in stopped-flow experiments with the phospholipid vesicle system. First, we demonstrated that the maximal activities for wild-type P450 11B1 and P450 11B2 in nanodiscs for the 11β-hydroxylase reaction were not demonstrably different than with phospholipid vesicles (Appendix Figure 3). All enzymes exhibited a Soret peak with a maximum absorbance of ~417 nm when unliganded, consistent with the low-spin state (Appendix Figure 4). Both DOC and corticosterone ligands induced type I spectral shifts to ~390 nm upon incubation with wild-type and mutant P450 11B enzymes (Appendix Figure 4), which indicates active-site binding and transition to the high-spin state (Figure 3.3). DOC binds tightly to both P450 11B2

and P450 11B1, with calculated K_d values of 0.28 ± 0.02 and 0.40 ± 0.07 µM, respectively (Table 3.2). Mutations P450 11B1-V320A and P450 11B2-A320V showed opposing effects on DOC affinity, resulting in K_d values of 0.12 ± 0.01 and 1.85 ± 0.13 µM, respectively. The most notable differences, however, were observed with corticosterone binding. P450 11B1 mutation V320A improved corticosterone affinity 10-fold, from 31 ± 5 to 2.96 ± 0.22 µM. In comparison, P450 11B2 mutation A320V prominently raised the K_d 62-fold to 236 ± 45 µM from 5.89 ± 0.94 µM. For all proteins, corticosterone binding remained significantly weaker than that of DOC, which is consistent with previous publications [7, 20].

Table 3.2 **Equilibrium Dissociation Constants (K_d) for Substrates with P450 11B Enzymes.**

	DOC		**Corticosterone**	
	K_d (µM)	**$\triangle A_{max}$**	**K_d (µM)**	**$\triangle A_{max}$**
P450 11B1	0.40 ± 0.07	0.016 ± 0.001	31 ± 5	0.006 ± <0.001
P450 11B1-V320A	0.12 ± 0.01	0.019 ± <0.001	2.96 ± 0.22	0.012 ± <0.001
P450 11B2	0.28 ± 0.02	0.026 ± <0.001	5.89 ± 0.94	0.014 ± 0.001
P450 11B2-A320V	1.85 ± 0.13	0.033 ± 0.001	236 ± 45	0.020 ± 0.001

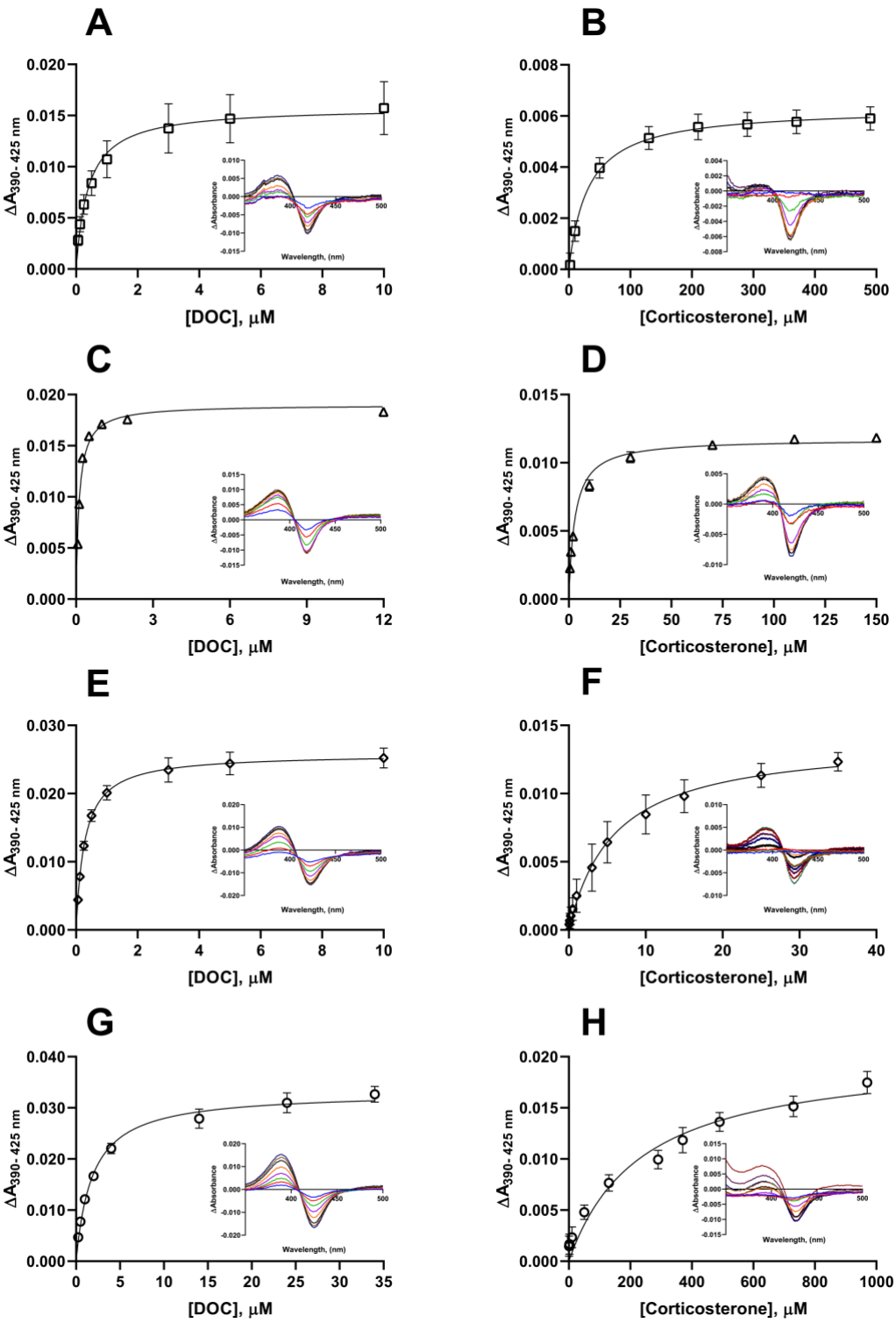

Figure 3.3 **Equilibrium binding titrations of DOC and corticosterone to P450 11B enzymes.** Panels A, C, E, and G show DOC binding to P450 11B1 (□), P450 11B1-V320A (Δ), P450 11B2 (◇) and P450 11B2-A320V (○), respectively. Panels B, D, F, and H show corticosterone binding to the same enzymes. The insets in each panel show the difference spectra at each ligand concentration. Data represent the mean ± standard deviation of three experiments. Error bars in panels C and D are smaller than the icons.

3.3.4 Substrate Binding Kinetics

The kinetics of substrate binding were elucidated by analyzing the kinetic traces obtained from absorbance changes in Soret bands overtime at 390 and 417 nm under stop-flow (rapid mixing) conditions. Single-exponential fits to the data were insufficient to describe DOC binding kinetics for either P450 11B1, P450 11B2, or the 320 mutant enzymes. Biexponential functions, however, fit the data well, consistent with at least two distinct binding steps in the overall mechanism (Figure 3.4, Panels A-D and E-H). The observed pseudo-first-order rate constants (k_{obs}) from the "fast" and "slow" components of the biexponential fits were then calculated and plotted as a function of ligand concentration. For all conditions, the k_{obs} of the "fast" phase increased linearly with increasing ligand concentration (Figure 3.4, Panels I-L), while the k_{obs} trends for the second phase were variable (Figure 3.4, Panels M-P). These results suggest that ligand binding to P450 11B enzymes might involve either conformational selection or induced fit mechanisms, analogous to what has been reported with other cytochrome P450 enzymes [21-24].

Regardless of the underlying mechanism, the k_{obs} for the "fast" phase describe a simple reversible binding step. In this case, plotting k_{obs} against [DOC] allows for the determination of the second-order binding rate constant ($\mu M^{-1} s^{-1}$) and dissociation rate constant (s^{-1}) from the slope and Y-intercept, respectively. The results obtained from this analysis are listed in Table 3.3. Our data suggest that while the rates of DOC binding to P450 11B1 and P450 11B2 are similar, their respective dissociation rates differ significantly (1.45 ± 0.07 and 0.69 ± 0.09, respectively) ($P = 0.0023$). As expected, while mutation A320V did not affect the k_{on} of DOC for P450 11B2, the dissociation rate of DOC from P450 11B2-A320V was 2.28 ± 0.22 s^{-1}, which is threefold higher than that of wild-type P450 11B2. The opposite trend was observed with P450 11B1-V320A, in which the dissociation rate of 0.18 ± 0.03 s^{-1} is significantly slower ($P < 0.0001$) than that of wild-

type P450 11B1, and the binding rate for DOC decreased by half, from 0.53 ± 0.01 to 0.28 ± 0.003 $\mu M^{-1} s^{-1}$.

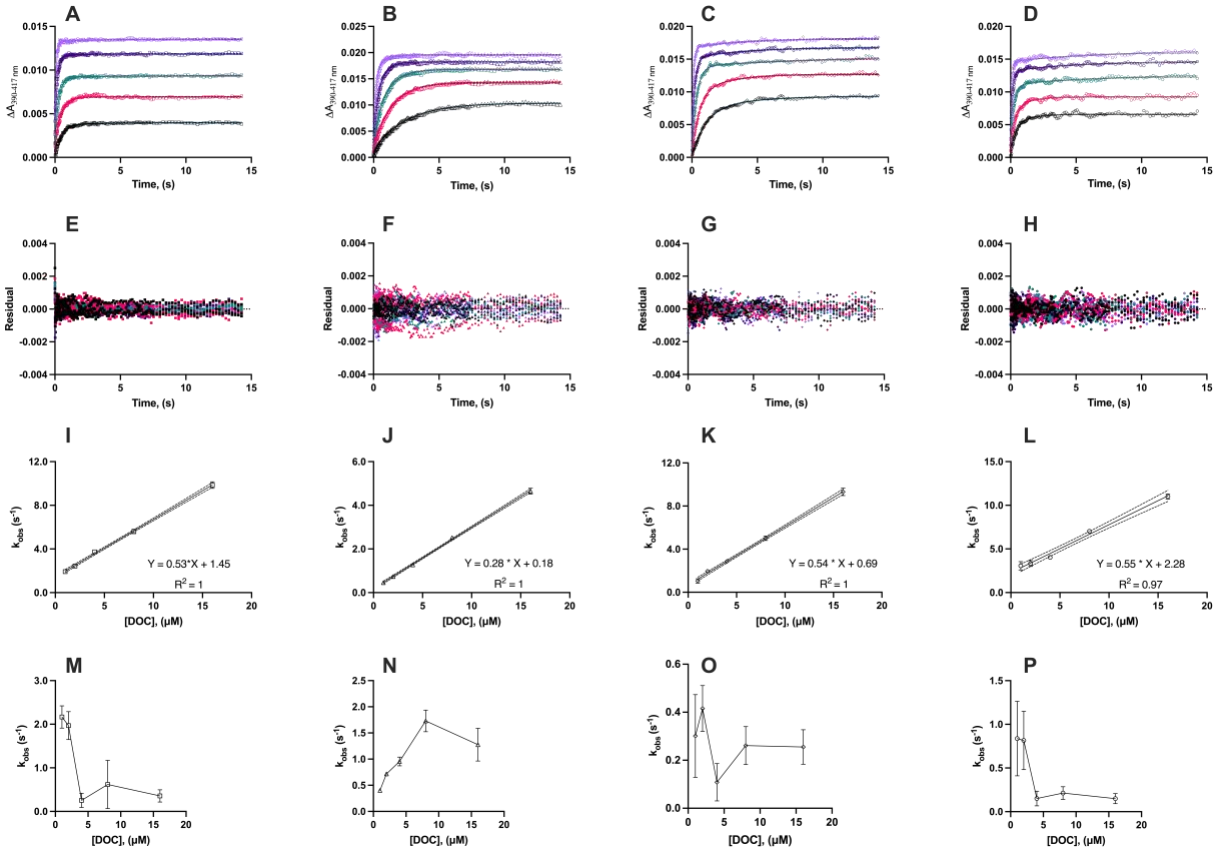

Figure 3.4 **UV-Visible stopped-flow analysis of P450 11B enzymes in nanodiscs.** Panels A, B, C, and D show the binding of 0.25 μM of P450 11B1 (□), P450 11B1-V320A (Δ), P450 11B2 (◇) and P450 11B2-A320V (○), respectively, with DOC at the following concentrations: 1 μM (black), 2 μM (magenta), 4 μM (aqua), 8 μM (purple), and 16 μM (lilac). The lines in panels A-D show the nonlinear regression fits to the traces obtained, which represent the mean of three technical replicates. Panels E-H show residual plots for curve fits to panels A-D, respectively. Panels I, J, K, and L show the linear analysis for the fast phase of the exponential fits as a function of [DOC], and the dashed lines represent the 95% confidence intervals. Panels M, N, O, and P show the calculated observed rate constants for the slow phase as a function of [DOC].

We also investigated the kinetics of corticosterone binding and dissociation with wild-type and mutant enzymes (Appendix Figure 5). Our findings revealed that corticosterone binding rates were significantly slower than those of DOC under all conditions; however, the dissociation rates of corticosterone were much faster than DOC. Additionally, P450 11B1 displayed a very high dissociation rate for corticosterone (19 ± 5 s^{-1}), which was twice as fast as that of P450 11B2 (8.60

± 0.40 s^{-1}). As anticipated, the k_{off} was considerably slower with P450 11B1-V320A (2.28 ± 0.30 s^{-1}), which decreased 8-fold from wild-type P450 11B1. Compared to DOC, the binding of corticosterone to P450 11B enzymes shows a much weaker spectrophotometric shift, especially for P450 11B1. Consequently, it is possible that the values calculated for the corticosterone dissociation rates were underestimated. Additionally, given the very weak binding (K_d) of corticosterone to P450 11B2-A320V, we did not attempt to calculate these parameters through this method.

Table 3.3 **Kinetic Parameters for DOC and Corticosterone Binding to P450 11B Enzymes Determined from Pseudo-First-Order Analysis.**

	DOC		**Corticosterone**	
	k_{on} (μM^{-1} s^{-1})	**k_{off} (s^{-1})**	**k_{on} (μM^{-1} s^{-1})**	**k_{off} (s^{-1})**
P450 11B1	0.53 ± 0.01	1.45 ± 0.07	0.24 ± 0.03	19 ± 5
P450 11B1-V320A	0.28 ± <0.01	0.18 ± 0.03	0.01 ± <0.01	2.28 ± 0.30
P450 11B2	0.54 ± 0.01	0.69 ± 0.09	0.07 ± 0.01	8.60 ± 0.40
P450 11B2-A320V	0.55 ± 0.03	2.28 ± 0.22	NM	NM

*NM = not measured

3.3.5 Direct Measures of DOC and Corticosterone Dissociation Rates

Given that trends in DOC and corticosterone dissociation rates from P450 11B1, P450 11B2, and their mutations aligned in the order predicted to enhance the processivity of P450 11B2, we sought to measure these rates directly. To perform these measurements, we monitored the transition from a high-spin to a low-spin state of enzyme-substrate complexes in the presence of 2-hydroxypropyl-β-cyclodextrin. Briefly, P450 11B enzymes were preincubated with either DOC or corticosterone at least two times their respective K_d to ensure that more than 50% of the enzyme population is in complex with the ligand used. The resultant samples were then rapidly mixed in the stopped-flow apparatus with a buffer containing an excess of 2-hydroxypropyl-β-cyclodextrin.

Upon dissociation from the enzyme, the 2-hydroxypropyl-β-cyclodextrin forms a complex with the free steroids and prevents their binding and rebinding once the samples are mixed.

The dissociation kinetics of DOC from P450 11B2, P450 11B1, and P450 11B1-V320A fit well to uniphasic exponential decay functions (Table 3.4), and in all cases, the dissociation rate constants (k_{off}) obtained from this method are similar to rate constants calculated from the conventional pseudo-first order analyses (Table 3.3). In contrast, DOC dissociation kinetics from P450 11B2-A320V fit biphasic kinetics (Figure 3.5), with a significantly faster ($P = 0.0378$) first rate compared to wild-type, 5.18 ± 1.59 versus 0.94 ± 0.04 s^{-1}, respectively, which might account for the differences in their respective K_d values (Table 3.2).

Corticosterone dissociation kinetics also fit uniphasic functions for all but P450 11B2-A320V (Appendix Figure 6). Only P450 11B2 showed a slow corticosterone dissociation rate constant of 0.45 ± 0.04 s^{-1}, and mutation A320V dramatically increased the rate of the first dissociation phase to 46.6 ± 8.6 s^{-1} (Table 3.4, 54% of total). Both wild-type P450 11B1 and P450 11B1-V320A exhibited very rapid corticosterone dissociation rates despite differences in DOC dissociation, which limited our ability to calculate accurate values. This rapid corticosterone dissociation when added directly might explain why the rates for the 18-hydroxylation remain similar for P450 11B1 and its mutation V320A under these conditions (Table 3.3), despite the enhanced 18-oxygenation activities of P450 11B1-V320A with DOC as the substrate (Table 3.1).

Table 3.4 **Dissociation Rates of DOC and Corticosterone from P450 11B Enzymes by Direct Method.**

	DOC	Corticosterone
	k_{off} (s^{-1})	k_{off} (s^{-1})
P450 11B1	1.28 ± 0.14	>6
P450 11B1-V320A	0.36 ± 0.02	>5
P450 11B2	0.94 ± 0.04	0.45 ± 0.04
P450 11B2-A320V	5.18 ± 1.59	46.6 ± 8.6

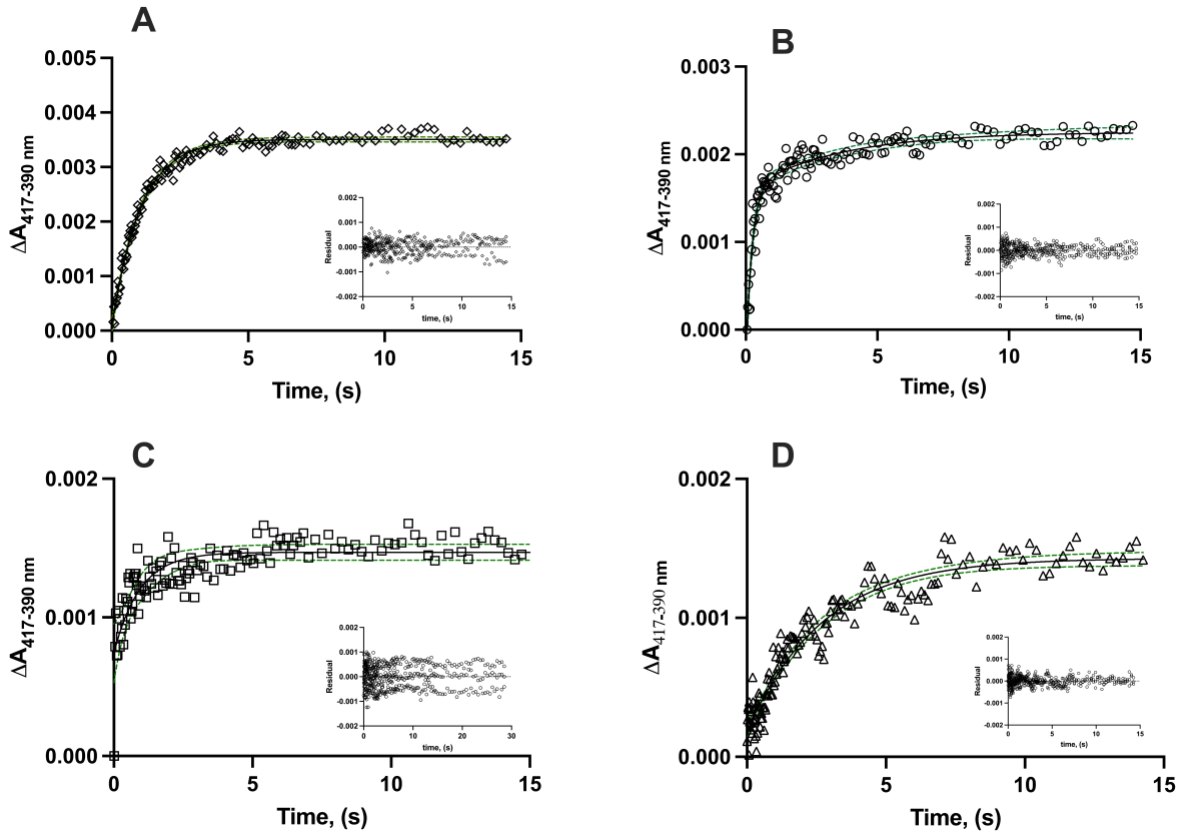

Figure 3.5 **Stopped-flow analysis of DOC dissociation from P450 11B enzymes by direct method.** Panels A, B, C, and D show the mixing of 0.5 µM of P450 11B2 (◇) and 11B2-A320V (○) and P450 11B1 (□), and 11B1-V320A (Δ), respectively, with an excess of cyclodextrin. The dashed lines represent the 95% confidence intervals, and the insets show residual plots.

3.3.6 Substrate Binding Kinetic Modeling

To better understand the binding mechanism(s) of substrates to P450 11B enzymes, data from kinetic traces were globally fitted to systems of differential equations that described lock and key (LK, simple reversible interaction) [25], or models that account for the dynamic nature of proteins, including conformational selection (CS), induced fit (IF), and mixed CS and IF (Table 3.5). The rates obtained from the fitting are summarized in Table 3.5. To assess goodness of fit, we report the ratio of chi-squared (χ^2) and Degrees of Freedom (DoF). A good fit is generally indicated by values of χ^2/DoF approaching 1.

As expected, given that the k_{off}/k_{on} ratios are up to 7-fold different than the K_d values in Table 3.2, the most simplistic mechanism of ligand binding, LK, does not provide good fits. More complex models provide better fits for P450 11B2 and P450 11B2-A320V but not for P450 11B1 and P450 11B1-V320A. In the CS model, a conformational change precedes ligand binding. Despite the CS mechanism being described in several cytochrome P450 enzymes [21, 22], the fit of the CS model (χ^2/DoF = 4.35) to P450 11B2 was not as satisfactory as that of the IF model (χ^2/DoF = 2.78), in which the conformational transition follows ligand binding [26]. This trend also holds for P450 11B2-A320V and for P450 11B1-V320A. Surprisingly, the combination of CS and IF models, while highly versatile, failed to enhance the quality of data fit across all conditions. In fact, for P450 11B1-V320A, the goodness of fit decreased (χ^2/DoF = 13.50). For P450 11B1, LK (χ^2/DoF = 4.64), CS (χ^2/DoF = 4.77), IF (χ^2/DoF = 4.66), and the mixed model (χ^2/DoF = 5.08) provided similar results, which might reflect the minimal biphasic nature of substrate binding compared to P450 11B2.

In considering the reasons for our results with the CS models, the forward rates (k_1) for the interconversion between enzyme conformations are, in all cases, significantly higher than the reverse rates (k_{-1}). This result implies that if two conformations are present, the enzyme primarily exists in one of these; therefore, the CS feature contributes little to the overall mechanism and data fitting. If this scenario is true, this skewed pre-equilibrium state distribution might also explain why adding a CS step does not improve the overall fitting of the mixed model. In addition, we could not measure conformational transitions or binding interactions faster than the dead time (2 ms) of the stopped-flow instrument. Consequently, we could not capture data in the time regime where very rapid conformational pre-equilibria might contribute to the substrate binding mechanism. Models with additional liganded and/or unliganded states might better fit the data.

Table 3.5 **Global Fitted Rates of DOC Binding to P450 11B Enzymes.***

Model	k_{on} ($\mu M^{-1}s^{-1}$)	k_{off} (s^{-1})	k_1 (s^{-1})	k_{-1} (s^{-1})	k_2 (s^{-1})	k_{-2} (s^{-1})	X^2/DoF
P450 11B1							
LK	0.69 ± 0.01	1.80 ± 0.02	-	-	-	-	4.64
CS	0.76 ± 0.25	1.81 ± 0.03	1000 ± ND	101 ± ND	-	-	4.77
IF	0.69 ± 0.05	1.93 ± 1.04	4.76 ± ND	70 ± ND	-	-	4.66
IF + CS	1.13 ± ND	1.82 ± ND	316 ± 262	198 ± 40	0.001 ± ND	69.62 ± ND	5.08
11B1-V320A							
LK	0.30 ± < 0.01	0.26 ± 0.00	-	-	-	-	8.06
CS	0.30 ± 0.06	0.27 ± 0.004	253 ± 106	0.001 ± ND	-	-	8.67
IF	0.28 ± < 0.01	0.38 ± 0.03	8.37 ± 2.38	13.35 ± 1.74	-	-	7.88
IF + CS	0.80 ± 0.20	0.60 ± 0.50	18.20 ± 2.37	22.75 ± 8.67	3.11 ± ND	3.92 ± 2.36	13.50
P450 11B2							
LK	0.50 ± < 0.01	0.49 ± 0.01	-	-	-	-	5.59
CS	0.50 ± 0.13	0.49 ± 0.01	467 ± 312	0.24 ± ND	-	-	5.89
IF	0.57 ±0.01	0.95 ± 0.03	0.34 ± 0.04	0.37 ± 0.03	-	-	2.86
IF + CS	0.58 ± 0.12	0.96 ± 0.04	908 ± 864	0.001 ± ND	0.33 ± 0.04	0.36 ± 0.03	2.94
11B2-A320V							
LK	0.74 ± 0.01	1.09 ± 0.02	-	-	-	-	4.09
CS	0.75 ± 0.28	1.12 ± 0.02	283 ± 117	0.001 ± ND	-	-	4.35
IF	0.84 ± 0.10	1.75 ± 0.06	0.27 ± 0.04	0.55 ± 0.06	-	-	2.78
IF + CS	0.86 ± 0.29	1.90 ± 0.10	316 ± 134	0.001 ± ND	0.34 ± 0.06	0.62 ± 0.06	2.92

*Data represent the fitted parameters ± standard error of the nonlinear regression; ND = not detected

3.4 Discussion

Despite a 93% sequence identity between the human P450 11B1 and P450 11B2, the reason(s) for minimal 18-hydroxylase activity and absent 18-oxidase activity of P450 11B1 have remained unknown. Using mutations at residue 320 that confer or reduce 18-hydroxylase

activities, our major finding is that changes in the rates of corticosterone dissociation for these mutations correlate with changes in 18-hydroxylase activities. In contrast, changes in coupling efficiencies are inconsistent with the loss or gain of 18-hydroxylase activities for these mutations. Our data are consistent with the processive catalytic mechanism for the 3-step production of aldosterone via P450 11B2 [7] and suggest that slow intermediate dissociation is essential for aldosterone biosynthesis, including via P450 11B1-V320A.

To elucidate the mechanism enabling aldosterone synthesis, we employed mutations P450 11B1-V320A and P450 11B2-A320V, which enhance or attenuate 18-oxygenation activities, respectively, relative to the wild-type enzymes. These substitutions provide a series of 4 enzymes with a range of 18-oxygenation activities, which we used to compare trends in microscopic steps or parameters with activities. The coupling of NADPH consumption with product formation was high (>35%) for the 11β-hydroxylase reactions with all enzymes using DOC as the substrate. Coupling efficiency for the 18-hydroxylase activity with corticosterone as the substrate, however, followed trends opposite to that expected if poor coupling limited 18-oxygenation via P450 11B1. Mutation P450 11B1-V320A, which acquires aldosterone synthase activity, showed lower coupling efficiency for the 18-hydroxylase reaction than wild-type P450 11B1; furthermore, mutation P450 11B2-A320V, which has limited aldosterone synthase activity, showed greater coupling efficiency than wild-type P450 11B2. In these experiments, we found that 18OHB and aldosterone production was lower using corticosterone as the substrate than when using DOC as the substrate, and minor amounts of downstream metabolites indicate that coupling efficiencies are likely underestimated. These findings also suggest that enzyme-substrate complexes with nascent corticosterone from DOC turnover are functionally different from those resulting from

direct corticosterone binding, which aligns with previous demonstrations that DOC is the optimal substrate for aldosterone synthesis via P450 11B2 [7, 9].

Since the coupling efficiency data did not explain differences in aldosterone synthesis, we directed our attention to the binding affinities and kinetic parameters for DOC and corticosterone interactions with both wild-type and mutant P450 11B enzymes. Our findings showed that all enzymes exhibited significantly lower K_d values for DOC than corticosterone. Our study also showed that P450 11B1-V320A exhibits substantially greater affinities for DOC and corticosterone than wild-type P450 11B1, which are comparable to that of P450 11B2. In contrast, P450 11B2-A320V has a notably lesser affinity for both substrates than wild-type P450 11B2, resembling P450 11B1. Given that high affinity for corticosterone correlated with aldosterone synthase activity, we next determined if the rates of binding or dissociation governed this trend.

Using stopped-flow spectroscopy for substrate binding titrations, the k_{on} rate constants for corticosterone with aldosterone-producing P450 11B2 and P450 11B1-V320A were slower (not faster) than for P450 11B1; however, the k_{off} constants for corticosterone dissociation from these two enzymes were much slower than for P450 11B1 (2.28-8.60 vs. 19 s^{-1}, respectively) by the pseudo-first-order method. To confirm these results, we directly measured corticosterone dissociation rates using cyclodextrin to complex free steroid and to limit rebinding. Although the values differed for the two methods, the trends are the same. For P450 11B2, the k_{off} of corticosterone was 100-fold slower than for P450 11B2-A320V and at least 10-fold slower than for P450 11B1. The rapid and weak spectral changes during corticosterone dissociation limited calculations for P450 11B1 and P450 11B1-V320A (Figure 3.4); however, trends for DOC dissociation followed those for corticosterone with greater accuracy (Table 3.4). Furthermore, based on activity assays, nascent corticosterone formed from DOC turnover appears to be even

more tightly bound than when added directly to enzymes with aldosterone synthase activity. We conclude that tight corticosterone binding, primarily due to slow dissociation, is a major factor in governing the processivity and the resultant aldosterone synthase activity of P450 11B2.

Figure 3.6 illustrates the possible origins of the differences in intermediate dissociation in P450 11B1 and P450 11B2. In P450 11B1, the side chain of V320 is within distance to make hydrophobic interactions with F321 (4.0 Å) and L324 (3.9 Å). This positioning allows F193 to rotate away from the active site, which exposes an extended break in the I-helix and a hydrogen-bonded water molecule (Figure 3.6A, C). In P450 11B2, the smaller A320 allows F193 to rotate in toward the active site (4.0 Å from A320) and to contribute hydrophobic interactions with F321 (3.3 Å), which reduces the I-helix break and excludes the water molecule (Figure 3.6B, D). This less hydrated active site with what appears to be more tightly arranged hydrophobic roof might allow the exceptionally tight binding and slow dissociation of DOC and corticosterone.

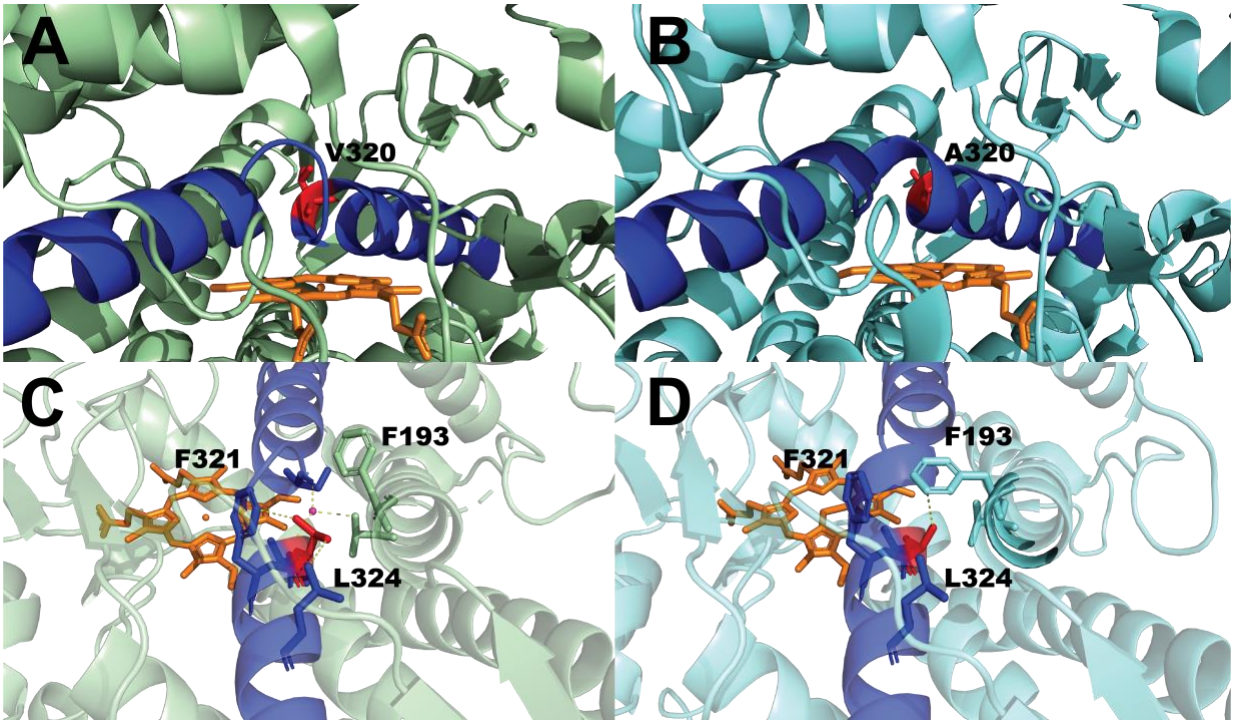

Figure 3.6 **Active site structures of P450 11B1 (PDB code 6M7X) and P450 11B2 (PDB code 7M8V) without ligand.** The I-helix is shown in blue, and the heme prosthetic group is presented in orange in all panels. Panel A shows the placement and location of the valine residue at position 320, as highlighted in red in P450 11B1 (green). Panel B shows the placement and location of the alanine residue at position 320, as highlighted in red in P450 11B2 (aquamarine). Panels C and D highlight interactions between the 320 residue in P450 11B1 and P450 11B2, respectively, and neighboring residues within less than a 5 Å distance, particularly F321 and L324. A water molecule (magenta) is represented as a sphere in panel C.

DOC binding to P450 11B enzymes occurs in at least two distinct steps, which is evident from the biphasic kinetic traces obtained (Figure 3.4), and we attempted to understand the binding mechanism by fitting the experimental data to kinetic models. In the case of a CS mechanism, as the ligand concentration increases, the pre-equilibrium converges towards a single conformation [27]. Assuming that only two conformations are present, the CS model would anticipate an exponential decrease in k_{obs} values for the second phase as [DOC] increases. On the contrary, the rate of conformational transition in the IF model increases with the concentration of the ligand [27]. This occurs because the enzyme changes from a single free conformation to an equilibrium state between two bound conformations. Although sometimes these patterns can be evident from

inspection of the data, our experimental data do not obviously reflect CS or IF kinetics. To address this uncertainty, we carried out global fitting of our kinetic traces to the differential equations that define each mechanism (Eq 1-4). In general, our results consistently favor an IF mechanism for ligand binding to P450 11B enzymes. Furthermore, binding and dissociation rates for the four P450 11B enzymes follow the same trends for all methods used to calculate these rates, which further strengthens our conclusions.

Several mammalian cytochrome P450 enzymes that catalyze sequential reactions, particularly cytochromes P450 19A1[21] and P450 17A1[22], demonstrate a preference for the CS mechanism; however, the IF mechanism describes the binding of certain ligands to P450 3A4[23] and P450 101A1 (P450cam) [24]. Nonetheless, even in the cases where IF is dominant, the presence of multiple enzyme states prior to ligand binding is not ruled out. The scientific literature on P450cam notes the existence of two conformational states: an "open"[28] and a "closed"[29] state. The "closed" conformation has been established as the more dominant of the two, as the transition from “closed” to “open” states was found to be significantly slower than the reverse transition [30]. Given these parameters, the authors concluded that P450cam would follow an IF mechanism, given that substrates would encounter the most prominent conformation at a higher rate, which was later confirmed experimentally [24].

Much like P450cam, P450 11B enzymes might exist in two distinct states. Utilizing the CS model, our computational analysis revealed forward reaction rates significantly faster than the reverse rates for the interconversion of the two enzymatic states. These results suggest that P450 11B enzymes might preferentially exist in one conformation, similar to that seen in P450cam. Furthermore, when considering the combination of both IF and CS, we observed the same pattern of one very dominant conformation, but without any significant improvement in the overall fitting

of the kinetic traces, as confirmed by the calculated χ^2/DoF (Table 3.5). These findings suggest a significant preference for IF in the homologous P450 11B enzymes. This IF mechanism might be directly influenced by the dissociation rates of substrates and intermediates. Therefore, to achieve this conformational transition and subsequent hydroxylation, it is crucial that the substrates and intermediates remain bound within the active site. In the case of P450 11B2, the slower rates of dissociation for both DOC and corticosterone might allow the enzyme to transition to a state that is more conducive for subsequent catalysis. In the case of P450 11B1, however, 18-hydroxylation is limited due to the fast dissociation rates of the intermediate corticosterone. Models that incorporate three or more states might provide greater insight into substrate binding; however, the overwhelming dominance of one conformation in the 2-state model suggests that more complex models will not alter our interpretations.

We conclude that slow corticosterone dissociation rates, rather than improved coupling efficiency, is a major mechanism that enables P450 11B2 but not P450 11B1 to synthesize aldosterone via a processive mechanism. Residues 320 and other active-site residues substantially regulate corticosterone dissociation kinetics and substrate orientation [8]; however, residue exchange alone is insufficient to endow P450 11B1 with all the catalytic properties of P450 11B2 [10]. Thus, it is likely that extrinsic factors, such as protein-protein interactions and membrane composition, also modulate their activities *in vivo* and account for the lower aldosterone production with purified, reconstituted P450 11B2 than in transfected cells. For all enzyme species, aldosterone production is highest with DOC as the substrate, which implies differences in enzyme-substrate complexes with nascent corticosterone derived from DOC than with solution-borne corticosterone. We also find that an IF mechanism best describes the binding of DOC to P450 11B enzymes, with one major binding state. Nonetheless, it is unclear how the "slow" phase contributes

to overall catalysis since the kinetic traces obtained show the "fast" phase as the most prominent component. Extrinsic factors such as temperature and lipid composition may impact the "slow" phase, which could be more pronounced *in vivo*. Therefore, additional computational and experimental studies of P450 11B1 and P450 11B2 dynamics in complex with substrates and adrenodoxin will provide valuable insights into steroid metabolism and cytochrome P450 biochemistry, particularly for enzymes with processive catalytic mechanisms.

3.5 Bibliography

1. Sparks, M.A., et al., *Classical Renin-Angiotensin system in kidney physiology.* Compr Physiol, 2014. **4**(3): p. 1201-28.
2. Schiffer, L., et al., *The CYP11B subfamily.* J Steroid Biochem Mol Biol, 2015. **151**: p. 38-51.
3. Byrd, J.B., A.F. Turcu, and R.J. Auchus, *Primary Aldosteronism: Practical Approach to Diagnosis and Management.* Circulation, 2018. **138**(8): p. 823-835.
4. Freeman, M.W., et al., *Phase 2 Trial of Baxdrostat for Treatment-Resistant Hypertension.* N Engl J Med, 2023. **388**(5): p. 395-405.
5. Gonzalez, E. and F.P. Guengerich, *Kinetic processivity of the two-step oxidations of progesterone and pregnenolone to androgens by human cytochrome P450 17A1.* J Biol Chem, 2017. **292**(32): p. 13168-13185.
6. Sohl, C.D. and F.P. Guengerich, *Kinetic analysis of the three-step steroid aromatase reaction of human cytochrome P450 19A1.* J Biol Chem, 2010. **285**(23): p. 17734-43.
7. Reddish, M.J. and F.P. Guengerich, *Human cytochrome P450 11B2 produces aldosterone by a processive mechanism due to the lactol form of the intermediate 18-hydroxycorticosterone.* J Biol Chem, 2019. **294**(35): p. 12975-12991.
8. Brixius-Anderko, S. and E.E. Scott, *Structure of human cortisol-producing cytochrome P450 11B1 bound to the breast cancer drug fadrozole provides insights for drug design.* J Biol Chem, 2019. **294**(2): p. 453-460.
9. Strushkevich, N., et al., *Structural insights into aldosterone synthase substrate specificity and targeted inhibition.* Mol Endocrinol, 2013. **27**(2): p. 315-24.
10. Bottner, B., K. Denner, and R. Bernhardt, *Conferring aldosterone synthesis to human CYP11B1 by replacing key amino acid residues with CYP11B2-specific ones.* Eur J Biochem, 1998. **252**(3): p. 458-66.
11. Bottner, B., H. Schrauber, and R. Bernhardt, *Engineering a mineralocorticoid- to a glucocorticoid-synthesizing cytochrome P450.* J Biol Chem, 1996. **271**(14): p. 8028-33.
12. Valentin-Goyco, J., et al., *Selectivity of osilodrostat as an inhibitor of human steroidogenic cytochromes P450.* J Steroid Biochem Mol Biol, 2023. **231**: p. 106316.
13. Peng, H.M., C. Barlow, and R.J. Auchus, *Catalytic modulation of human cytochromes P450 17A1 and P450 11B2 by phospholipid.* J Steroid Biochem Mol Biol, 2018. **181**: p. 63-72.

14. Turcu, A.F., et al., *Comprehensive Analysis of Steroid Biomarkers for Guiding Primary Aldosteronism Subtyping.* Hypertension, 2020. **75**(1): p. 183-192.
15. Brixius-Anderko, S. and E.E. Scott, *Aldosterone Synthase Structure With Cushing Disease Drug LCI699 Highlights Avenues for Selective CYP11B Drug Design.* Hypertension, 2021. **78**(3): p. 751-759.
16. Luthra, A., et al., *Nanodiscs in the studies of membrane-bound cytochrome P450 enzymes.* Methods Mol Biol, 2013. **987**: p. 115-27.
17. Woods, S.T., et al., *Expression of catalytically active human cytochrome p450scc in Escherichia coli and mutagenesis of isoleucine-462.* Arch Biochem Biophys, 1998. **353**(1): p. 109-15.
18. Wright, C., et al., *Abiraterone acetate treatment lowers 11-oxygenated androgens.* Eur J Endocrinol, 2020. **182**(4): p. 413-421.
19. Johnson, K.A., *Fitting enzyme kinetic data with KinTek Global Kinetic Explorer.* Methods Enzymol, 2009. **467**: p. 601-626.
20. Hobler, A., et al., *Human aldosterone synthase: recombinant expression in E. coli and purification enables a detailed biochemical analysis of the protein on the molecular level.* J Steroid Biochem Mol Biol, 2012. **132**(1-2): p. 57-65.
21. Zarate-Perez, F. and J.C. Hackett, *Conformational selection is present in ligand binding to cytochrome P450 19A1 lipoprotein nanodiscs.* J Inorg Biochem, 2020. **209**: p. 111120.
22. Guengerich, F.P., et al., *Conformational selection dominates binding of steroids to human cytochrome P450 17A1.* J Biol Chem, 2019. **294**(26): p. 10028-10041.
23. Sweeney, D.T., et al., *Induced fit describes ligand binding to membrane-associated cytochrome P450 3A4.* Mol Pharmacol, 2023.
24. Guengerich, F.P., et al., *Kinetic Evidence for an Induced Fit Mechanism in the Binding of the Substrate Camphor by Cytochrome P450(cam).* ACS Catal, 2021. **11**(2): p. 639-649.
25. Fischer, E., *Einfluss der Configuration auf die Wirkung der Enzyme.* Berichte der deutschen chemischen Gesellschaft, 1894. **27**(3): p. 2985-2993.
26. Koshland, D.E., *Application of a Theory of Enzyme Specificity to Protein Synthesis.* Proc Natl Acad Sci U S A, 1958. **44**(2): p. 98-104.
27. Di Cera, E., *Mechanisms of ligand binding.* Biophys Rev (Melville), 2020. **1**(1): p. 011303.
28. Lee, Y.T., et al., *P450cam visits an open conformation in the absence of substrate.* Biochemistry, 2010. **49**(16): p. 3412-9.
29. Poulos, T.L., B.C. Finzel, and A.J. Howard, *Crystal structure of substrate-free Pseudomonas putida cytochrome P-450.* Biochemistry, 1986. **25**(18): p. 5314-22.
30. Dandekar, B.R., N. Ahalawat, and J. Mondal, *Reconciling conformational heterogeneity and substrate recognition in cytochrome P450.* Biophys J, 2021. **120**(9): p. 1732-1745.

Chapter 4
Future Directions & Concluding Remarks

4.1 Summary

The purpose of this dissertation was to gain a better understanding of the biochemical mechanisms that regulate cytochrome P450 11B2 catalysis and inhibition. The study had two main objectives. First, we aimed to investigate the impact of osilodrostat (LCI699), a drug initially developed as a selective P450 11B2 inhibitor, on steroidogenesis. We evaluated the drug's pharmacological effectiveness by analyzing steroid production in adrenal cells. Moreover, we studied osilodrostat's direct effect on specific enzymes, including P450 11B1 and 11B2, by using purified proteins and stable cell lines. Secondly, we aimed to define the kinetic parameters that regulate the 18-hydroxylase and 18-oxidase activities of P450 11B2 with purified enzymes incorporated in lipid nanodiscs and phospholipid vesicle systems. Overall, these studies represent a significant advancement in the field of steroid biosynthesis, and our results have important implications for future research in the cytochrome P450 field.

Our research has shown that LCI699 is a potent inhibitor of P450 11B1 and P450 11B2, which has been confirmed through experiments carried out in three different model systems. We conducted cellular assays with NCI-H295R cells and found that LCI699 effectively inhibited cortisol and aldosterone production, with IC_{50} values of 8.4 nM and 3.2 nM, respectively. Similar results were observed in V79 cells stably expressing these enzymes, where LCI699 was approximately 34-fold more potent in inhibiting P450 11B2 than P450 11B1. Additionally, both P450 11B enzymes integrated into phospholipid nanodiscs demonstrated K_d values of around 1

nM for LCI699. Our research also revealed a partial inhibition and weak binding of LCI699 to P450 11A1. These results suggest that LCI699 is a highly potent inhibitor of the P450 11B enzymes. Its lack of selectivity towards P450 11B2, however, limits its use for the treatment of primary aldosteronism.

Our study also uncovered an intriguing finding regarding the impact of LCI699 on bound DOC and its metabolism. Specifically, we have observed that the addition of LCI699 does not entirely displace the bound DOC, nor does it prevent its metabolism to aldosterone. In contrast, in the case of P450 11B1, the addition of LCI699 resulted in the complete displacement of the bound DOC. This opposing behavior can be attributed to the presence of two distinct populations of P450 11B2 enzymes, one of which is more tightly bound to DOC, or extremely slow dissociation rates.

To elucidate the mechanism underlying the synthesis of aldosterone from DOC, we utilized the mutant P450 11B1-V320A and P450 11B2-A320V. These genetically engineered variants exhibit varied 18-oxygenation activities, with the former potentiating and the latter attenuating these activities. The research findings indicate that aldosterone production is modulated by the rate of corticosterone dissociation rather than the NADPH coupling efficiency. In all enzymes, including mutant and wild-type, the NADPH coupling efficiency was higher with DOC than corticosterone. All enzymes also exhibited significantly higher K_d values for corticosterone than for DOC. Altogether, these results provide compelling evidence that confirms that DOC is the ideal substrate for aldosterone synthesis.

The results of the study also revealed that both P450 11B homologous enzymes exhibit biphasic binding kinetics, although the behavior was found to be more pronounced in P450 11B2. This suggests that DOC binding to P450 11B enzymes occurs in at least two distinct steps. We attempted to understand the binding mechanism by fitting the experimental data into kinetic

models. In general, our results favor an induced fit mechanism for ligand binding to P450 11B enzymes, although we cannot fully exclude the presence of a conformational selection step.

This IF-binding mechanism might explain the behavior observed with LCI699 and DOC-bound P450 11B2. DOC binding to P450 11B2 might elicit a conformational transition to a species that has a very slow dissociation rate, and that is conducive to hydroxylation. This may explain why the addition of LCI699 still leads to aldosterone formation when P450 11B2 is pre-incubated with DOC. On the other hand, when P450 11B2 is pre-incubated with LCI699, the production of aldosterone is entirely abrogated. Nonetheless, the presence of more than two enzyme conformations might be possible, and other factors, such as substrate cooperativity, may also be worth investigating.

Both P450 11B1 and 11B2 are promising targets for treating endocrine-related disorders, such as primary aldosteronism. However, as seen in the literature, and throughout this Dissertation, selectively targeting P450 11B2 is challenging, given its 93% sequence similarity to P450 11B1. Our data with LCI699 indicate that successful 11B2 inhibitors must be several orders of magnitude more selective to avoid potential side effects associated with P450 11B1 and even P450 11A1 inhibition. Given this finding, it is important to be able to biochemically distinguish between these two highly similar enzymes. Regarding those differences, we have been able to determine some of the parameters that regulate aldosterone production, as we have shown that slow corticosterone dissociation rates, rather than coupling efficiency, is a major mechanism that enables P450 11B2 but not P450 11B1 to synthesize aldosterone. It is plausible that extrinsic factors, such as protein-protein interactions and membrane composition, might also exert a regulatory influence on their *in vivo* activities. Therefore, additional computational and experimental studies of P450 11B1 and

P450 11B2 can provide valuable insights into steroid metabolism and cytochrome P450 biochemistry.

4.2 Modulation of Aldosterone Synthase Activity by Membrane Composition

As highlighted in this dissertation, the lipid composition of the membrane is an extrinsic factor that has been shown to modulate the activity of cytochrome P450 enzymes [1, 2]. Human cell membranes are composed of a diverse array of lipids, which exhibit considerable variation across tissues and are susceptible to alterations in response to disease states. Since the F/G loop and various other parts of P450 enzymes are buried within the membrane [3], the lipid composition has the potential to exert a significant influence on protein activity, dynamics, and stability. Due to the intricate nature of cellular membranes and their diverse range of lipid compositions, our current model systems are insufficient to replicate native cellular environments. As such, more effort should be made to characterize these lipid model systems, which are restricted to single lipid-containing bilayers or basic lipid mixtures in the form of phospholipid vesicles or nanodiscs.

The literature has documented that phospholipids can modulate the activity of P450 11B1 and P450 11B2. A study found that dioleoyl phosphatidylcholine (DOPC) enhances the 18-oxidase activity of P450 11B2 [1]. In contrast, DOPC was found to decrease the 11β-hydroxylation of P450 11B1, while 1,2-dilauroyl-sn-glycero-3-phosphocholine (DLPC) enhanced that activity. This study also emphasized the importance of the P450 to lipids ratio, with P450 11B2 exhibiting the highest 18-hydroxylase and 18-oxidase activities when the lipids were present at a 200-fold excess.

To understand the effects of lipid model systems, we incorporated P450 11B1 and P450 11B2 into phospholipid nanodiscs and compared their binding to the phospholipid vesicle model. Our findings revealed that P450 11B homologous enzymes bind more tightly to DOC and corticosterone in nanodiscs than in lipid vesicles (Appendix Table 1). The most notable difference

was observed with the binding of corticosterone. While the binding of corticosterone was measurable with P450 11B2 in phospholipid vesicles, no high-spin change was observable with P450 11B1 in this system. P450 11B2 also showed a 75-fold improvement in corticosterone affinity in nanodiscs, from 444 ± 50 µM to 5.89 ± 0.94 µM.

The binding kinetics of DOC to P450 11B1 and P450 11B2 were also examined in nanodiscs and phospholipid vesicles. The study involved obtaining kinetic traces from absorbance changes in the Soret bands over time, as delineated in Chapter 3. By analyzing these kinetic traces, the binding (k_{on}) and dissociation (k_{off}) rates of DOC were determined (Appendix Table 2). Our findings revealed that in both model systems used, P450 11B1 displayed a much higher k_{off} for DOC than P450 11B2. A notable finding, however, is that the dissociation rate remained relatively unchanged between these two systems. For example, P450 11B2 showed a k_{off} of 0.69 ± 0.09 s^{-1} in nanodiscs, while in phospholipid vesicles, it was determined to be 0.46 ± 0.01 s^{-1}. The main difference observed was in the binding rates calculated, as they were more than three times slower in phospholipid vesicles compared to nanodiscs in both enzymes.

These results highlight the importance of evaluating the interactions between P450 enzymes and lipids. Although we observed differences in the binding kinetics of P450 11B enzymes, it is possible that their processivity may also be influenced by the membrane's lipid composition. This modulation of activity could result from changes in substrate accessibility, as endogenous ligands must traverse the cellular membranes to access the substrate access channel in P450 enzymes. Furthermore, the membrane environment may also impact conformational changes, as has been reported to occur with P450 1A2 [4].

4.3 Modulation of Aldosterone Synthase Activity by Protein-protein Interactions

All heterologous P450 11B2 systems produced less aldosterone than 18-hydroxycorticosterone due to incomplete 18-oxidase activity. This fact raises the question: are our current *in vitro* systems missing an essential *in vivo* component? Extrinsic factors, such as lipid composition, have been shown to impact the activity of P450 11B enzymes [1]. Furthermore, the ratio of P450 enzyme to redox partners is also important for catalysis, and studies have shown that increasing the ratio of P450 11B2 and 11B1 to adrenodoxin enhances substrate turnover and affinity [5, 6]. While favorable lipid compositions and P450 11B2 to redox partner ratios have been established, aldosterone synthesis via P450 11B2 *in vitro* remains incomplete.

Recently, the steroidogenic acute regulatory (StAR) protein has been shown to enhance P450 11B2 activity [7]. In steroidogenic cells, full-length (37-kDa) StAR drives the transfer of cholesterol from the outer to the inner mitochondrial membrane for conversion to pregnenolone [8]. Upon mitochondrial entry, StAR is cleaved to a 30-kDa form, which was thought to have no activity. A recent study, however, found that the 30-kDa StAR protein promoted aldosterone production from DOC *in vitro* in H9c2 embryonic rat heart cells [7]. This study also found P450 11B2 to be in complex with the 30-kDa StAR and the translocase protein TOM22 *in vivo* and *in vitro*.

To assess if 30-kDa StAR can modulate the activity of P450 11B2 *in vitro* directly, soluble StAR was expressed and purified in *E. coli*. To accomplish StAR expression, a plasmid containing a fusion protein consisting of the 30-kDa StAR domain (residues 66-285) and maltose-binding protein (MBP) at the C-terminus was obtained [9]. Prior to this fusion protein being developed, previous biochemical studies relied on StAR purified from inclusion bodies [10]. These inclusion bodies were denatured with high concentrations of urea and then slowly refolded by removing urea

through dialysis over several days. While this method resulted in functional StAR, concerns regarding the protein's correct folding remained. In contrast, the MBP-StAR fusion allows for soluble protein expression and fast purification. The MBP domain contains a histidine tag attached to the N-terminus. The C-terminus of MBP was also connected to StAR through an Asn-rich linker followed by a human rhinoviral 3C protease cleavage site. This 3C protease cleavage site allows for the removal of the MBP after purification through affinity chromatography. Overall, with the use of the MBP-StAR plasmid, we successfully expressed and purified 30 kDa StAR with a high degree of purity (Appendix Figure 7A).

To assess that the purified 30 kDa StAR was functional, a binding assay with a fluorescent cholesterol analog, 25-NBD cholesterol, was carried out (Appendix Figure 7B). In this experiment, the purified 30 kDa StAR protein was incubated in increasing concentrations of 25-NBD cholesterol at 37 ^{o}C. After pre-incubation, fluorescence was excited at 483 nm and recorded at 523 nm. The data obtained suggest that 30 kDa StAR binds to 25-NBD with high affinity (K_d = 47.2 ± 6.7 nM), resembling what was previously published [9]. After confirming protein functionality, an activity assay with P450 11B2 in the presence and absence of 30 kDa StAR and cholesterol was carried out (Appendix Figure 8), and no difference was observed between all the conditions. This result suggests that 30 kDa StAR does not potentiate P450 11B2-catalyzed aldosterone formation directly. This discrepancy might be due to the TOM22 protein being a requirement for this interaction, given that all three proteins were found in the complex [7]. Furthermore, a higher concentration of 30 kDa StAR might be needed to observe such effects *in vitro*, although this is less likely given that the highest molar concentration was 10 times more than P450 11B2. Regardless, these results emphasize the need to investigate protein-protein interactions for a better comprehension of P450 11B enzymes.

4.4 Alternative Aldosterone Synthase Substrates

As discussed in Chapter 1, the adrenal glands are responsible for the secretion of a diverse range of steroids, including androstenedione (A4) and testosterone. Both A4 and testosterone have been shown to be substrates for P450 11B1 and P450 11B2. P450 11B enzymes convert A4 into 11β-hydroxyandrostenedione (11OHA4), which is further metabolized into 11-keto androstenedione and then 11-ketotestosterone (11KT) in peripheral tissues [11]. Although the 11β-hydroxylation of A4 in the human adrenal is well-established, the study of A4 to 18-oxygenated steroids is a relatively recent development in the field of steroid metabolism.

A study conducted with purified P450 11B2 has demonstrated the enzyme's ability to metabolize A4 into 18-hydroxyandrostenedione and dihydroandrostenedione [12]. Despite their efforts, however, the authors of the study were unable to identify a fourth metabolite resulting from this reaction. Therefore, it is feasible that A4 metabolism by P450 11B2 may yield 11β,18-dihydroxyandrostenedione. Given that A4 does not possess a C_{20}-C_{21} side-chain, 11β,18-dihydroxyandrostenedione would be unable to form a cyclic lactol like what has been reported to occur with 18-hydroxycorticosterone [13]. Because of this property, A4 and its metabolites could potentially serve as tools for studying the activities of P450 11B2. In particular, the use of 11β, 18-dihydroxyandrostenedione would allow for more detailed studies of P450 11B2's 18-oxidase activity.

4.5 Development of Selective P450 11B2 Inhibitors

Although osilodrostat was not a selective P450 11B2 inhibitor, it has paved the way for the development of drugs to treat primary aldosteronism (PA). While drugs that target

mineralocorticoid receptors are used to treat PA, their use is limited by side effects, as discussed in Chapter 1. Furthermore, first-generation aldosterone synthase inhibitors have shown promising results in clinical studies for the treatment of PA [14, 15]. Nonetheless, as highlighted in Chapter 2, several limiting factors prevent the production of potent and selective P450 11B2 inhibitors. Ideal selective inhibitors for P450 11B2 would primarily abolish its 18-oxidase activity to limit the accumulation of DOC, which is itself a mineralocorticoid, and have little to no effect on cortisol synthesis.

Drug discovery approaches have significantly expanded and streamlined over the past years, which offer new avenues for the discovery of promising P450 11B2 inhibitors with unique mechanisms of action. These approaches identify lead compounds ("hits") by screening molecular libraries using target-based or phenotypic approaches. Target-based approaches screen a small molecule library against a specific biological target, while phenotypic approaches rely on a cellular system. Among these high-throughput target-based methods, DNA-encoded library (DEL) technology has been shown to be a promising and efficient tool [16]. DNA-encoded libraries (DELs) are composed of molecules that are connected to a unique DNA tag functioning as a barcode. Hits are identified by sequencing the DNA tags after separating the target-ligand complex. DELs have an advantage over other methods as they contain a larger library of molecules (2 – 200 billion), and campaigns can be carried out relatively quickly (less than 6 months) [17]. The success of DEL screens, however, depends on having a stable protein system. In the case of P450 11B enzymes, their expression and purification have been well-characterized, along with those of their redox partners. Therefore, both P450 11B1 and 11B2 can be screened against these large DELs to identify drugs that selectively bind to P450 11B2. This approach would identify both active-site (competitive) inhibitors and non-active site-directed allosteric modulators. The

two types of compounds can then be further characterized by spectral changes with and without substrate and by activity assays, such as the ones discussed in Chapter 2.

Computational techniques also represent a promising approach to identifying potential inhibitors for P450 11B2 [18]. In addition to using DELs, *in silico* screening of virtual libraries through computational methods presents a cost-effective strategy that is possible given the availability of high-resolution structures of P450 11B enzymes [6, 19, 20]. This approach could also assist in identifying allosteric binding pockets and other unique means to selectively target P450 11B2. Nevertheless, computational tools alone are insufficient to identify inhibitors. Validating and assessing possible hits require benchwork. Therefore, a comprehensive approach comprising both computational and experimental methods would be beneficial to identify promising drug candidates for treating PA.

4.6 Conclusions

Both P450 11B1 and P450 11B2 are of significant scientific and medical interest due to their pivotal roles in steroid biosynthesis and endocrine disorders. While crystallographic structures and kinetic analyses have elucidated important distinctions between these two homologous enzymes, several questions regarding their respective catalytic functions still need to be answered. The findings presented in this Dissertation highlight the significant differences in the binding of DOC and corticosterone to P450 11B1 and P450 11B2, which may result from their distinct dynamic behavior. Although intrinsic factors such as structure and amino acid composition play a significant role in regulating catalytic activity, extrinsic factors such as protein-protein interactions and membrane composition might also have an impact. Therefore, conducting additional computational and experimental studies on P450 11B1 and P450 11B2 could provide valuable insights into these processes.

4.7 Bibliography

1. Peng, H.M., C. Barlow, and R.J. Auchus, *Catalytic modulation of human cytochromes P450 17A1 and P450 11B2 by phospholipid.* J Steroid Biochem Mol Biol, 2018. **181**: p. 63-72.
2. Sumangala, N., et al., *Influence of cholesterol on kinetic parameters for human aromatase (P450 19A1) in phospholipid nanodiscs.* J Inorg Biochem, 2023. **247**: p. 112340.
3. Headlam, M.J., M.C. Wilce, and R.C. Tuckey, *The F-G loop region of cytochrome P450scc (CYP11A1) interacts with the phospholipid membrane.* Biochim Biophys Acta, 2003. **1617**(1-2): p. 96-108.
4. Yun, C.H., M. Song, and H. Kim, *Conformational change of cytochrome P450 1A2 induced by phospholipids and detergents.* J Biol Chem, 1997. **272**(32): p. 19725-30.
5. Loomis, C.L., S. Brixius-Anderko, and E.E. Scott, *Redox partner adrenodoxin alters cytochrome P450 11B1 ligand binding and inhibition.* J Inorg Biochem, 2022. **235**: p. 111934.
6. Brixius-Anderko, S. and E.E. Scott, *Structural and functional insights into aldosterone synthase interaction with its redox partner protein adrenodoxin.* J Biol Chem, 2021. **296**: p. 100794.
7. Bose, H.S., et al., *A Novel Mitochondrial Complex of Aldosterone Synthase, Steroidogenic Acute Regulatory Protein, and Tom22 Synthesizes Aldosterone in the Rat Heart.* J Pharmacol Exp Ther, 2021. **377**(1): p. 108-120.
8. Bose, H.S., V.R. Lingappa, and W.L. Miller, *Rapid regulation of steroidogenesis by mitochondrial protein import.* Nature, 2002. **417**(6884): p. 87-91.
9. Sluchanko, N.N., et al., *High-yield soluble expression, purification and characterization of human steroidogenic acute regulatory protein (StAR) fused to a cleavable Maltose-Binding Protein (MBP).* Protein Expr Purif, 2016. **119**: p. 27-35.
10. Bose, H.S., M.A. Baldwin, and W.L. Miller, *Incorrect folding of steroidogenic acute regulatory protein (StAR) in congenital lipoid adrenal hyperplasia.* Biochemistry, 1998. **37**(27): p. 9768-75.
11. Bernhardt, R. and J. Neunzig, *Underestimated reactions and regulation patterns of adrenal cytochromes P450.* Mol Cell Endocrinol, 2021. **530**: p. 111237.
12. Glass, S.M., et al., *Characterization of human adrenal cytochrome P450 11B2 products of progesterone and androstenedione oxidation.* J Steroid Biochem Mol Biol, 2021. **208**: p. 105787.
13. Reddish, M.J. and F.P. Guengerich, *Human cytochrome P450 11B2 produces aldosterone by a processive mechanism due to the lactol form of the intermediate 18-hydroxycorticosterone.* J Biol Chem, 2019. **294**(35): p. 12975-12991.
14. Freeman, M.W., et al., *Phase 2 Trial of Baxdrostat for Treatment-Resistant Hypertension.* N Engl J Med, 2023. **388**(5): p. 395-405.
15. Mulatero, P., et al., *CYP11B2 inhibitor dexfadrostat phosphate suppresses the aldosterone-to-renin ratio, an indicator of sodium retention, in healthy volunteers.* Br J Clin Pharmacol, 2023. **89**(8): p. 2483-2496.
16. Gironda-Martinez, A., et al., *DNA-Encoded Chemical Libraries: A Comprehensive Review with Succesful Stories and Future Challenges.* ACS Pharmacol Transl Sci, 2021. **4**(4): p. 1265-1279.

17. Foley, T.L., et al., *Selecting Approaches for Hit Identification and Increasing Options by Building the Efficient Discovery of Actionable Chemical Matter from DNA-Encoded Libraries.* SLAS Discov, 2021. **26**(2): p. 263-280.
18. Sadybekov, A.V. and V. Katritch, *Computational approaches streamlining drug discovery.* Nature, 2023. **616**(7958): p. 673-685.
19. Brixius-Anderko, S. and E.E. Scott, *Structure of human cortisol-producing cytochrome P450 11B1 bound to the breast cancer drug fadrozole provides insights for drug design.* J Biol Chem, 2019. **294**(2): p. 453-460.
20. Strushkevich, N., et al., *Structural insights into aldosterone synthase substrate specificity and targeted inhibition.* Mol Endocrinol, 2013. **27**(2): p. 315-24.

Appendix

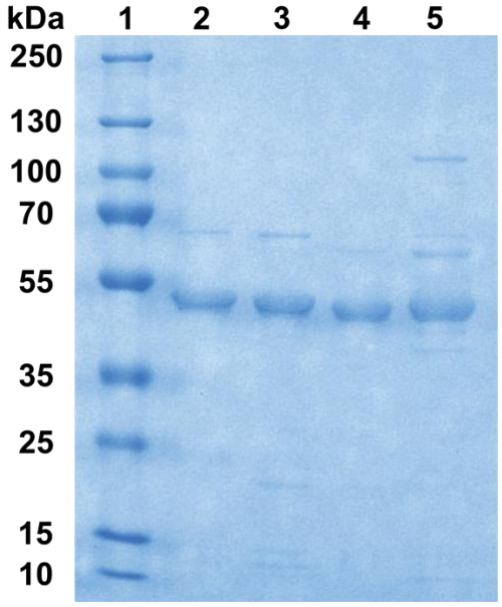

Appendix Figure 1 **SDS-PAGE analysis of purified P450 11B1 and 11B2 wild-type and mutant enzymes**. Lane 1: Molecular weight markers, Lane 2: Purified P450 11B1, Lane 3: Purified P450 11B1 A320V, Lane 4: Purified P450 11B2, Lane 5: Purified P450 11B2 A320V. The purified P450 11B enzymes migrate at the expected molecular weight of ~ 55 kDa.

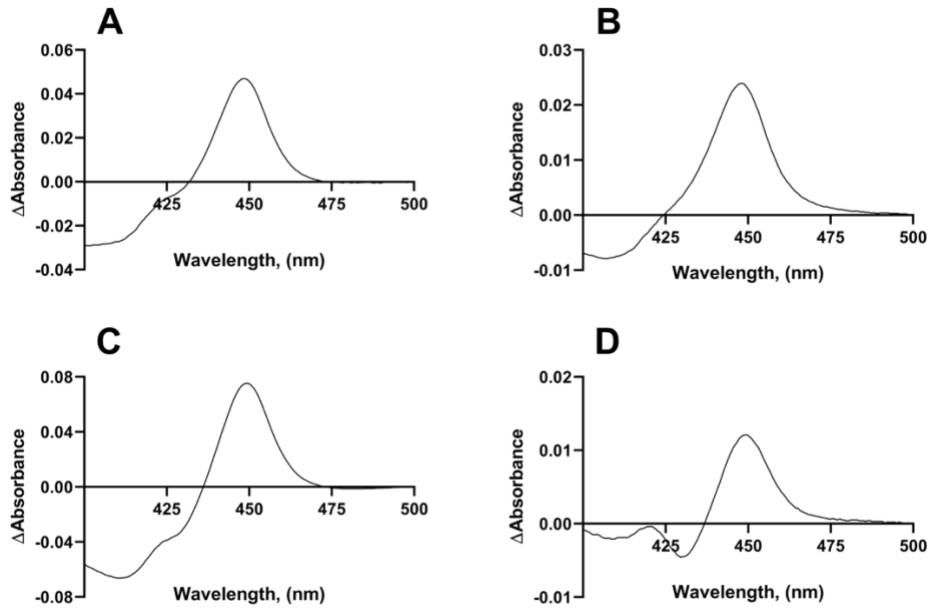

Appendix Figure 2 **Representative CO-reduced difference spectrum of purified cytochrome P450 11B enzymes.** Panels A and B correspond to P450 11B1 and P450 11B1-V320A, respectively. Panels C and D correspond to P450 11B2 and P450 11B2-A320V, respectively. All purified proteins have very little or negligible P420 content.

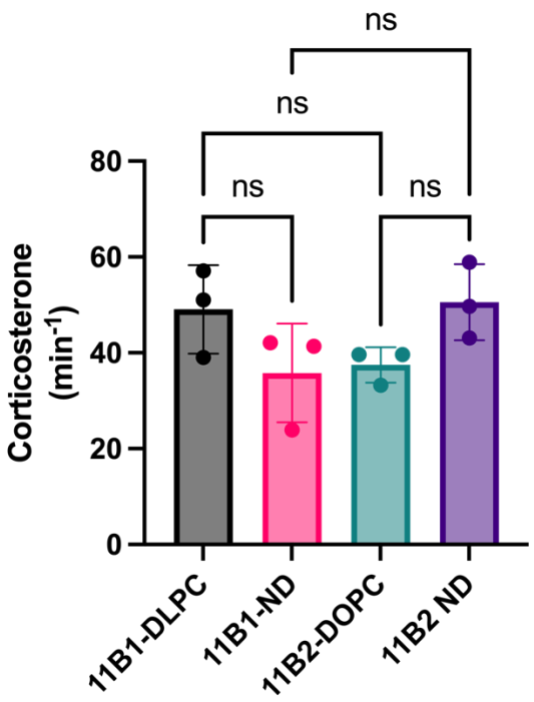

Appendix Figure 3 **11β-hydroxylase activity of P450 11B1 and P450 11B2 in phospholipid vesicles and nanodiscs.** Products were quantified by HPLC analysis. Data represent the mean ± standard deviation of three technical replicates (circles). Statistical analysis was carried out by using one-way ANOVA.

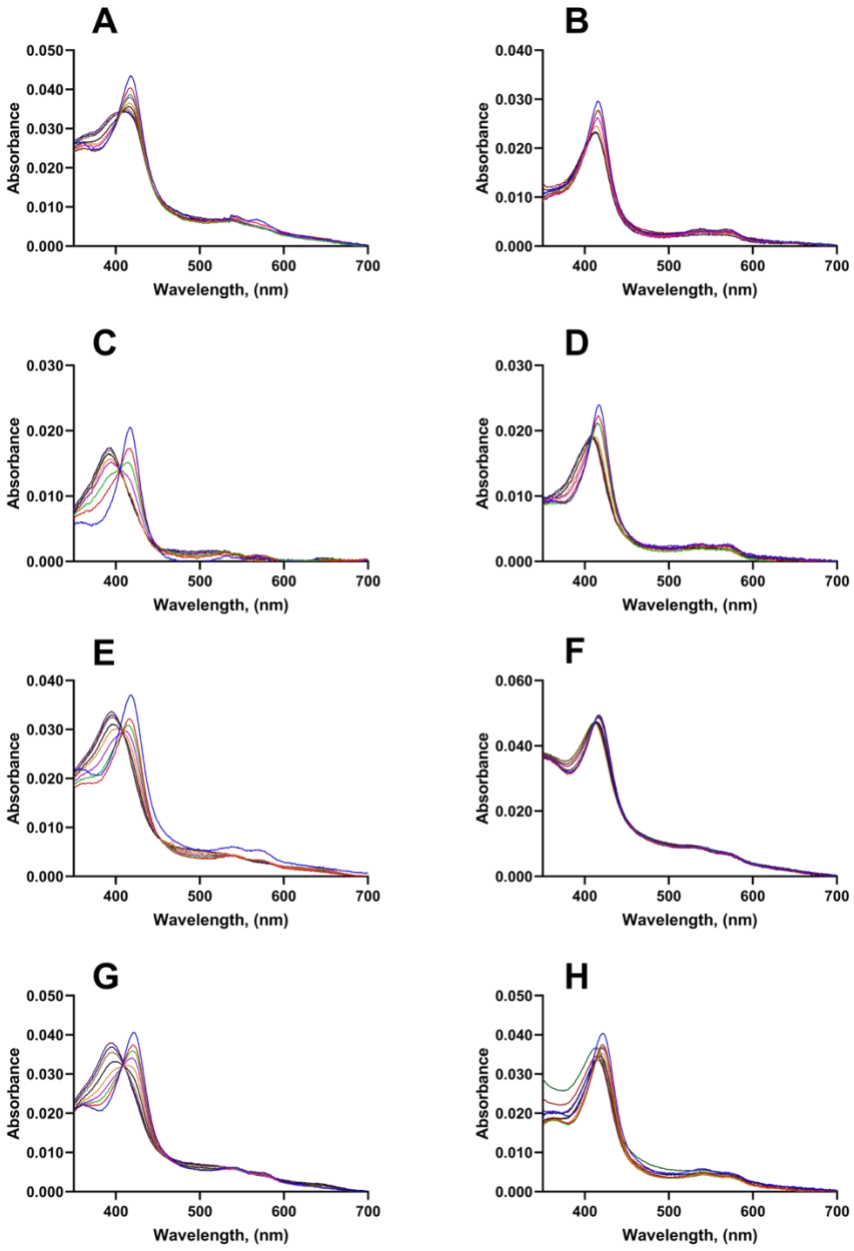

Appendix Figure 4 **Representative UV-visible spectra of P450 11B wild-type and mutant enzymes in the absence and presence of either DOC or corticosterone.** Panels A, C, E, and G correspond to the titration of DOC to P450 11B1, P450 11B1-V320A, P450 11B2, and P450 11B2-A320V, respectively. Panels B, D, F, and H correspond to the titration of corticosterone to P450 11B1, P450 11B1-V320A, P450 11B2, and P450 11B2-A320V, respectively. All P450 11B enzymes exhibit a Soret band at 417 nm in their unliganded state. Upon titration with ligand, the Soret band shifts to 390 nm.

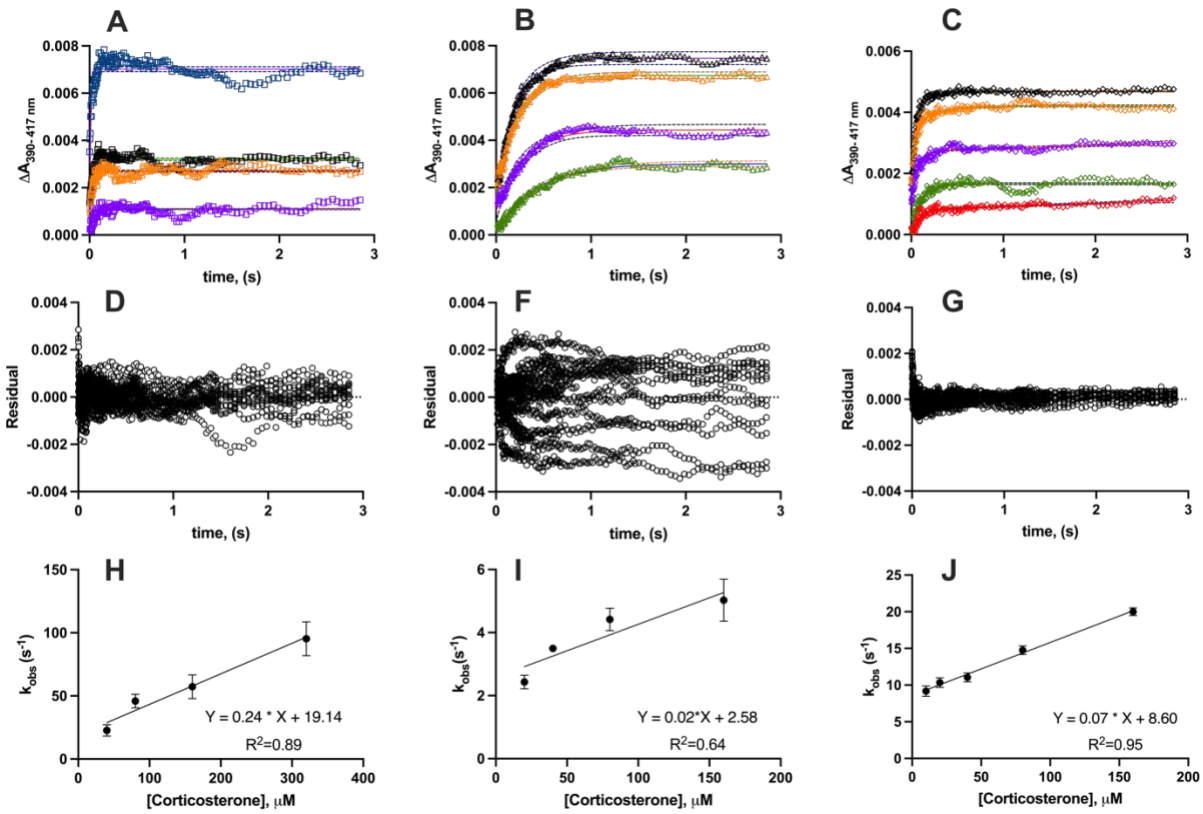

Appendix Figure 5 **UV-Visible stopped-flow analysis of P450 11B enzymes in nanodiscs.** Panels A, B, and C show the binding of 0.25 μM of μM of P450 11B1 (□), P450 11B1-V320A (Δ), and P450 11B2 (◇)respectively, with Corticosterone at the following concentrations: 10 μM (red), 20 μM (green), 40 μM (purple), 80 μM (orange), 160 μM (black), and 320 μM (blue). The lines in panels A-D show the nonlinear regression fits to the traces obtained, which represent the mean of three technical replicates. Panels D-G show residual plots for curve fits to panels A-C, respectively. Panels H, I, and J show the linear analysis of the exponential fits as a function of [Corticosterone]. Dashed lines represent the 95% confidence intervals. The observed rate constants were calculated by fitting kinetic traces to an uniphasic exponential function.

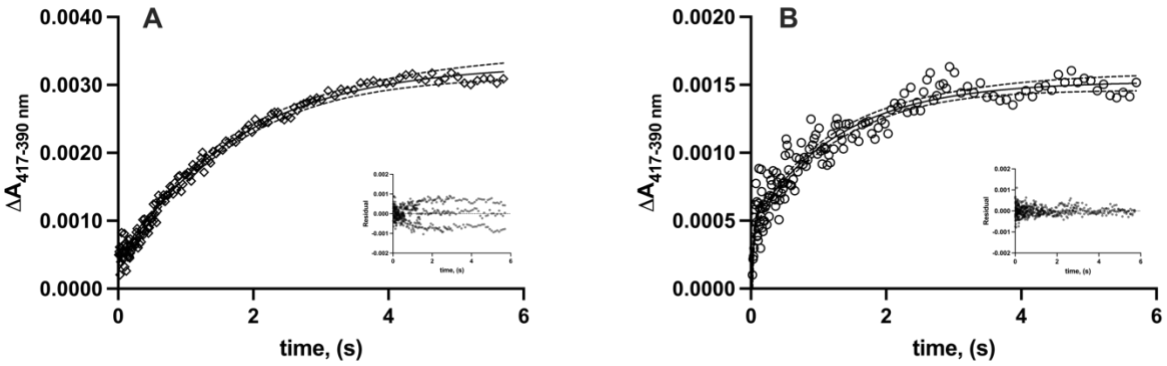

Appendix Figure 6 **Stopped-flow analysis of Corticosterone dissociation from P450 11B enzymes by direct method.** Panels A and B show the mixing of 0.5 µM of P450 11B2 (◇) and 11B2-A320V (○), respectively, with an excess of cyclodextrin. The dashed lines represent the 95% confidence intervals, and the insets show residual plots.

Appendix Table 1 **Equilibrium Biding Titrations of P450 11B2 and P450 11B1 in Nanodiscs and Phospholipid Vesicles.***

	DOC, K_d (µM)		Corticosterone, K_d (µM)	
	Nanodiscs	**Vesicles**	**Nanodiscs**	**Vesicles**
P450 11B1	0.45 ± 0.08	14.12 ± 0.54	31 ± 5	n.d.
P450 11B2	0.12 ± 0.01	10.05 ± 1.34	5.89 ± 0.94	444 ± 50

*Data represent the mean ± standard error of three replicates; n.d. = not determined

Appendix Table 2 **Kinetic Parameters for DOC Binding to P450 11B1 and P450 11B2 in Nanodiscs and Phospholipid Vesicles from Pseudo-first-order Analysis.***

	Nanodiscs		Vesicles	
	k_{on} (μM^{-1} s^{-1})	k_{off} (s^{-1})	k_{on} (μM^{-1} s^{1})	k_{off} (s^{-1})
P450 11B1	0.53 ± 0.01	1.45 ± 0.07	0.14 ± 0.00	1.77 ± 0.00
P450 11B2	0.54 ± 0.01	0.69 ± 0.09	0.16 ± 0.02	0.46 ± 0.01

* Data represent the mean ± standard error of three replicates. Values for P450 11B2 in vesicles are reported from duplicate measurements.

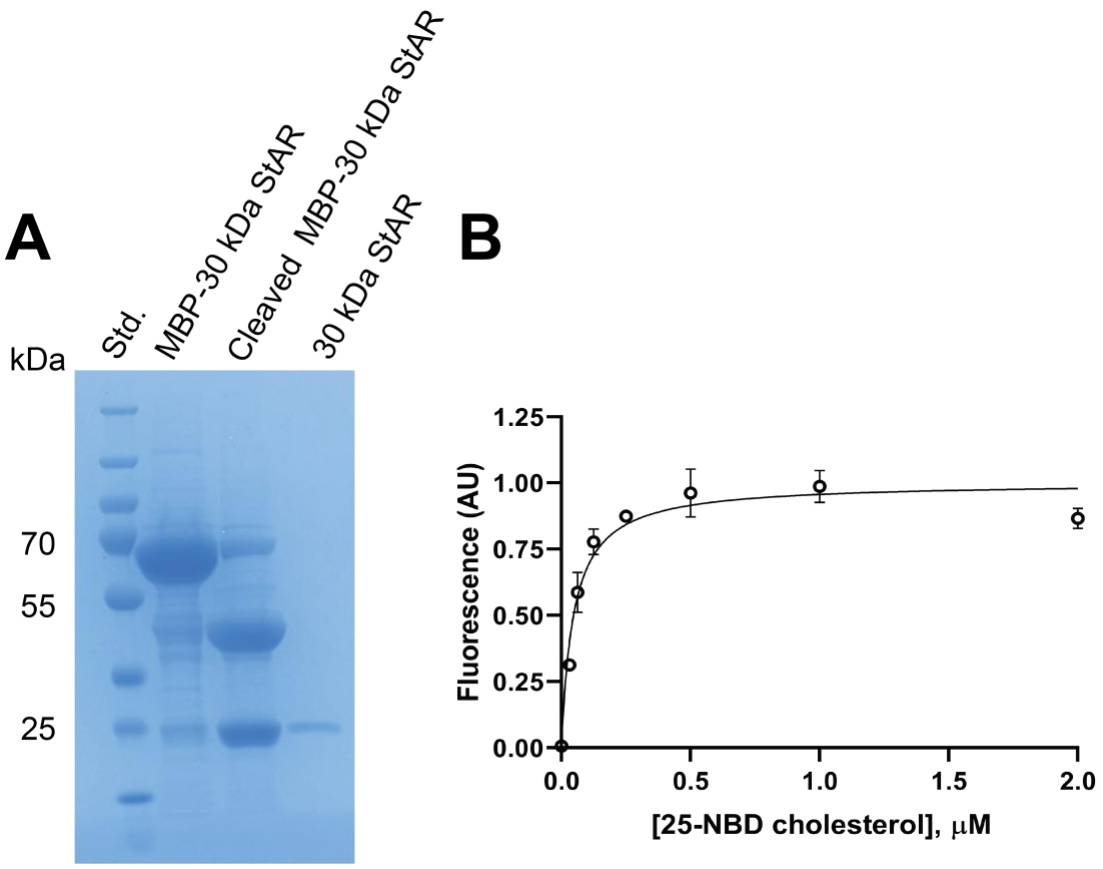

Appendix Figure 7 **SDS gel of purified StAR and binding assay by fluorescent cholesterol analog 25-NBD.** Panel A shows the cleavage of the MBP-StAR fusion protein (lane two) by 3C protease and the purified StAR (lane four) by subsequent size exclusion chromatography. Molecular masses of the protein standards (Std., lane one) are indicated in kDa to the left. Panel B shows the of 0.5 μM of 30-kDa StAR to 25-[N-[(7-nitro-2-1,3-benzoxadiazol-4-yl)methyl]amino]-27-norcholesterol (25-NBD cholesterol). Data represent the mean ± standard deviation of three replicates.

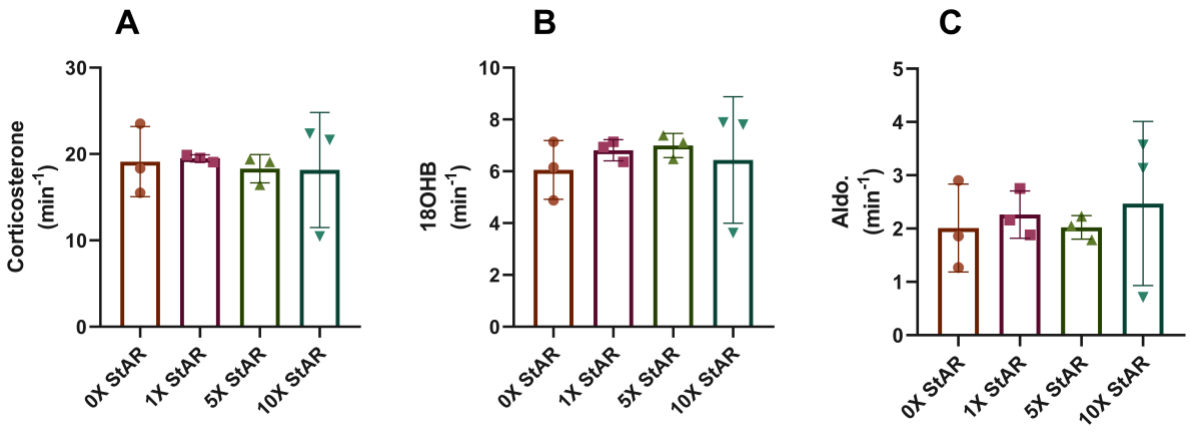

Appendix Figure 8 **P450 11B2-nanodiscs activity assay in the presence and absence of StAR (30 kDa).** Panels A, B, and C, show the rates of corticosterone, 18-hydroxycorticosterone (18OHB), and aldosterone (Aldo.), respectively. Data represent the mean ± standard deviation of three replicates.